Technische Universität München
TUM School of Engineering and Design

Control of the Weld Depth for Deep Penetration Laser Beam Welding

Maximilian Schmöller

Vollständiger Abdruck der von der TUM School of Engineering and Design der Technischen Universität München zur Erlangung des akademischen Grades eines

Doktors der Ingenieurwissenschaften (Dr.-Ing.)

genehmigten Dissertation.

Vorsitz: Prof. Dr.-Ing. Wolfram Volk

Prüfer*innen der Dissertation:

1. Prof. Dr.-Ing. Michael F. Zäh
2. Prof. Dr. techn. Peter Mayr

Die Dissertation wurde am 30.08.2022 bei der Technischen Universität München eingereicht und durch die TUM School of Engineering and Design am 08.02.2023 angenommen.

Preface

This dissertation was elaborated during my work as a research associate at the Institute for Machine Tools and Industrial Management (*iwb*) of the Technical University of Munich (TUM).

First of all, I would like to thank Prof. Dr.-Ing. Michael F. Zaeh, full professor of the Chair of Machine Tools and Manufacturing Technology, for the opportunity to pursue a doctorate and for his valuable supervision. During my work at the *iwb*, you provided me with the necessary scientific skills and excellently promoted my abilities and talents. Furthermore, I would like to thank the second examiner and the examination board chairman.

A special thanks goes to my colleagues at the institute, especially to the Laser Manufacturing Technology Department members. The creative and motivating mindset at the institute has facilitated the elaboration of this thesis. I have a close friendship with many of you, which has left a permanent impression on my life through shared ups and downs. Let us not forget the good times we were able to enjoy with each other outside of our work, which contributed to a well-balanced experience at the institute. It is my wish to preserve and cherish this friendship in the future. I would like to particularly mention my colleagues Johannes Kriegler, Jan Bernd Habedank, Jan Hagemeister and Christian Stadter. You all gave me valuable advice on my scientific work and contributed to a successful result. Furthermore, I would like to thank all my students and co-authors of the publications for the exciting and inspiring discussions during our scientific work.

Finally, I would like to extend a heartfelt thank you to my family. My parents Anna Katharina Schmoeller and Helmut Schmoeller, my brother Philipp Schmoeller and my grandmothers Anni Grundmueller and Anni Schmoeller have all encouraged me since my childhood. They have made me understand the value of education on my life's path. Thank you for your enduring support and for teaching me the values of solidarity and integrity.

Munich, March 2023 *Maximilian Schmöller*

Table of Contents

Table of Contents

List of Abbreviations

Acronym	Description
1D	One-dimensional
3D	Three-dimensional
AI	Artificial Intelligence
ANN	Artificial Neural Network
BIBO	Bounded-Input-Bounded-Output
BPP	Beam Parameter Product
BPTT	Backpropagation through time
β-VAE	Beta-Variational Autoencoder
CNC	Computerized numerical control
CNN	Convolutional Neural Network
CT	X-ray Computed tomography
cw	Continuous-wave
D	Differential
DNN	Deep Neural Network
DPLW	Deep penetration laser beam welding
FD	Frequency Domain
FEM	Finite Element Method
FFNN	Feed Forward Neural Network

Acronym	Description
FFT	Fast Fourier Transformation
FPH	Full penetration hole
GA	Genetic algorithm
HAZ	Heat-affected zone
I	Integral
ICALEO	Intl. Congress on Applications of Lasers and Electro-Optics
IIR	Infinite impulse response
IR	Infrared
iwb	Institute for Machine Tools and Industrial Management
LapSVM	Laplacian Graph Support Vector Machine
LSTM	Long-Short-Term-Memory
LTI	Linear time-invariant
ML	Machine Learning
MM	Multi-mode
µCT	Microfocus X-ray computed tomography
OCT	Optical Coherence Tomography
P	Publication
P	Proportional
PID	Proportional-Integral-Differential
PLC	Programmable logic controller
RMSE	Root mean square error
RNN	Recurrent Neural Network
SM	Single-mode
SO	Sub-objective

Acronym	Description
SVM	Support Vector Machine
TD	Time Domain
TEM	Transverse Electromagnetic Mode
TEM_{00}	Fundamental Transverse Electromagnetic Mode
TUM	Technical University of Munich
VAE	Variational Autoencoder

List of Symbols

Variable	Unit[1]	Description
Roman variables		
c_p	J·(kg·K)$^{-1}$	Specific isobaric heat capacity
d	m	Distance
d_f	m	Focus diameter
d_k	m	Keyhole depth
d_w	m	Weld depth
E	J	Energy
E_I	V·m^{-1}	Complex electric field
E_R	V·m^{-1}	Electric field in the OCT reference path
E_S	V·m^{-1}	Electric field in the OCT measurement path
e	-	Error
F_G	N	Gravitational force
f	m	Focal length
f_{12}	Hz	Excitation frequency of an atom
g	m·s^{-2}	Gravitational acceleration
h	J·s	Planck constant
I	W·m^{-2}	Intensity

[1] The units are specified in their respective standard form without prefixes.

Variable	Unit[1]	Description
I_0	$W \cdot m^{-2}$	Maximum radiation intensity
I_D	A	Photocurrent in an OCT detector
I_{Mot}	A	Motor current
i	-	Imaginary number
k	-	Wavenumber
k_{abs}	-	Absorption index
l_d	m	Distance beween radiation source and detector
l_s	m	Distance beween radiation source and sample
l_α	m	Absorption length
M	Nm	Motor torque
M^2	-	Beam quality factor
m	kg	Mass
N	-	Counter variable
N_r	-	Discrete reflections
n	-	Real part of the fraction index
P_{abs}	W	Absorbed laser power
P_L	W	Laser power
$P_{L,s}$	W	Setpoint laser power
P_{ref}	W	Reflected laser power
P_{trans}	W	Transmitted laser power
R_R	-	Power reflectivity at a reference reflector
R_S	-	Power reflectivity at a sample
r	m	Radius
r_R	-	Intensity reflectivity at a reference reflector

Variable	Unit[1]	Description
r_S	-	Intensity reflectivity at a sample
S	-	Spectral power
s	-	Electric field amplitude
T	K	Temperature
T_m	K	Melting temperature
T_v	K	Vaporization temperature
t	s	Time
t_l	m	Melt layer thickness
u	-	Manipulated variable
u_R	-	Controller output variable
u_S	-	Setpoint variable
v_w	$m \cdot s^{-1}$	Feed rate
w	-	Reference variable
w_o	m	Focus radius of a laser beam
w_i	-	Weighting factor *i*
w_L	m	Laser beam radius in the focusing lens
w_R	m	Laser beam radius at Rayleigh length
x, y, z	-	Cartesian coordinates
x_c	-	Controlled variable
x_i	-	Input values of an artificial neuron
x_o	-	Output value of an artificial neuron
x_s	-	Expected output variable
z_R	m	Reference length
z_S	m	Distance to a sample

Variable	Unit[1]	Description
z_c	-	Disturbance variable
z_r	m	Rayleigh length
z_α	m	Optical penetration depth
Greek variables		
α	°	Angle of incidence
α_{abs}	m^{-1}	Absorption coefficient
β	-	Hyperparameter
Δk	-	Spectral bandwidth
ΔP	W	Power offset value
λ	m	Wavelength
λ_{th}	$W \cdot (m \cdot K)^{-1}$	Thermal conductivity
μ_{dyn}	$(N \cdot s) \cdot m^{-2}$	Dynamic viscosity
φ	°	Deflection angle
φ_a	-	Activation function of an artificial neuron
φ_{ref}	°	Reference angle
ρ	-	Reflection coefficient
ρ_m	$kg \cdot m^{-3}$	Mass density
ρ_s	-	Responsitivity of an OCT sensor
Σ	-	Activation function of an artificial neuron
τ	-	Transmission coefficient
θ	°	Aperture angle
θ_p	-	Threshold value in artificial neurons

1 Introduction

1.1 Laser beam welding – a keystone of fully automated production

As a joining process in fully automated production, laser beam welding is becoming increasingly important. This technology offers the potential to achieve high quality and productivity for a safe and efficient production with a high degree of automation in the coming years (WEBSTER ET AL. 2014). An essential prerequisite for the employment of the novel process in industrial manufacturing is the feasibility of assuring and consistently documenting the product quality. With the joining processes typically being located at a late stage of the value chain, e.g., in the production of electrical energy storage systems, very low defect rates must be achieved (KAMPKER & NOWACKI 2014, pp. 57 ff.). Inline process monitoring systems can be employed to detect low-quality joints caused by irregularities in the welding process. The acquired data offers great potential for reducing rejects by improving and stabilizing production processes. Efficient and close-to-process utilization of the data requires inline control systems (KATAYAMA 2020, p. 135). By their employment, the transition from the detection to the prevention of insufficient product quality can be accomplished.

1.2 Challenges, objectives and approach

Laser beam welding is characterized by a highly concentrated energy input on a confined area due to the high radiation intensity used as a heat source. Consequently, the component to be welded is exposed to a low total energy input, resulting in a small heat-affected zone (HAZ) during the joining process compared to other fusion welding processes. Above a threshold intensity of the laser radiation, the evaporation temperature of metallic materials is exceeded. The result is the formation of a so-called keyhole maintained by the escaping metal vapor and the high pressure inside

the capillary. The deep penetration welding process is characterized by a high efficiency, since the laser radiation is reflected by the keyhole walls multiple times and is partially absorbed during each impact (SIMONDS ET AL. 2018). However, the high temperature gradients lead to dynamic fluctuations in the welding process due to a decrease from the evaporation to the ambient temperature in a range of a few millimeters. If these instabilities lead to a collapse of the keyhole, spatter ejection or a change in the penetration depth can result (VOLPP & VOLLERTSEN 2016). For many technical applications, a constant weld depth is essential. Figure 1 shows three different scenarios for the weld depth exemplified by a weld seam in overlap configuration. In case a), no fusion of the two layers is achieved, as the upper joining partner is not fully penetrated. Many applications require case b), in which a complete attachment of the subjacent joining partner is achieved without a full penetration of the lower joining partner. Case c) shows a contrary situation to case a), as the joining partners are completely penetrated. Damage to the component or a vulnerable area below can result. Particularly, welding configurations, where full penetration welding should be avoided, often have vulnerable areas on the backside of the welding zone, e.g., battery cells or electronic components.

The weld depth control for deep penetration laser beam welding (DPLW) has been the subject of research for many years. In this context, the development of a precise and real-time capable method for the inline measurement of the weld depth is essential. A possible solution is based on an interferometric measurement principle, Optical Coherence Tomography (OCT), in which a measuring laser beam is directed coaxially to the processing laser beam to the process zone (BAUTZE & KOGEL-HOLLACHER 2014). The keyhole depth d_k can be measured with a frequency of several kilohertz and an axial accuracy in the range of a few micrometers. The sensor signal is strongly influenced by the dynamic fluctuations of the keyhole, by the material of the components to be joined and by the process parameters. The result is an inherent challenge regarding the interpretation of the OCT measurement signal.

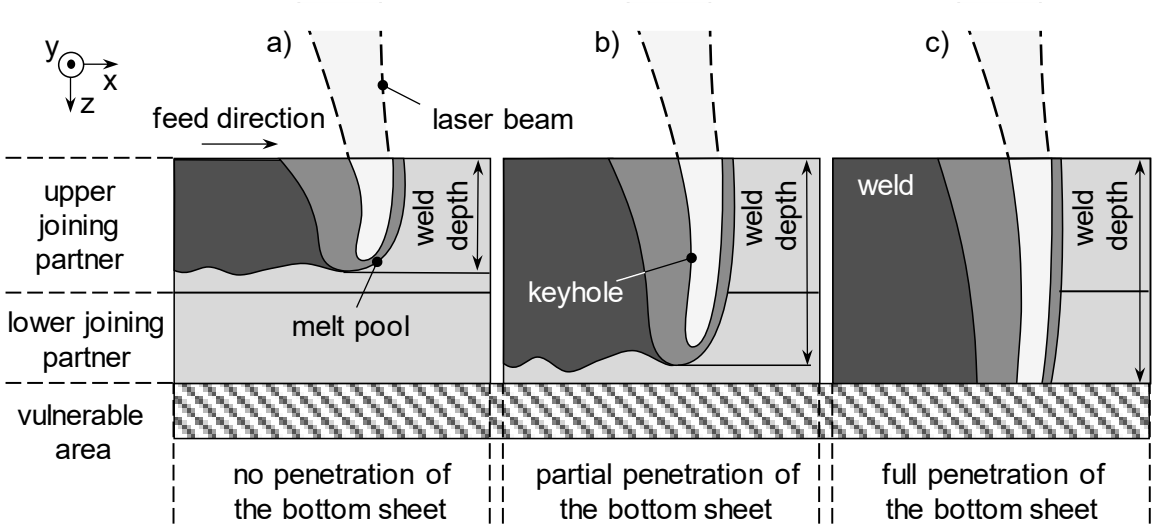

Figure 1: Cross-sectional illustration of a laser welding process for joining two components in an overlap configuration; a) insufficient weld depth; b) desired weld depth; c) full penetration of both joining partners

In the scope of this thesis, an inline weld depth control is to be developed. It is based on a numerical simulation of the melt pool geometry and on flexible and adaptive data processing methods for the keyhole measurement signal. A profound understanding of the measuring method and the process-determining variables in DPLW must be gained to use the signal of an OCT sensor as an input signal for controlling the weld depth. First of all, the optimal OCT data-set structure is analyzed as a function of the material of the components to be joined and the process parameters during welding with a continuously emitting, i.e., a continuous-wave (cw) laser beam source. Besides that, a numerical simulation model is employed to investigate the relationship between the measurable depth of the keyhole and the resulting weld depth. A deviation between these two quantities results from a melt layer below the keyhole (cf. Figure 1). The influences on the OCT signal and the thickness of the melt layer are the basis for interpreting the keyhole depth measurement regarding the weld depth. Machine Learning (ML) methods are used for the regression of structured data. In addition to a well-understood input signal, precise knowledge of the possible reactions to actively influence the weld depth is required to control the DPLW process. For this purpose, ML-methods are used to evaluate the relationships between the process parameters and the weld depth. To apply ML-methods for processing inline measurement data, extensive training data-sets are to be obtained. Computed Tomography (CT) images of welding samples provide a consistent data-set, which can be used in a comparison with the inline evaluated weld depths as reference data. The gained knowledge forms the basis for developing a weld depth control for DPLW.

1.3 Structure of the thesis

This publication-based thesis is divided into six chapters. After the introduction, chapter 2 provides the fundamentals contributing to understanding the DPLW process and the control of the weld depth based on inline process monitoring data. It includes laser material processing, inline weld depth measurement, Artificial Intelligence (AI) methods for data processing and control architectures for industrial processes. In chapter 3, the state of the art is presented. The focus is on inline weld depth measurement in DPLW, ML-methods for data processing and numerical weld pool simulation. Chapter 4 describes the research approach, which includes the scientific objectives of this thesis, the methodological approach, the assignment of the embedded publications and the experimental set-up. The scientific results, which were presented in five scientific publications, are summarized and distinguished from the state of the art in chapter 5. The publications include the knowledge gained on interpreting the OCT keyhole depth measurement signal, the weld pool simulation results and the fundamentals and implementation of inline weld depth control. In chapter 6, the results are summarized and discussed, followed by an outlook on possibilities for weld depth control advancement.

2 Fundamentals

2.1 Chapter overview

This chapter, dedicated to the fundamentals, is divided into five sections. In section 2.2, laser material processing basics are provided, followed by a description of the inline weld depth determination during laser beam welding in section 2.3. The basics of Artificial Intelligence for data processing in industrial environments are explained in section 2.4. A detailed discussion of industrial process control strategies is given in section 2.5.

Based on an explanation of the scientific terminology regarding laser material processing in sub-section 2.2.1, sub-section 2.2.2 describes the fundamental properties of laser radiation. Sub-section 2.2.3 addresses the generation of laser radiation and the technical principles of a laser beam source. The interactions between laser radiation and matter, which are the basis for the use of laser radiation in materials processing, are discussed in sub-section 2.2.4. Particular emphasis is devoted to aspects with relevance for process control.

Sub-section 2.3.1 focuses on possibilities for inline process monitoring of laser beam welding. An overview of process monitoring systems in broad scope is followed by an in-depth discussion of methods for the acquisition of measurement data in the process zone during laser beam welding. Based on this, sub-section 2.3.2 describes the principles of keyhole depth measurement using Optical Coherence Tomography.

Sub-section 2.4.1 gives an overview of Machine Learning methods for data processing. In sub-section 2.4.2, Neural Networks are discussed. In particular, approaches suitable for the analysis of OCT measurement data are addressed in detail.

An overview of methods for industrial process control is given in sub-section 2.5.1. Based on this, fuzzy-based control approaches are described in sub-section 2.5.2. A summary of the fundamentals is presented in sub-section 2.6.

2.2 Laser material processing

2.2.1 General remarks

The term *laser* is an acronym for *light amplification by stimulated emission of radiation*, describing the physical process of amplifying radiation by stimulated emission. In this section, the laser technology and the basics of laser welding are explained. For further information on these topics, reference is made to the works of POPRAWE (2005), HÜGEL & GRAF (2009) and GRAF (2015).

2.2.2 Characteristics of laser radiation

The wave-particle duality can describe the propagation of electromagnetic radiation. According to the model, a light beam can be described both as an infinitesimal, rectilinearly propagating beam (ray optics) and as a superposition of radially propagating waves (wave optics) (DIMITROVA & WEIS 2008). As a combination of the described domains, the Gaussian beam is a suitable model for the description of laser light propagation. The following explanation refers to a beam in the fundamental Transverse Electromagnetic Mode TEM_{00} with a radially symmetric intensity distribution that corresponds to the Gaussian bell curve (BLIEDTNER ET AL. 2013, pp. 33–34).

Figure 2 shows a Gaussian beam with the essential geometrical quantities describing the laser beam propagation properties. Since, in theory, light has an infinite propagation, a convention for the expansion of a laser beam is needed. The radial propagation limit of the beam is defined as the radius r at which the intensity I is as low as the value of I/e^2 with respect to the maximum intensity I_{00} in the center of the beam (HÜGEL & GRAF 2009, p. 22). Coherence is an essential property of laser radiation, which implies a linear and directed propagation of the radiation. Furthermore, an ideal (coherent and high-quality) laser beam has one discrete frequency, i.e., one characteristic wavelength λ. The wavelength significantly influences the geometric properties of propagating laser radiation. The beam radius in the focal point w_0 is preferably used to describe the geometric properties of the laser beam:

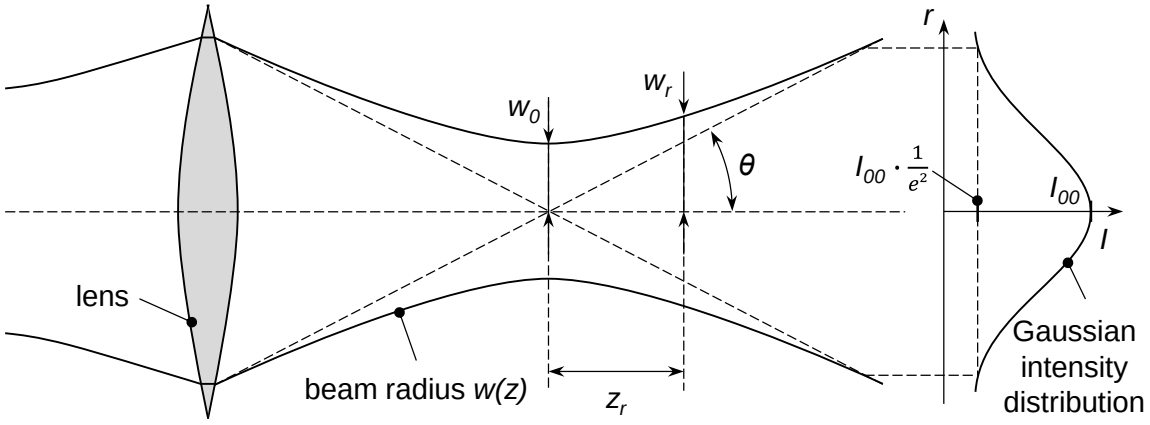

Figure 2: Caustics of a Gaussian laser beam with optical parameters for beam characterization; based on EICHLER & EICHLER (2010, p. 235)

$$w_0 = \sqrt{\frac{\lambda\, z_r}{\pi}} \tag{2-1}$$

Distant to the focal plane, the beam diameter expands along the beam axis. The distance at which the cross-sectional area doubles compared to the beam area at the beam waist is described by the Rayleigh length z_r:

$$z_r = \frac{\pi w_0^2}{\lambda} \tag{2-2}$$

The beam radius w can be described as a function of the position z along the propagation axis:

$$w(z) = w_0 \sqrt{1 + \left(\frac{z}{z_r}\right)^2} \tag{2-3}$$

At the Rayleigh length the radius $w(z_r)$ has the specific value w_r. The focusing property of a laser beam, i.e., the product of the focus radius and the divergence angle, is specified by the beam parameter product (*BPP*):

$$BPP = w_0 \cdot \theta \tag{2-4}$$

The expansion of a laser beam along the propagation axis is described by the divergence angle θ:

$$\theta = \frac{\lambda}{\pi \cdot w_0} \tag{2-5}$$

Compared to the ideal Gaussian beam, which offers the highest attainable focusing possibility, the quality of a laser beam is described by the beam quality factor M^2:

$$M^2 = \frac{\pi}{\lambda} \cdot w_0 \cdot \theta \tag{2-6}$$

It represents the ratio of the *BPP* of the considered beam to the *BPP* of an ideal Gaussian beam of the same wavelength. In addition to the fundamental mode TEM_{00}, there are several higher modes with multiple maxima in the radial intensity distribution. The result is a flat intensity distribution for a high number of superimposed modes and an increased focal diameter compared to the TEM_{00}. Beam sources emitting radiation in the fundamental mode are called single-mode (SM) beam sources. They have a higher beam quality than multi-mode (MM) beam sources, in which the radiation is composed of multiple superimposed modes.

2.2.3 Generation of laser radiation

A resonator is used in a laser beam source to generate laser radiation by exciting a laser-active medium by light of a specific wavelength. The resonator, whose schematic structure is shown in Figure 3, determines the basic properties of the laser beam. Essential elements of a resonator are two mirrors, the laser-active medium and the pumping source. While the laser-active medium primarily determines the laser radiation wavelength, the beam profile results mainly from the mirror arrangement.

Independent of the resonator design, the generation of laser radiation is based on the stimulated, i.e., technically induced emission. The required energy must be supplied to the laser-active medium by an external energy supply, referred to as a pumping source. The semi-transparent mirror contributes to maintaining the energetically excited state in the resonator. It allows only a defined fraction of the radiation to be transmitted, while the reflected fraction stimulates the laser-active medium.

The physical fundamentals of absorption and emission are explained by the *Bohr model* of the atom, according to which atoms have discrete energy levels and always aspire to the state of lowest energy. By adding energy, excited states are reached, which corresponds to an over-occupation of a higher energy level on the atomistic scale. The emission of radiation is always preceded by absorption. Excitation only occurs through radiation providing the appropriate energy, i.e., if the radiation energy introduced is equal to the energetic difference between two energy states. Naturally occurring radiation results from spontaneous emission. By incident radiation, an atom can be excited to a higher energy level. When the excited atom falls back to the lower energy level, an undirected photon is emitted. It is characteristic that the lower energy level is always over-occupied in thermal equilibrium (RENK 2012, p. 55).

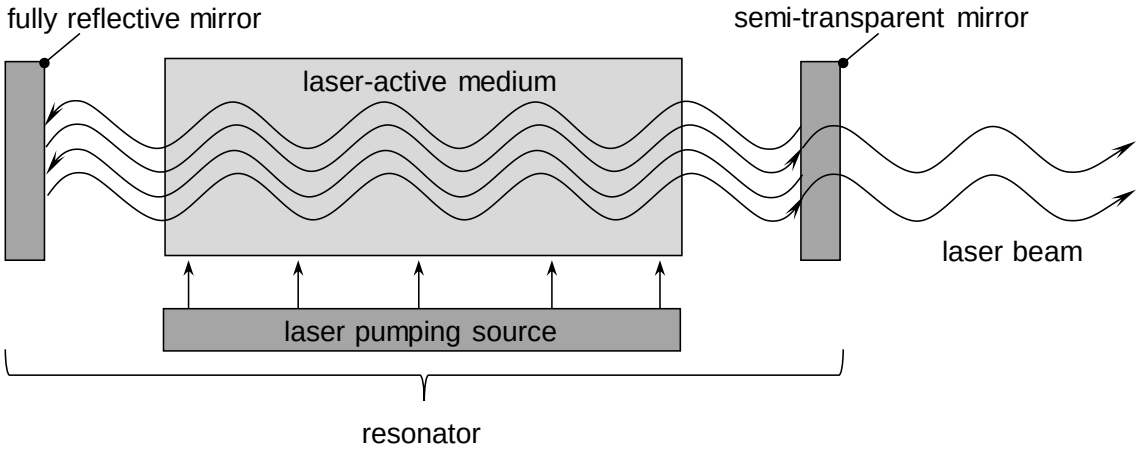

Figure 3: Schematic representation of a laser resonator for the generation of laser radiation; based on TRÄGER (2012, p. 643)

In contrast, the stimulated emission in a laser beam source requires an inversion of the occupation at the respective energy levels of the atoms in the laser-active medium. To obtain the inverted occupation state, a major fraction of the atoms has to be in the excited energy state, i.e., the excited state has to be overoccupied. This can be achieved by applying energy to the atoms with a pumping process. The resulting inverted state is an essential prerequisite for the generation of laser radiation (GRAF 2015, pp. 142–143). When no energy is supplied by a pump source, the electrons are in the state of lowest energy E_1. If a photon of the frequency f_{12} hits an atom or molecule, the hit particle changes to a higher energy state E_2. The transition from the ground state to the excited state follows the energy conservation principle:

$$E_2 - E_1 = \mathrm{h} \cdot f_{12} \tag{2-7}$$

Thereby, a photon of energy $\mathrm{h} \cdot f_{12}$ is retracted from the light and the intensity of the light decreases. From equation 2-7 follows that energy can occur only as an integer manifold of the *Planck constant* h. Particles in the excited state fall back into the ground state after a specific time. With a spontaneous emission, a photon of the energy $\mathrm{h} \cdot f_{12}$ is emitted. However, if a particle in the excited state is hit by a light quantum again, it falls to a lower energy state while energy is released. This so-called stimulated emission releases significantly more light quanta, which results in usable laser radiation with high energy, coherence and a uniform direction. (HÜGEL & GRAF 2009, pp. 50 ff.; RENK 2012, pp. 55 ff.; GRAF 2015, pp. 153 ff.)

2.2.4 Interaction of the laser beam and the material

For this work, laser radiation was used as a heat source for the welding of metals, i.e., for forming a cohesive joint between metallic components by melting and intermixing the materials in the area of the weld joint. An essential requirement is that the workpieces partially absorb the laser radiation. Depending on the material, the laser intensity in the interaction zone, the laser radiation wavelength and the traversing speed of the spot, different process regimes can be distinguished (KATAYAMA 2020, pp. 25–26). These are depicted in Figure 4 in a simplified representation. At a low beam intensity, the workpiece is only heated by the absorbed part of the laser radiation without melting. The workpiece volume potentially modified by the heat of the laser process is referred to as the heat-affected zone (HAZ)[2]. Above a threshold intensity at which sufficient energy is absorbed by the material, the melting temperature T_m is exceeded. In the heat conduction welding regime, a lenticular melt pool is formed due to the absorption of radiation energy on the workpiece surface. A further increase of the beam intensity results in exceeding the evaporation temperature T_v in the interaction zone. A vapor capillary (keyhole) is then formed within the melt pool, within which the laser beam is reflected multiple times. Due to the evaporation of the material, the pressure within the keyhole increases, causing an increase in its volume. Within the expanding vapor capillary, the amount of energy absorbed by the workpiece and the weld depth increase with the intensity. The resulting process regime is referred to as deep penetration laser beam welding (DPLW).

Fundamental to the efficiency of a process are the interaction processes of a laser beam with the material. In a simplified description, absorption, reflection and transmission can occur (ALLMEN & BLATTER 1995). Neither reflected nor transmitted radiation contribute to the heating of the material and can be summarized as power loss. The absorptivity represents the proportion of the energy absorbed by the workpiece when the laser impacts the workpiece surface only once. In contrast, the total absorption coefficient α_{abs} describes the fraction of the energy absorbed in the interaction zone, when considering multiple laser-material interactions.

[2] The heat-affected zone (HAZ) is a non-molten area of the workpiece in proximity to the process zone that potentially undergoes a change in the material properties as a result of the heat exposure during the welding process.

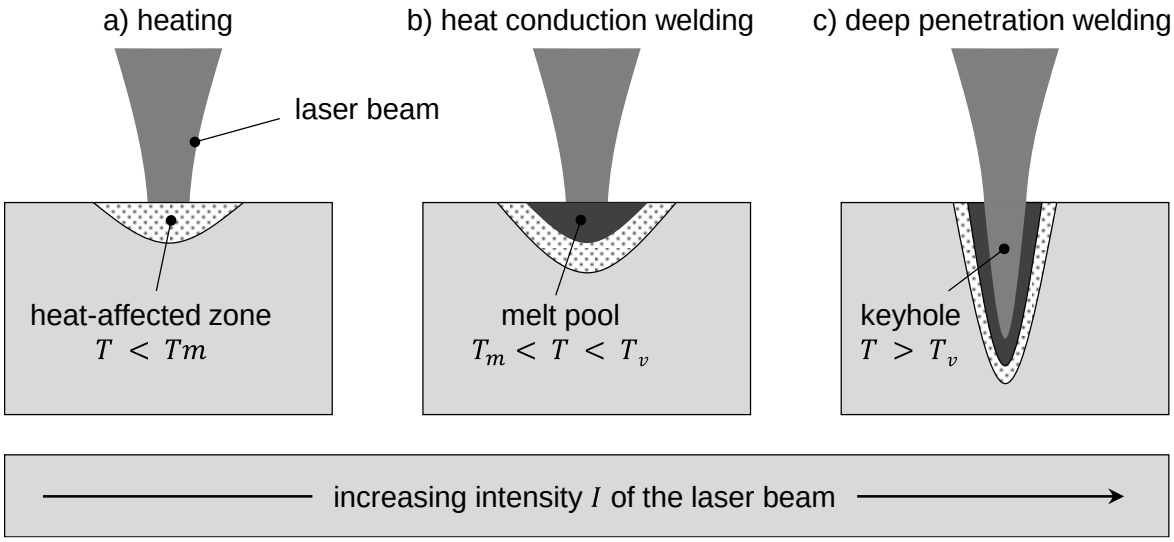

Figure 4: Process regimes of laser beam welding for an increasing radiation intensity; a) heating; b) heat conduction welding; c) deep penetration welding; based on KATAYAMA (2020, p. 25)

Considering the conservation of energy, a simple equation for the absorption, reflection and transmission can be obtained (BÖCKH & WETZEL 2014, p. 204; DAHOTRE & HARIMKAR 2008):

$$1 = \alpha_{abs} + \rho + \tau \tag{2-8}$$

The fractions of reflected and transmitted radiation energy are represented by the reflection coefficient ρ and the transmission coefficient τ. Subsequently, the power balance for laser beam welding with the total laser power P_L, the absorbed power share P_{abs}, the reflected power share P_{refl} and the transmitted power share P_{trans} can be derived (BEYER 1995, p. 27):

$$P_L = P_{abs} + P_{refl} + P_{trans} \tag{2-9}$$

For a DPLW process conducted on metallic material, absorption and reflection are the main interaction processes, while the transmission is typically not relevant. As described above, the deep penetration welding regime is characterized by a keyhole. Within this cavity, multiple laser radiation reflections occur at the capillary wall. Due to the repeated impingement of the laser radiation, the proportion of absorbed energy increases compared to heat conduction welding, where the laser radiation interacts with the material only once at the workpiece surface (KATAYAMA 2020, p. 20). Figure 5 schematically shows the resulting propagation of laser radiation within a keyhole. A high temperature gradient from the vaporization temperature inside the keyhole to the temperature of the base material is inherent to the deep penetration

welding process. The resulting temperature field within the process zone causes a melt layer surrounding the keyhole (KARKHIN 2019, p. 289). The weld depth d_w results from the keyhole depth d_k and the thickness of the melt layer t_l.

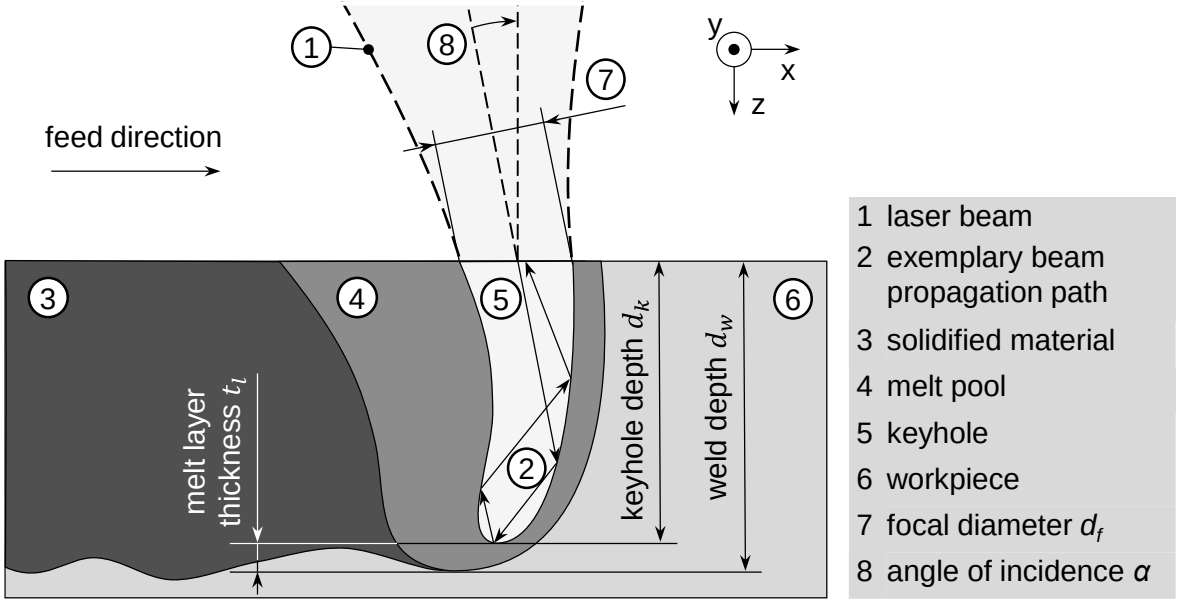

Figure 5: Schematic illustration of a DPLW process with an exemplary propagation path of laser radiation within the keyhole

2.3 Weld depth evaluation

2.3.1 General remarks

In automated manufacturing, monitoring systems for product quality are installed along the process chain. Process steps with a significant influence on the mechanical or optical properties of weld seams are usually inspected (SCHAUMBERGER ET AL. 2019). The central terms related to process monitoring in laser material processing are explained in the following. A distinction between the methods can be made by the timing of the process monitoring information relative to the machining process. In general, process monitoring methods can be divided into four groups (DAGGE ET AL. 2009):

- Inline
- Online
- Atline
- Offline

A measurement method is referred to as inline if the sensor technology is located close to the process and continuously provides measurement data from the process zone during an ongoing process (cf. Figure 6 (a)). The measurement results can be used directly for immediate data evaluation and process control. An advantage of the inline measurement is the continuous correlation of the obtained information with the specified characteristics of the process or the product. As the data acquisition and processing is generally fully automated, there is no need for manual inspection of the component. With inline process monitoring, a higher effort must be devoted to the calibration of the systems, because process influences directly affect the sensors involved and disturbing influences from the process zone must be considered. (KESSLER 2006, pp. 17–18)

Online process monitoring, like inline monitoring, is performed automatically during the process runtime. However, selected test specimens are extracted from the production line and measured in a bypass to the main production line (cf. Figure 6 (b)). To avoid a delay in the production process, the cycle time for measuring the specimens in the bypass must be shorter than the cycle time of the production process. Consequently, the information obtained can be used to control the process flow. In general, online monitoring is more cost-intensive than inline process monitoring, since an additional test line has to be established. (KESSLER 2006, pp. 15–16)

In contrast to continuous inline and online techniques, atline process monitoring is performed discontinuously and remotely from the process. Due to the decoupling of the inspection and the process, the state of the machining process can change during the analysis (cf. Figure 6 (c)). In atline testing, the workpiece or sample is extracted manually and analyzed, for example, with this technique in a laboratory close to production. In most cases, specially designed instruments are used to test the samples rapidly. The process flow can be adjusted manually based on the information obtained. (KESSLER 2006, p. 15)

Offline analysis of the process is another discontinuous procedure in which a workpiece or sample is manually transferred to a remote testing site (cf. Figure 6 (d)). As a result, direct process control is not possible with this technique. The inspection frequency is determined manually, which requires expert knowledge. This is crucial for ensuring a correct process flow. An advantage of offline process monitoring is the high flexibility in the occasional performance of complex testing tasks. (KESSLER 2006, p. 15)

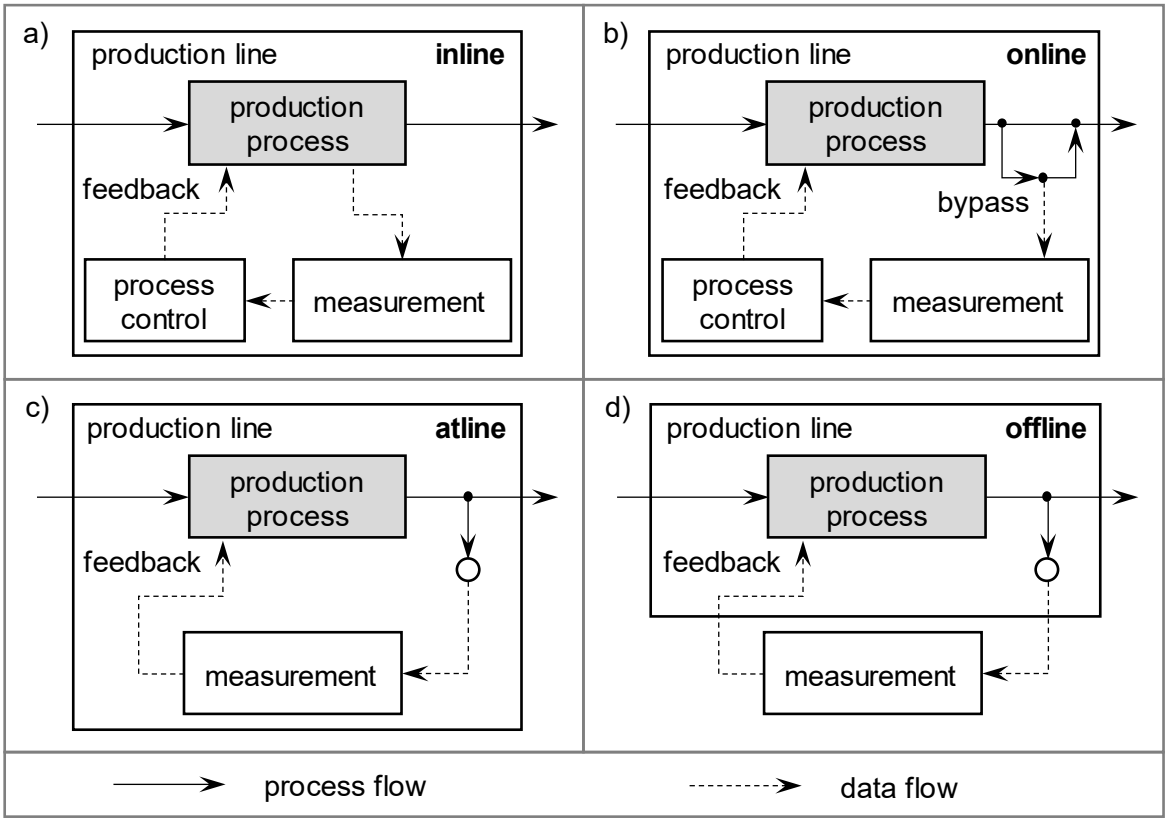

Figure 6: Classification of process monitoring methods; a) inline monitoring; b) online monitoring; c) atline monitoring; d) offline monitoring

The following sub-section focuses on inline process monitoring systems, since for the efficient use of measurement data in a closed control loop with direct feedback to the process, the shortest possible delay between the acquisition of measurement data on the process state and the feedback of reaction variables is required.

2.3.2 Inline process monitoring of laser beam welding

Process monitoring is of central importance in laser beam welding to ensure weld seam quality. The welding area can be divided into three observation domains: the pre-process zone, the process zone and the post-process zone (cf. Figure 7).

Pre-process zone

The pre-process zone comprises the unprocessed material with geometric features that provide a reference for the positioning of the weld seam. Among the characteristics are, for example, sheet edges in welding zones or markings (STADTER ET AL. 2019). Sensor systems used in the pre-process zone mainly employ non-contact, camera-based measurement principles. For example, the light section method projects one or more laser lines laterally onto the component and captures their

reflection with a camera coupled in the beam path (LEE & NA 2002). An offset in the line image indicates a sheet edge. Another sensor solution is the gray image evaluation with a camera and coaxial illumination. The gray images show a characteristic pattern of shaded areas and highlights caused by reflection at the sheet edge. Utilizing image processing, the sheet edge position can be determined and used inline for the path correction of the processing laser beam. (PURTONEN ET AL. 2014)

Process zone

The laser beam used for processing hits the material in the process zone, usually causing a melt pool and sometimes a keyhole. Instabilities in the keyhole or the melt flow directly influence the subsequent welding results (AALDERINK ET AL. 2007). Due to the high difference in brightness between the keyhole and the surrounding material as well as the high dynamics in the melt pool, process observation is difficult. For these reasons, cameras or photodiodes with a high dynamic range and a high temporal resolution are typically used. A method for analyzing the melt pool is recording the process emissions by photodiodes (YOU ET AL. 2013). If the threshold values of the measurement signal, predetermined with reference measurements of high- and low-quality welds, are exceeded, irregularities of the welding process can be detected and correlated to seam defects.

Post-process zone

The weld seam can be observed in the post-process zone, in which superficial connection defects, pores and other irregularities can occur (VALAVANIS & KOSMOPOULOS 2010). Camera systems with a detection wavelength in the visible or near-infrared (IR) spectral range are mainly used to detect defective areas on the weld seam surface. For this purpose, the light section method is also frequently used. A projection laser is moved along the seam bead, detecting superficial defects.

Another approach aims at analyzing the cooling behavior of the weld seam by active or passive thermography. Based on temperature distributions with a deviation from a reference, a locally insufficient connection between the sheets can be observed (SRAJBR ET AL. 2011). Melt pool ejections and pores can be detected by a changed thermal radiation characteristic. Nearly all post-process seam evaluation methods are performed in the offline mode in cost-intensive test stations (HEBER ET AL. 2013; STENBERG ET AL. 2017).

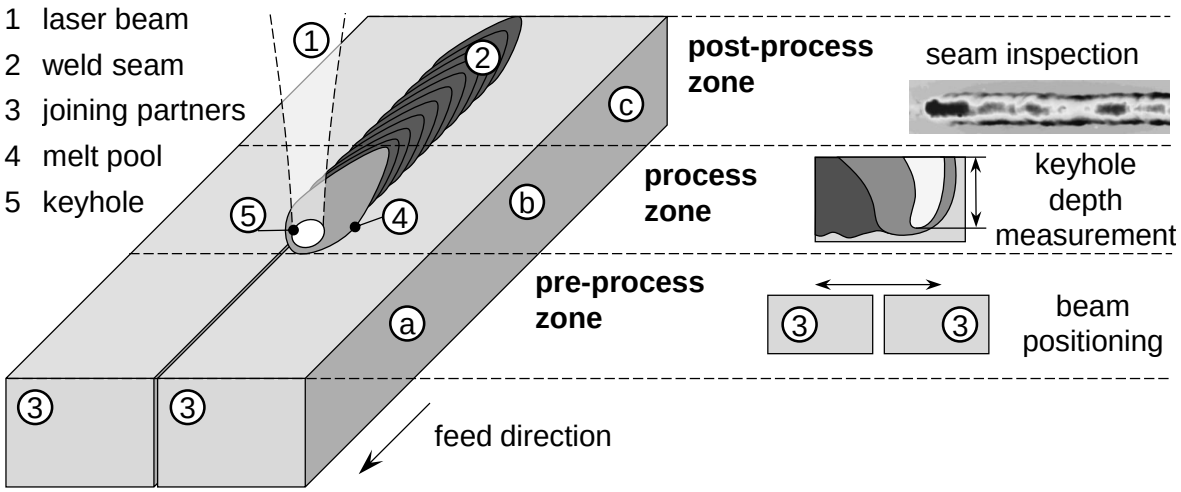

Figure 7: Spatial assignment of the observation domains for the inline monitoring of a laser beam welding process; a) pre-process zone; b) process zone; c) post-process zone

The measurement methods presented in this section cover a wide range of the sensor systems available on the market. They all can primarily be used in a single process observation domain, i.e., either in the pre-process, process or post-process zone. The following sub-section covers the fundamentals of Optical Coherence Tomography, which can be used to observe the pre-process, process and post-process zones. Of particular interest for this work is the ability to detect the depth of the keyhole in the process zone.

2.3.3 Optical Coherence Tomography for keyhole depth measurement

Based on a modification of the optical interferometer design proposed by *Michelson*, Optical Coherence Tomography (OCT) has been established as a method for high precision distance measurements. OCT is a common term for the technical application of the principle of Low Coherence Interferometry (LCI). An absolute path length difference between the reference and the measurement distance can be determined by substituting the single-mode light source of a *Michelson*-interferometer with a wide-band laser beam source. The measuring principle is based on the interference pattern that is created by the interference of the measuring and the reference beam (DREXLER & FUJIMOTO 2015). Since 1991 OCT has been a well-established measurement technique in ophthalmology, that is used to obtain topographic scans of the eye (HUANG ET AL. 1991). It has been proven that already a fraction of the reflected radiation in the order of 10^{-10} of the incident optical power is sufficient for a robust

distance measurement. With regard to the design, OCT sensors operating in the Frequency Domain (FD) and in the Time Domain (TD) can be distinguished. With FD-OCT sensors, a significantly reduced acquisition time for topographic scans is possible compared to TD-OCT sensors. The sensitivity of the FD-OCT is superior to that of TD-OCT (CHINN ET AL. 1997). As a result, high-precision measurements with a temporal resolution of several kilohertz are possible. Figure 8 shows the optical set-up with the essential components (a) and the arrangement of the measurement and the reference beam path (b) for an FD-OCT.

Fundamentals of an FD-OCT

An FD-OCT is characterized by a fixed reference path free of moving parts. Since no mirror adjustment is necessary, the acquisition rate of distance measurement points is only limited by the detector array sampling rate. The spectral analysis of the interference between the reference beam and the measuring beam is performed with the help of a spectrometer. Based on the polychromatic illumination, the complex electric field E_I can be described:

$$E_I = s(k,\omega)e^{i(kz-\omega t)} \tag{2-10}$$

Here, s is the amplitude of the electric field, defined as a function of the wave-number k and the angular frequency ω. The coordinate in the direction of beam propagation is represented by z and the time by t. With a wavelength-independent splitting ratio of the beam splitter of 0.5, the electric fields in the reference path E_R and in the measurement path E_S can be determined (DREXLER & FUJIMOTO 2015, p. 71):

$$E_R = \frac{E_i}{\sqrt{2}} r_R e^{i2kz_R}, \quad E_S = \frac{E_i}{\sqrt{2}} \sum_{n=1}^{N_r} r_{Sn} e^{i2kz_{Sn}} \tag{2-11}$$

For the case of transparent media, multiple reflections n at the positions z_{Sn} and the respective n-discrete power reflectivities $R_{Sn} = |r_{Sn}|^2$ with the n-discrete intensity reflectivities r_{Sn} at the sample and the intensity reflectivities r_R at the reference reflector are considered. The photocurrent in the detector I_D results from the superposition of the electric fields from the reference and the measurement path (DREXLER & FUJIMOTO 2015, p. 72):

$$I_D(k,\omega) = \frac{\rho_s}{2}\langle|E_R + E_S|\rangle^2 \tag{2-12}$$

Here, ρ_s describes the responsitivity of the sensor. The integration over the response time of the detector $\langle \cdots \rangle$, i.e., the time average (DREXLER & FUJIMOTO 2015, p. 72)

$$\langle f \rangle = \lim_{T \to \infty} \frac{1}{2T} \int_{-T}^{T} f(t) dt, \tag{2-13}$$

quantifies together with equations 2-10 and 2-11 the temporally invariant terms of the detector current $I_D(k)$ (DREXLER & FUJIMOTO 2015, p. 73):

$$\begin{aligned} I_D(k) = \frac{\rho_s}{4}[S(k)(R_R + R_{S1} + R_{S2} + \cdots)] \\ + \frac{\rho_s}{4}\left[S(k)\sum_{n=1}^{N_r}\sqrt{R_R R_{Sn}}(e^{i2k(z_R - z_{Sn})} + e^{-i2k(z_R - z_{Sn})})\right] \\ + \frac{\rho_s}{4}\left[S(k)\sum_{n \neq m=1}^{N_r}\sqrt{R_{Sn} R_{Sm}}(e^{i2k(z_{Sn} - z_{Sm})} + e^{-i2k(z_{Sn} - z_{Sm})})\right] \end{aligned} \tag{2-14}$$

Here, R_R describes the power reflectivity at the reference reflector. As a function of the central wavenumber k, the spectral power $S(k)$ of light sources typically used for FD-OCT can be simplified. With the assumption of a Gaussian spectrum, the spectral power can be described (DREXLER & FUJIMOTO 2015, p. 73):

$$S(k) = \langle |s(k, \omega|^2 \rangle = \frac{1}{\Delta k \sqrt{\pi}} e^{-\left[\frac{k - k_0}{\Delta k}\right]^2} \tag{2-15}$$

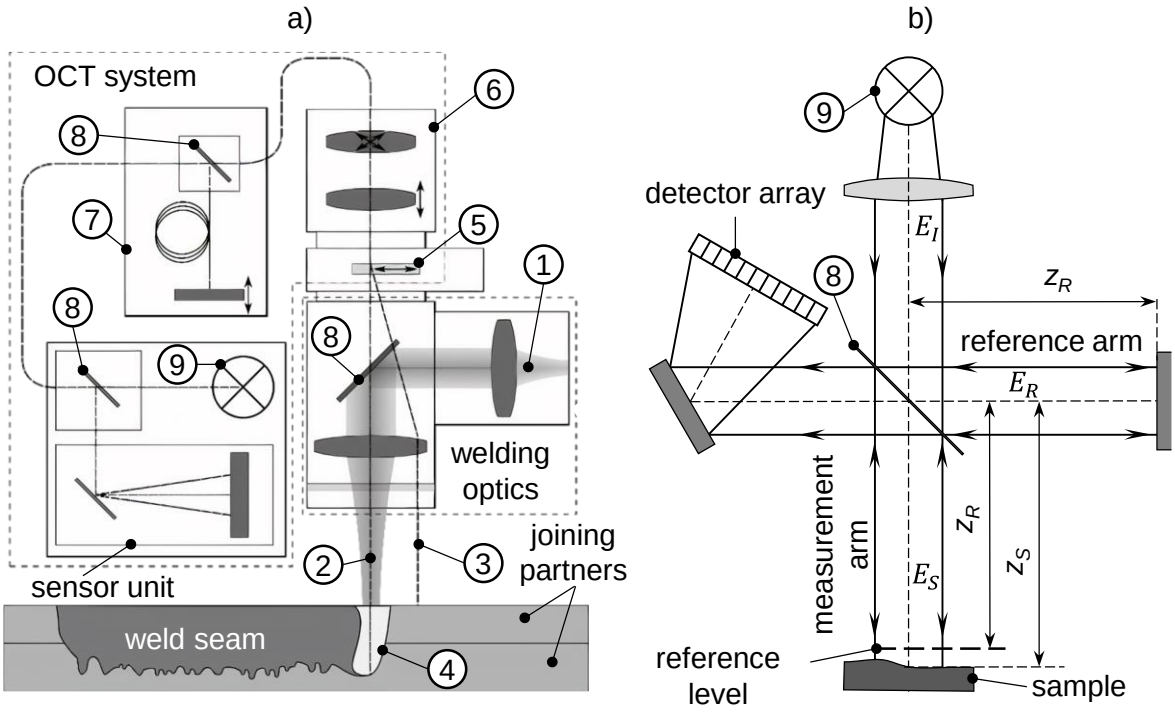

1	laser beam	2	keyhole measurement beam	3	surface measurement beam
4	keyhole	5	beam splitter	6	OCT beam positioning unit
7	reference unit	8	semi-transparent mirror	9	superluminescent diode (SLD)

Figure 8: Schematic structure of an OCT sensor for process monitoring in laser material processing; a) optical components of an OCT sensor and their integration into a laser processing optics; b) illustration of the beam paths of an OCT sensor; based on DONGES & NOLL (2015, pp. 236–238)

Here, Δk is the spectral bandwidth of the light source. To determine the distance z_s, the following relationship applies in the case of discrete reflections N_r (DREXLER & FUJIMOTO 2015, p. 76):

$$\sqrt{R_S(z_S)} = \sum_{n=1}^{N_r} \sqrt{R_{Sn}}\, \delta(z_S - z_{Sn}) \tag{2-16}$$

The inverse Fourier transformation of equation 2-13 provides the axial position of the reflection planes, i.e., their distance to the reference plane.

Characteristics of the OCT measurement signal

Figure 9 (a) shows an exemplary detector signal of an FD-OCT and the corresponding signal after *Fast Fourier Transformation* (FFT) (cf. Figure 9 (b)). In the plot, two reflections in the measurement path are considered, one in the reference plane and one approximately in the middle of the OCT measurement range. It is relevant for the technical application of an FD-OCT that only relative distances between the reference and other reflection planes can be determined. Thus, the measurement signal does not contain any absolute information about the occurrence of the reflections before or after the reference plane, i.e., there is an upper and a lower measuring range providing identical distance information. The relative position of the measurement to the reference plane must be technically verified to avoid measurement errors. A detailed mathematical derivation of the appropriate simplifications considering the OCT measurement principle is described by DREXLER & FUJIMOTO (2015). For a comprehensive description of measurement parameters as a function of optical properties, reference is made to TOMLINS & WANG (2005).

By OCT, high-frequency distance measurements to a high number of reflection planes can be performed. The technique is used to measure the keyhole depth d_k in laser beam welding by combining an OCT sensor according to the concept shown in Figure 10 with a laser welding system. Within the technical implementation, specific enhancements are introduced to the set-up. The reference axis is adjustable in its length so that the reference plane's axial position can be displaced relative to the reflection planes of the sample. Also, the measuring beam is divided by a beam splitter to obtain reflections from the component surface and the keyhole. The respective arrangement of the measuring and processing beams is shown in Figure 10 (a).

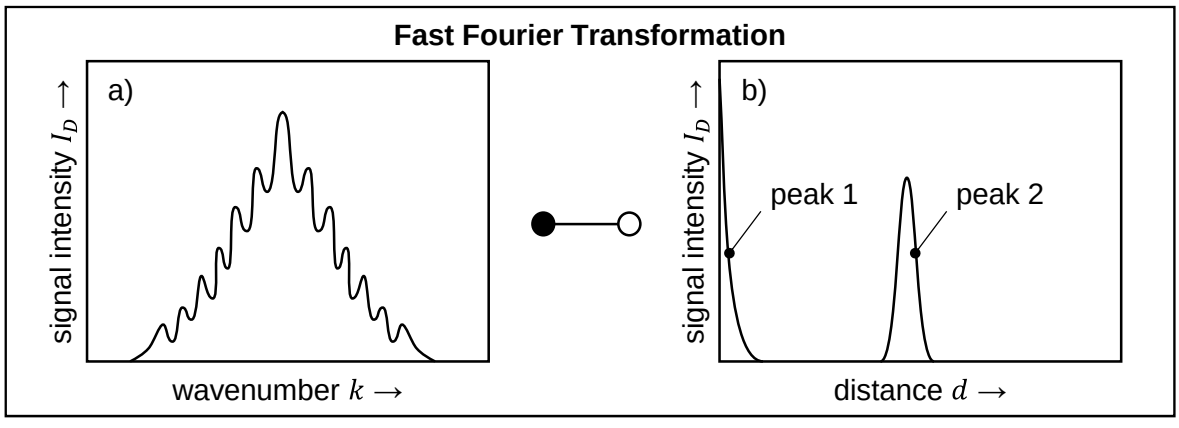

Figure 9: a) Typical signal of an FD-OCT detector as a function of the wavenumber k and b) Fourier-transformed signal; based on DONGES & NOLL (2015, p. 241)

Typically, a large portion of the measuring beam power is directed coaxially to the processing beam into the keyhole opening on the workpiece surface. The unabsorbed part is reflected towards the processing optics after traveling along the propagation path inside the capillary and can be detected by the OCT sensor. The radiation directed to the workpiece surface next to the process zone is also partially reflected. It provides a second distance value in the Fourier-transformed OCT signal. The difference between the two path lengths provides the keyhole depth. A reference can be obtained by detecting the component surface, considering surface irregularities.

OCT for keyhole depth measurement

An exemplary OCT signal for a keyhole depth measurement during DPLW is shown in Figure 10 (b). Here, a considerable difference in the signal characteristics of the keyhole compared to the surface signal is apparent. The keyhole distance values show a strong fluctuation over time and are scattered in the *z*-direction. In contrast, the surface signal shows a low scattering. This variation is due to process dynamics and multiple reflections during the keyhole depth signal evaluation.

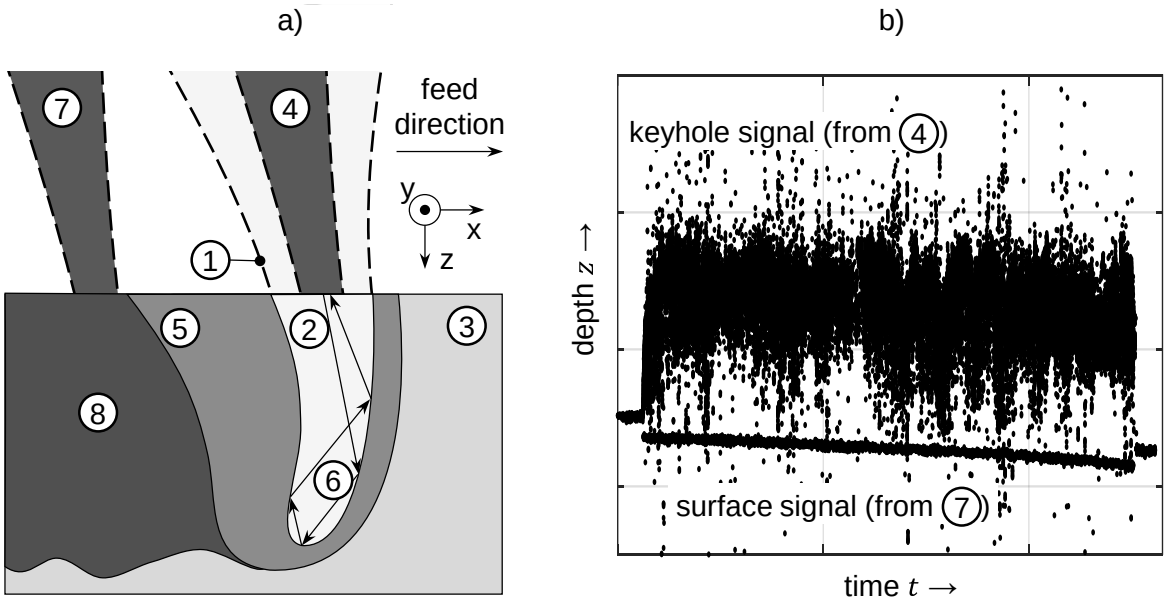

1	laser beam	2	keyhole	3	workpiece
4	keyhole measurement beam	5	melt pool	6	propagation of the incident beams
7	surface measurement beam	8	weld seam		

Figure 10: OCT for measuring the keyhole depth in DPLW; a) arrangement and propagation of measurement and processing laser beams; b) signal from the keyhole depth measurement with surface reference and keyhole signal

Resulting from fluid dynamic effects, changes of the keyhole geometry in the welding process lead to changes in the propagation path length (DORSCH ET AL. 2017). Given the various influences on the measurement signal characteristics, such as process parameters, material or penetration depth, no clear conclusion about the weld depth can be drawn from the depth signal without subsequent data processing and interpretation.

For the inline interpretation of the high-frequency OCT-signal for the weld depth, computationally efficient data processing methods are required. The process influences on the signal, which have a significant impact on the reliability of the evaluation, pose a further challenge. Besides conventional signal filters, Artificial Intelligence and, in particular, Machine Learning (ML) methods offer proven potential for signal interpretation (ERTEL 2016, p. 257). The fundamentals of ML, together with the architectures of algorithms suitable for processing sensor signals, are discussed in the following section.

2.4 Artificial Intelligence for data processing

2.4.1 Overview of Machine Learning algorithms

Artificial Intelligence (AI) is a discipline of computer science. It describes the attempt to imitate the human decision-making behavior to create autonomously acting systems within a hardware or software environment. The objective is to develop an intelligent behavior that allows a system to make autonomous decisions within defined constraints (ERTEL 2016, p. 191). Figure 11 shows a selection of human capabilities that can be simulated with AI. Machine Learning (ML) is a subfield of AI representing the human ability to learn from observations and experiences. It includes algorithms for recognizing patterns and regularities in data-sets to derive forecasts for data previously unknown to the system. Artificial knowledge is generated in a learning phase, in which experience is made available to the ML-system as a training basis (MARSLAND 2014, pp. 4–5). ML-algorithms learn iteratively from a fixed data-set in contrast to conventional programming approaches. Thus, patterns in the database can be detected even if the algorithm is not specifically instructed to search for regularities. ML-methods can be divided into the three categories *unsupervised learning*, *supervised learning* and *reinforcement learning*, depending on the form of

the input variables and the desired output (cf. Figure 11) (SHALEV-SHWARTZ & BEN-DAVID 2014, pp. 22–24).

In *supervised learning*, expert knowledge in the form of hypotheses is provided to the algorithm in the training phase as a support for decision-making with the aim that the trained ML-algorithm can imitate the procedure in the application phase (CARNEIRO ET AL. 2007). With supervised models, regression and classification problems can be solved (JAIN ET AL. 1999). *Unsupervised learning* does not provide the algorithm with a basis for decision-making. Therefore, the training is carried out without previously known target values and without a reward for correct decisions, which means that the algorithm must independently identify correlations and regularities in the training data-set (NIEBLES ET AL. 2008). The learned behavior can be used to solve classification and data compression problems in the application phase. Fundamentally, the algorithm learns how to decide which non-specified category the individual elements of a data-set are to be assigned to (NOROOZI & FAVARO 2016). In dimension reduction, relevant data elements are separated from irrelevant elements. *Reinforcement learning* represents a further possibility for training ML-algorithms. A so-called agent is responsible for independent decision-making. The agent's goal is to maximize the positive reward it receives for a correct decision. Based on the rewards received, the algorithm independently approximates a utility function that describes the value of a condition at a certain point in time (MNIH ET AL. 2015).

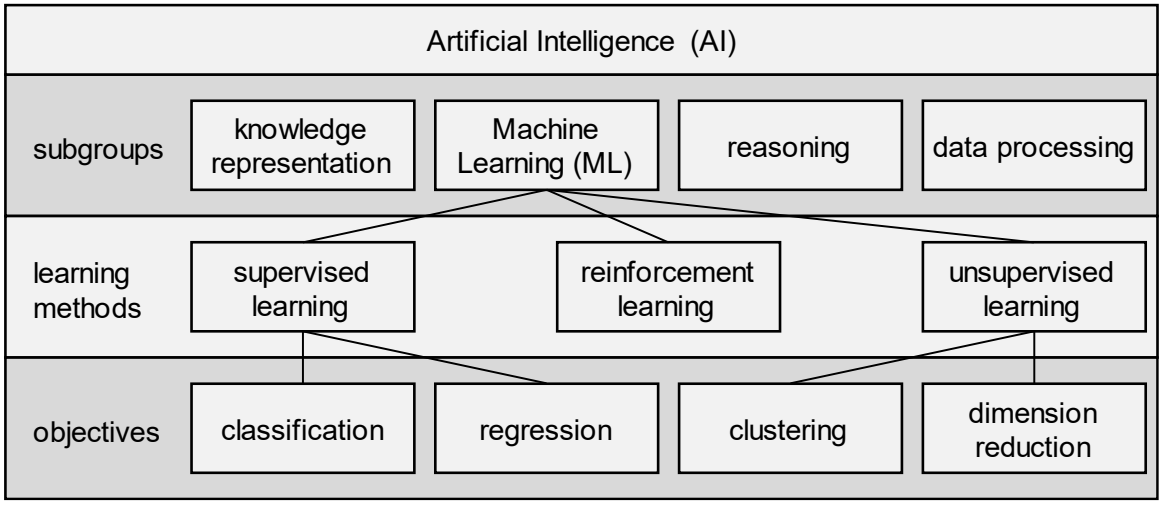

Figure 11: Overview of AI disciplines with a focus on ML-methods; based on SHALEV-SHWARTZ & BEN-DAVID (2014)

2.4.2 Artificial Neural Networks

This sub-section describes the fundamentals of Artificial Neural Networks (ANNs), representing a major category of AI-algorithms. ANNs can be applied to all subgroups of AI (cf. Figure 11). In the following, special consideration will be given to ANNs for use in ML.

Structure of Artificial Neural Networks

Artificial neurons are biologically inspired mathematical models. They consist of activation functions connected in layers mimicking human neural systems. The input variables x_i scaled with weighting factors w_i enter a propagation function Σ. The output of this function is the network input net_i, which in turn feeds the activation function φ_a. The activation function determines the output value x_o of the artificial neuron. If necessary, a threshold value θ_p is imposed. The combination of artificial neurons allows for the creation of ANNs, where neurons are arranged in consecutive layers. The layers inside the network, which are not located at the input or the output, are called hidden layers. Classical ANNs typically have a small number of hidden layers (ERTEL 2016; MACKAY 2011).

Feed-Forward Neural Networks

Network architectures with a strictly forward-oriented information flow are referred to as Feed-Forward Neural Networks (FFNNs). Figure 12 presents the overall structure of an FFNN and the design of an artificial neuron. However, various other neuron connections can be established within and between the layers. Depending on the connection layout, the activation of an artificial neuron can act as input to the artificial neurons of the following layer, to itself or to the preceding layers. Some of the specialized network architectures are explained in the following.

Frequently used activation functions are the step function, the semi-linear activation function and the tangent hyperbolic function. For the step function, a threshold value θ_p is defined. The neuron provides a constant output of 1 only if the net input value net_i from the propagation function is equal to or higher than the threshold value. For a net input value smaller than the threshold, the output value is 0. The semi-linear activation function propagates the net value itself in a defined range around the threshold. Outside the linear interval, either the values 0 or 1 are passed as output. The tangent hyperbolic function converts any net inputs to values between -1 and 1. Thus, the activation functions have the purpose of exchanging output values ranging from -1 to 1 between the neurons.

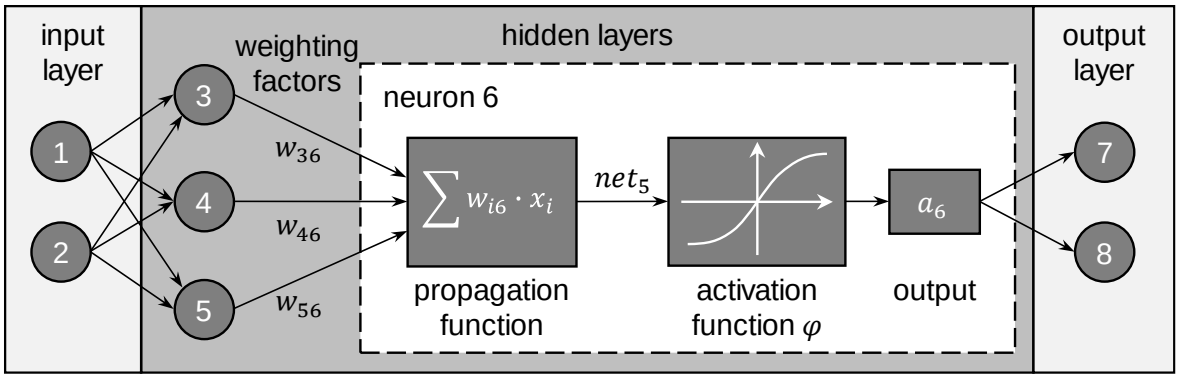

Figure 12: Structure of an FFNN with eight neurons (numbered from 1 to 8), two hidden layers and internal structure of an artificial neuron

An essential characteristic of ANNs is the ability to gain knowledge based on training data. The training process is designed iteratively and aims at minimizing the deviation between the output value of the ANN and a predefined target value. After each training run, the output of an ANN is compared to the target values from the training data-set. Subsequently, the error, commonly expressed as the root mean square error (RMSE), of the training results is calculated. If the error exceeds a defined maximum value, i.e., the termination criterion, a backpropagation algorithm is activated, which calculates new values for the weights w_{ij}. Adjusting the weighting factors ensures a reduction in the RMSE across all results in the following run. Until the termination criterion is reached, an iterative process is performed to adjust the weights for the execution of the training runs. (KRAMER 2009, pp. 128–133)

Deep Neural Networks

Deep Neural Networks (DNNs) refer to an ANN architecture that has become well-known through the extraordinary success of algorithms such as *AlphaGO* by the company DeepMind (SILVER ET AL. 2016). A characteristic feature of DNNs is a large number of hidden layers between the input and the output layers. While conventional ANNs usually contain two to three hidden intermediate layers, DNNs often consist of well over 100 layers. The main difference compared to conventional FFNNs is the ability of DNNs to work directly with unprocessed raw data and learn from complex data-sets, referred to as Deep Learning. DNNs require very large data-sets and powerful computers for training but potentially can reach superior accuracy. They independently extract features from the data and directly deliver the prediction result (LECUN ET AL. 2015). This learning behavior is referred to as end-to-end learning. DNNs play a significant role in speech and image recognition (ERTEL 2016).

Convolutional Neuronal Networks

Convolutional Neural Networks (CNNs) are based on a Deep Learning architecture and are used especially for processing image data. In contrast to classical neural networks, that require input data in the form of a vector, CNNs can directly process two-dimensional data such as the pixel matrix of an image (TURAGA ET AL. 2010). A CNN essentially consists of an alternating sequence of filters (convolutional layers) and aggregation layers (pooling layers), merged into a classical ANN. The filters and the aggregation layers are only connected to a limited extent. Each neuron of the hidden layer of the ANN uses only a small contiguous area of pixels as input. Thus, a CNN processes an image as a unit but considers a multitude of small areas for classification. This approach ensures that, for example, the rotation or position of an object in the image does not influence the classification (DÖRN 2018, p. 131).

Recurrent Neuronal Networks

FFNNs, as previously described, are generally unsuitable for processing sequential data, since, in the computational flow, each processing step is performed independently of the previous one. Consequently, no regularities or commonalities between temporally staggered inputs can be detected in the data. FFNN are stateless and are defined by the parameterization and the input vector (ZHANG ET AL. 2015).

By extending the FFNN architecture, neural networks can be employed for processing sequential data-sets such as time series. An example of an adapted structure are Recurrent Neural Networks (RNNs), which have an internal state influencing future computational steps. The difference between RNNs and FFNNs is the feedback of the output into a neuron of the same or of a previous layer at the transition to the next time step (GOODFELLOW ET AL. 2016; CONNOR ET AL. 1994). Figure 13 shows the structure of an RNN and the sequence of feedback. Analogous to the FFNN, an RNN can be composed of multiple layers. Due to the temporal variability of the internal state of an RNN, a temporal component is added to the optimization algorithm. The modification also has to be considered in the training of the RNN, which typically requires the employment of a *Backpropagation-through-time* (BPTT) algorithm (WERBOS 1990).

During the training of multilayer ANNs, such as RNNs, the weighting factors in the neurons are adjusted beginning from the output, i.e., against the data flow direction. In this process, a learning experience may not reach the layers located closer to the input. The connection of activation functions may correspond to a repeated multiplication with values between 0 and 1 or values > 1, respectively, causing the

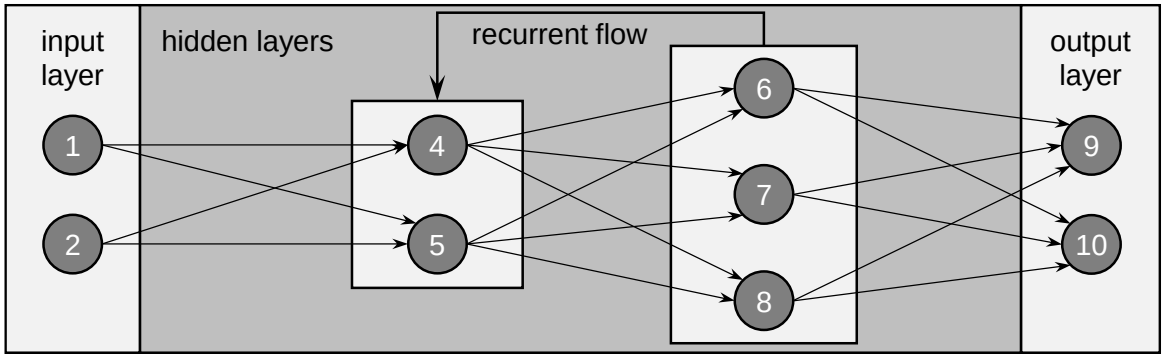

Figure 13: Structure of an RNN with two hidden layers and an information feedback loop

returned weighting values to approach zero or infinity. An RNN is often subject to vanishing or exploding gradients with increasing network complexity. Two approaches to solving this problem have been established. First, a non-gradient-based training algorithm can be used. Examples are the heuristic approximation method of simulated cooling and discrete error feedback (BENGIO ET AL. 1994), the introduction of an explicit time delay or the introduction of time constants (MOZER 1992). The second approach involves an extension of the network architecture to a Long-Short-Term-Memory-RNN (LSTM-RNN), according to HOCHREITER & SCHMIDHUBER (1997). LSTM-RNNs are used to preserve the error returned during training over time and across layers, reducing the risk of vanishing and exploding gradients. An LSTM element consists of an artificial neuron interconnected with additional elements called gates (GERS ET AL. 2000):

- Input gate: An input gate determines the extent to which new information flows into the cell.
- Forget gate: A forget gate determines the extent to which a value is forgotten in the cell.
- Output gate: An output gate determines the extent to which the value in the cell is passed to the next module in the chain.

With this architecture, the information in a neuron can be remembered or forgotten. Activation functions are used to decide what information is to be stored, overwritten or erased. However, unlike digital storage on computers, these gates are designed to be analog. Analog gates are necessary for the differentiability of subsequent error feedback. Like the nodes of an FFNN, the LSTM modules block or route information based on the signal weighting. The output of the module is multiplied by the internal weights. Through the learning process, both the internal weights of the module and the external weights between modules are adjusted. (HOCHREITER & SCHMIDHUBER 1997)

RNNs and LSTM-RNNs are well suited for processing sequential data. Thus, the influences of short- and long-term trends in sensor data can be distinguished and considered in the data interpretation.

With the help of the previously described ML approaches, it is possible to process data with high efficiency and superior accuracy compared to conventional data processing approaches. That potential can be used, e.g., in the interpretation of sensor signals from process monitoring systems, such as an OCT sensor for keyhole depth measurement. Due to the rapid evaluation of incoming signals, information about the process state can be made available almost in real-time. It can be utilized as an input variable for a closed-loop control system. The underlying fundamentals and concepts of process control are described in the following section.

2.5 Control strategies for industrial processes

2.5.1 Overview of process control strategies

The main objective in control engineering is to influence the behavior of technical systems and especially of temporally fluctuating processes to achieve the desired response. The selection of the controlled variables within a system significantly influences the functionality of a control system. They must be selected with the aim that their modification allows a precise and efficient adaptation of the process variables to specified setpoints or setpoint curves (KIENDL 1997, p. 10). Since the control variable is based on determining the deviation between the setpoint and the actual value, a control loop is formed. Both variables are compared cyclically and the deviation is minimized (LUNZE 2020, pp. 1–3). The independent reaction of a controller can increase the degree of automation of a technical system by reacting to temporally changing influences on the system. This results in increased operator comfort, enhanced productivity of technical systems and improved product quality.

The behavior of a motor-driven rod pendulum can exemplify the operation principle of a closed-loop control (cf. Figure 14 (a)). As a first step, all input and output variables of the dynamic system must be determined. Depending on the system complexity, defined by the number of input and output variables, a suitable method for system characterization is selected. The determining factors are the time variances occurring during the measurement of the variables and the linearity of the system behavior. A rod pendulum is a non-linear, time-variant system with one input variable, the motor torque M, and one output variable, the angle φ. Assuming that

only the gravitational force $F_G = m \cdot g$ is applied to the pendulum, the rest position $\varphi = 0$ can be determined. To displace the pendulum, a torque M has to be applied to the rod by the motor. This torque is induced by applying a motor current I_{Mot}. If the output variable φ is to be varied over a period of time, an offset can be applied to the value of the manipulated variable M in the actuator by a control system. Due to the design of the physical system, the actuating variable M is coupled to the output variable φ. Figure 14 (b) shows the resulting open chain of action from the motor torque M to the deflection angle of the rod pendulum φ.

In contrast to an open control chain, in a closed-loop system the output variable of the technical system, in this case the angle φ, is recoupled in a control loop. In the event of unforeseen disturbance variables z acting on the system, the resulting angle φ differs from the reference angle φ_{ref}. For the resulting error $e = x_s - x_c$, the controller must generate an output variable u_R, which causes the error e to converge to zero. Depending on the functional relationship

$$u_R = F\big(e(t)\big), \tag{2-17}$$

which is established by the controller between the error e and the controller output variable u_R, the success of the control operation is determined (KIENDL 1997, p. 7).

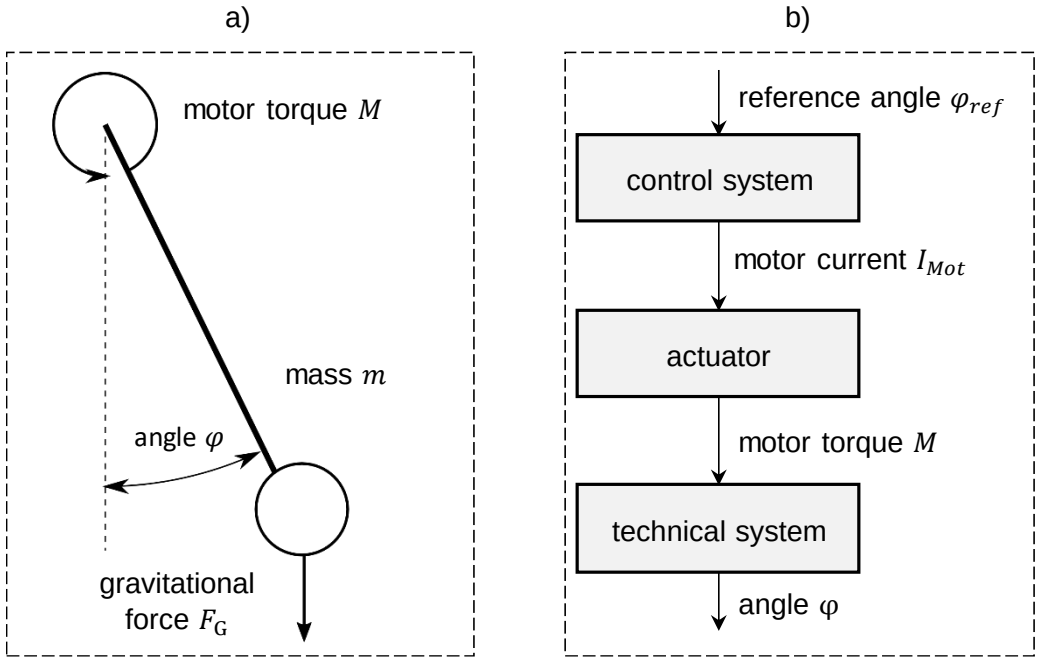

Figure 14: Rod pendulum as a physical system for the illustrative description of a closed-loop control; a) physical relationships in the system; b) open chain of action for the control of the deflection angle

Figure 15 shows the basic structure of a control loop with a pilot control[3] and a closed-loop controller. The reference variable w is converted to a setpoint variable u_S and to an expected output variable x_S by the pilot control system. In the process, the manipulated variable u is converted into the controlled variable x_c by the system dynamics involving the occurring disturbance variable z_c. To determine the error, which is used for the generation of controller output variable u_R, the sensor-based acquisition of the output variable x_c is essential (FÖLLINGER ET AL. 2013, pp. 1–3).

In general, four different requirements apply to the design of a control system regarding the behavior of the control loop. Optimum control systems aim at the highest possible fulfillment of all quality criteria. (LUNZE 2020, p. 353)

Stability: A dynamic system is called *transmission-stable* if it can calculate a limited output signal for each limited input signal. Transmission stability is also called Bounded-Input-Bounded-Output-stability (BIBO-stability).

Interference compensation and setpoint tracking: A control loop must have the ability to track the controlled variable as precisely as possible in relation to the reference variable when the influence of the disturbance variable z_c is low.

Dynamics: A specific dynamic relationship is required between the reference variable, the disturbance variable and the controlled variable. The step response can characterize the approximation of the controlled variable to the reference variable in case of a deviation from the setpoint position. A fast approach and a low overshooting behavior are usually required. An example of the response of a controlled variable x_c to an abrupt change in the reference variable φ_{ref} is shown in Figure 15 (b). The overshoot represents the exaggeration of the controlled variable regarding the setpoint, and the regulation time is the duration until the controlled variable has stabilized in the settling tolerance.

Robustness: A control loop must be designed with regard to a robust behavior, which is present when changes in the parameters of the controlled system caused by external influences or errors in the system model have a low influence on the behavior of the dynamic system. (LUNZE 2020, pp. 353–357)

[3] A pilot control refers to an element of a control loop applying a value to the reference variable that is independent of the states of the controlled system and resulting measurements (FÖLLINGER ET AL. 2013)

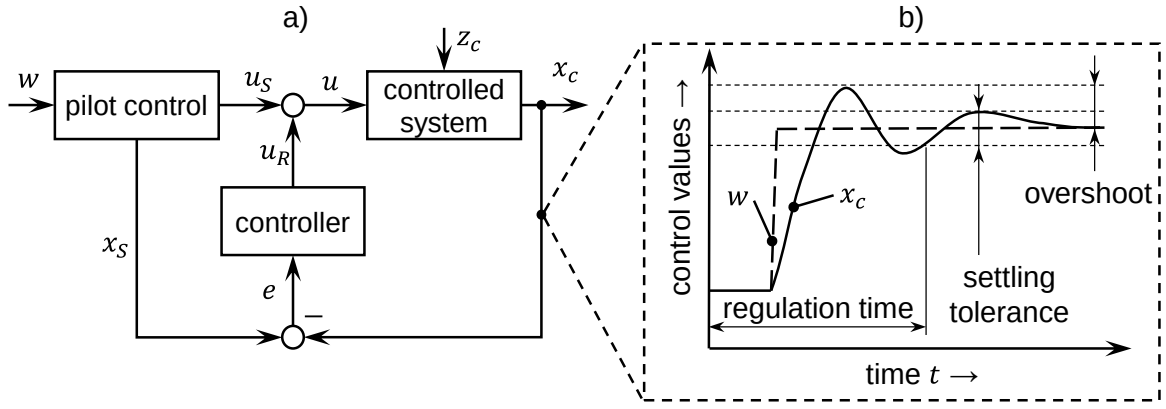

w	reference variable	u_S	setpoint variable	u	manipulated variable
x_c	controlled variable	x_s	expected output variable	u_R	controller output variable
z_c	disturbance variable	e	error		

Figure 15: Structure of a control loop; a) closed-loop control with pilot control; b) settling process of the output value by a controller for an abrupt change of the setpoint value

For the design of a technical control system, a given system model is generally used as a basis. The model is a simplified representation of the system, which covers all essential characteristics and behaviors. Different modeling approaches can be used to identify the system, which essentially differ in the required background knowledge of the system structure. How well the model structure and its parameters are determined is essential, since they describe the system behavior. (BOHN & UNBEHAUEN 2016)

White-Box model: The model structure is determined from known physical properties. No measurements or experiments are required to determine the model, since both the model structure and the parameters (e.g., masses in Newtonian mechanics) are known or given by the system design. Consequently, the White-Box model represents a theoretical approach. (BOHN & UNBEHAUEN 2016, p. 242)

Black-Box model: Black-Box models are used if no knowledge of the model structure is available or existing previous knowledge is not applicable. General approximation approaches help to derive the model structure. Model parameters are not based on physical quantities and are determined by system identification methods from measured input and output data. (BOHN & UNBEHAUEN 2016, pp. 242–243)

Gray-Box model: Gray-Box models combine approaches of White- and Black-Box modeling. The model equations are partly derived from physical laws or preliminary considerations. The unknown parameters occurring in the model equations are

determined by a system identification on the basis of measured input and output data. (BOHN & UNBEHAUEN 2016, p. 243)

For the control of linear, time-invariant systems (LTI systems), it is common to use linear controllers (LUNZE 2020, p. 111). Standardized procedures exist for the design of these control systems. Like the systems to be controlled, these control systems can be represented with transfer functions. By determining the zeros, linear factors can be obtained from the transfer functions. Different basic types of controllers are available, composed of proportional (*P*), integral (*I*) and differential (*D*) components. The transfer functions are represented by linear factors in the frequency domain. The individual factors serve different purposes in influencing the controller behavior:

- *P*-component: The proportional component of the controller leads to a proportional amplification of the control deviation. This causes a fast approach of the controlled variable to the reference variable (LUNZE 2020, p. 413).
- *I*-component: The integrating behavior of the *I*-component is required to achieve steady-state accuracy in the control loop. The dynamics are low compared to the P-component (LUNZE 2020, p. 413).
- *D*-component: The differential component reacts to a change in the control deviation over time. As a result, a strongly filtered signal of the controlled variable is required to prevent destabilization of the system by short-term high-frequency disturbance signals (LUNZE 2020, p. 413).

P-, *PI*-, *PD*- and *PID*-controllers are mostly used in practical application. Analytical and heuristic methods can be used to determine the controller parameters. As an analytical method, the controller design based on the pole-zero diagram can be applied. By specifically influencing the position of the pole and zero points of the closed-loop transfer function, the stability or properties such as the closed-loop damping can be influenced. If no model of the circuit is available, heuristic methods can be used. The controller parameters are searched for experimentally and iteratively. It should be noted that often only low requirements on the quality of the control loop can be met. In addition, the controlled system must have high stability in order to allow for experiments at the outer limits of the process stability range (LUNZE 2020).

Proceeding from the fundamentals of control engineering, the following section focuses on rule-based control concepts and in particular on the group of fuzzy controllers. Such controllers are preferably used when no mathematical model of the controlled system can be determined.

2.5.2 Fuzzy control

The operation of a fuzzy[4] controller is adapted from human behavior in reacting to occurring disturbances. For this purpose, a process model is represented with the aid of a large number of verbal rules, whereby a high degree of transparency can be created even for complex and multi-criteria problems.

Fuzzy controllers feature several advantages over classical control engineering approaches: (SCHNEIDER 2008, pp. 377–378)

- No mathematical process model is required for the controller design.
- Linear and non-linear fuzzy controllers[5] have a high degree of transparency.
- A large number of possible influences during parameterization results in a high flexibility of fuzzy controllers.
- Qualitative information, e.g., expert knowledge that cannot be formulated mathematically, can be embedded in the controller design.

The following main disadvantages of fuzzy controllers can be stated: (SCHNEIDER 2008, pp. 377–378)

- A standard design procedure is not available.
- For non-linear fuzzy controllers, a stability investigation based on mathematical methods is challenging.
- Fuzzy controllers require comparatively high computing power.

The basic principle of fuzzy control includes the three operations of *fuzzification*, *inference* and *defuzzification*. Prior to a detailed description of these operations, the two main fuzzy control concepts are introduced using examples. Fuzzy models are based on a model description using indistinct quantities, so-called fuzzy sets (BOHN & UNBEHAUEN 2016, p. 321). A simple fuzzy controller, referred to as a *Mamdani* controller, uses rules of the following form (SCHRÖDER & BUSS 2017, pp. 871–873):

[4] Fuzziness is defined as the uncertainty of the membership of states to a category. According to set theory, the membership of a state to a category depends on a probability function.
[5] A fuzzy controller is considered non-linear if the defuzzified output of the controller is a non-linear function of the inputs (YING ET AL. 1990).

$$\begin{aligned}&\text{IF } input\ variable\ 1 = term\ A_{k1}\\&\quad \text{AND } input\ variable\ 2 = term\ A_{k2}\\&\quad \text{AND } input\ variable\ 3 = term\ A_{k3}\\&\quad \ldots\\&\quad \text{OR } input\ variable\ n\ = term\ A_{kn}\\&\text{THEN } control\ variable = term\ B_l\end{aligned} \tag{2-18}$$

A *Sugeno* fuzzy controller, on the other hand, uses fuzzy rules to merge the results of several conventional control laws $y = f_l(x_1, x_2, \ldots, x_n)$ and represents a hybrid concept between conventional control and fuzzy control (SCHRÖDER & BUSS 2017, pp. 871–873):

$$\begin{aligned}&\text{IF } input\ variable\ 1 = term\ A_{k1}\\&\quad \text{AND } input\ variable\ 2 = term\ A_{k2}\\&\quad \text{AND } input\ variable\ 3 = term\ A_{k3}\\&\quad \ldots\\&\quad \text{OR } input\ variable\ n\ = term\ A_{kn}\\&\text{THEN } y = f_l(x_1, x_2, \ldots, x_n)\end{aligned} \tag{2-19}$$

Prior to explaining the operations of *fuzzification*, *inference* and *defuzzification* in a fuzzy controller, the theory of fuzzy sets is discussed in detail.

Fuzzy sets

The fuzzy logic is based on the fuzzy sets. It is therefore a characteristic of the fuzzy sets proposed by ZADEH & ALIEV (2019) that a binary distinction does not determine the inclusion or non-inclusion of an element, e.g., the state of a system, in a set. In classical set theory, on the other hand, a set x is determined entirely by the specification of all elements:

$$A = \{a_1, a_2, \ldots, a_n\} \tag{2-20}$$

The elements $a_1, a_2, \ldots, a_n$ are characterized by the membership function $\mu_A(x)$:

$$\mu_A(x) = \begin{cases}1\ for\ x \in A\\0\ for\ x \notin A\end{cases} \tag{2-21}$$

Accordingly, an element x either belongs to a set A or not. However, in a fuzzy set, the characteristic function can have values in the interval [0,1], assigning a degree of set membership to an element. This method of the set definition is called fuzzy logic.

Fuzzification

Fuzzification is understood as converting a sharp input value into a non-sharp description. The degrees of membership, described by the functions $\mu_{A_1}(x), \mu_{A_2}(x), \dots, \mu_{A_n}(x)$, are assigned to the respective input value. In the design of a fuzzy controller, the definition of the terms $A_1, \dots, A_n$ (cf. equation 2-20) and their sets of significance with the membership functions have a great influence on the control behavior. First, the number of terms must be defined, depending on how detailed the range of values is to be subdivided. The terms are often referred to as *negative-big* via *zero* to *positive-big*. Secondly, the type of membership function must be chosen. The most common types are trapezoidal or triangular membership functions. Figure 16 shows a selection of different types of membership functions. The third step is to arrange the membership functions to cover the whole range of allowed values. The membership functions should overlap to an appropriate degree to model the transition between terms. (SCHRÖDER & BUSS 2017, pp. 873–876)

Inference

Applying the rules to the fuzzy input variables is called inference. Usually, the rules have the form as shown in equation 2-18. Any logical operator (e.g., AND, OR, NOT) can be used to define the rule preconditions. Usually, an AND operation is initially used for a rule, while the individual rules are often linked with OR operators. (SCHRÖDER & BUSS 2017, p. 875)

Defuzzification

After *inference*, the values of the output variables are available in a fuzzy form. However, to control an actuator, the degrees of validity must be translated back into sharp values. The step of selecting a valid and explicit output value is called *defuzzification*. Essentially, two methods exist for this purpose: the *center-of-area (*or *center-of-gravity)* method and the *center-of-maxima* method (SCHRÖDER & BUSS 2017, pp. 379–382). As a result of the *inference*, a discrete spectrum of recommendations is provided. The *center-of-area* method compromises the recommended actions of individual rules when interpreting the inference results. The *center-of-maxima* method was developed based on the *center-of-area* method and offers the advantage of reduced computational effort. For a control system, a trade-off is often appropriate.

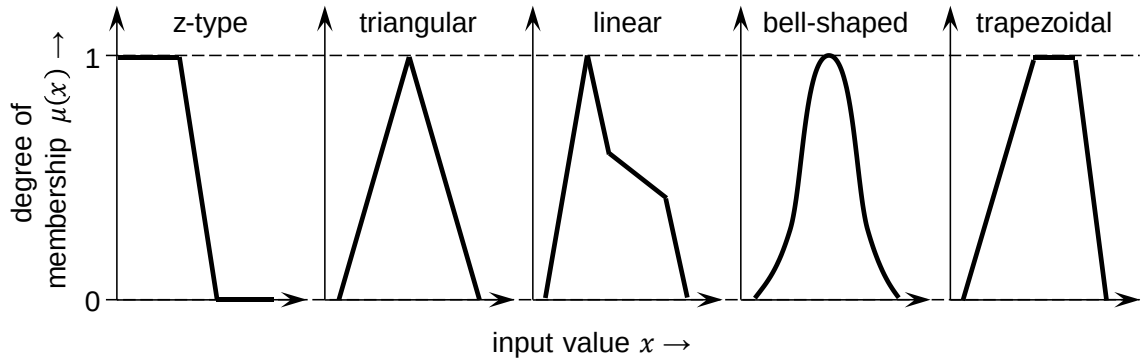

Figure 16: Examples of membership functions for the fuzzy description of input variables in a fuzzy control system

Both methods are shown in Figure 17 for an exemplary progression of the membership as a function of the output value x. The maximum-based method provides the most significant output value. This is especially convenient when fuzzy modules are not used as controllers but for process monitoring to determine whether certain events are present or not. (KIENDL 1997, p. 25)

Design of a fuzzy control system

For the design of a fuzzy control system, no standardized procedure exists. Commonly, empirical knowledge about a process is introduced into the controller in the form of rules. This design strategy is used mainly for controlled systems with a high degree of complexity, unknown internal operating mechanisms or an insufficiently accurate process model. In this way, a controlled system can be represented and optimized based on experiments (KIENDL 1997, p. 27). Alternatively, known process data can be used to set up a fuzzy model of the controlled system. This model can then serve as the basis for controller design by representing the desired behavior of the control system. Modeling from the data can be based, for example, on the characterization of a correlation between the manipulated variable u and the controlled variables x with $u = f(x_1, x_2, \dots, x_n)$. Also, a signal or image analysis of the result of the controlled system can be evaluated according to characteristics of different features and their connection with the manipulated variable u. (KIENDL 1997, p. 27)

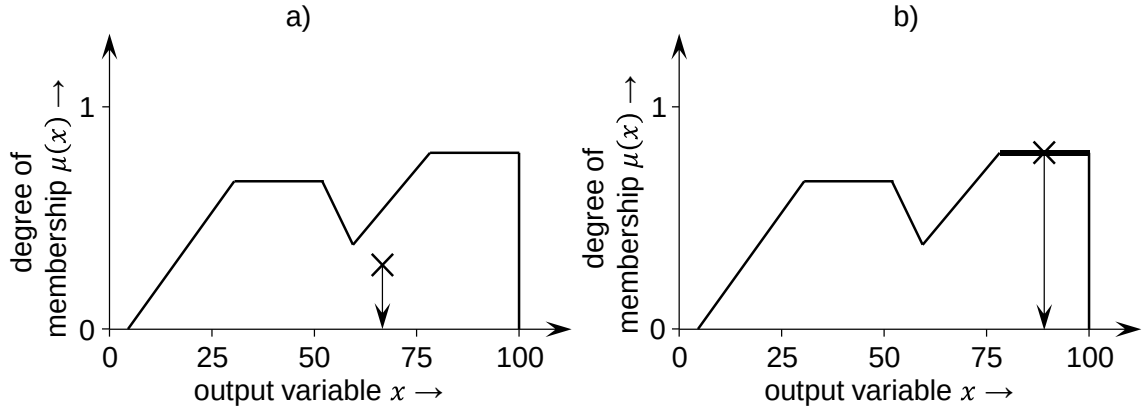

Figure 17: Methods of defuzzification; a) center-of-area method; b) center-of-maxima method

2.6 Concluding remarks

In this chapter, laser material processing basics were presented at the beginning (section 2.2). Properties of laser radiation were described, followed by an explanation of the principle of laser beam generation. Based on this, the beam-material interactions relevant to laser beam welding were discussed. Subsequently, the fundamentals of inline weld depth determination were provided in section 2.3, which included a classification of process monitoring methods and a description of the operation principle of OCT. A summary of AI-methods was presented in section 2.4, which included a description of the integration of ML into AI and a summary of the function of ANN. Finally, the required basics of control engineering for industrial processes were summarized (section 2.5). Following an overview of general control strategies, fuzzy control was described in detail. The fundamentals presented in sections 2.2 to 2.5 describe the functioning of the individual components of a laser system with inline weld depth control. Particular attention was given to the processing steps of signals that must be passed through from acquisition to controller intervention by the actuator system. Based on the described framework, the state of the art in process monitoring and control is presented in chapter 3.

3 State of the Art

3.1 Chapter overview

Numerous methods for monitoring laser beam welding processes exist, as described in sub-section 2.3.2. These approaches usually aim at ensuring the quality of joints and help to detect deviations of the production process from the desired operation. Particularly in automated laser welding systems with high throughput rates, sensor-based monitoring of the processes plays an increasingly important role. An essential property of welded joints is their mechanical strength, which is primarily determined by the weld cross-section and accordingly by the weld depth. Several research activities have addressed the inline detection of this property during DPLW. The approach employed in this dissertation aims at using the signal from an inline keyhole depth measurement to control the weld depth. Detected deviations of the measured depth from a given value can be compensated by adjusting the process parameters. An interpretation algorithm based on ML-methods allows to determine the weld depth from the OCT keyhole depth measurement signals. The resulting depth value serves as an input variable of a process control, with fuzzy control as an architectural concept.

Chapter 3 provides an overview of the state of the art in process monitoring and control of laser beam welding processes. Section 3.2 discusses the sensing of process variables in laser material processing. Approaches to OCT employment in DPLW are discussed in section 3.3. The focus is on the acquisition of measured variables in the keyhole area, i.e., in the process zone. Approaches to process control in laser beam welding are presented in section 3.4, while section 3.5 summarizes the current state of research and identifies the need for action.

3.2 Process monitoring in laser material processing

For process monitoring in laser beam welding, a wide range of sensor systems can be employed to detect, e.g., physical effects related to the process stability or the product quality. Cameras, photodiodes, pyrometers, microphones or distance measuring systems are used. In the following, relevant scientific works, which use the sensor technologies mentioned above for monitoring, will be discussed in detail. A comprehensive overview of process monitoring and quality assurance in laser material processing beyond the presented work is provided by STAVRIDIS ET AL. (2018) and PURTONEN ET AL. (2014).

An investigation of different sensors and measurement principles for process monitoring in laser beam welding has been carried out by STRITT ET AL. (2016). To generate data for an evaluation and gain a higher understanding of the process, welding tests were performed on copper, steel and aluminum specimens. Bead on plate welds of individual materials and linear welds for joining two sheets of different materials in an overlap configuration were investigated. In the experiments, a high-speed camera, an inline X-ray device, an OCT sensor, a pyrometer and an IR camera were evaluated regarding their suitability for process monitoring. The data obtained was analyzed for typical weld defects, such as pores and hot cracks. Using a high-speed camera, defects on the surface and spatter formation during the welding process of the case-hardening steel 16CrMn5 were detected. A relationship was found between the number and the direction of weld spatters and the welding speed. At a low processing speed of 1 m/min, small spatters occurred without a preferred direction. In contrast, at high feed rates around 10 m/min, large spatters detached against the welding direction (STRITT ET AL. 2016, p. 5). Thermographic images from an IR camera during welding of AA6014 aluminum sheets near the edge of the specimen provided a further insight. The temperature difference between the center of the specimen and the sheet edge was larger when hot cracks occurred. The indirect methods investigated by STRITT ET AL. (2016) were associated with uncertainty in concluding on the stability of the welding process. Direct measurement methods, such as an OCT-based measurement of the keyhole depth, were shown to be more precise and allowed for conclusions, e.g., on the stability of the welding process.

YOU ET AL. (2014) used a camera-based monitoring system combined with an ultraviolet filter and a bandpass filter for the visible wavelength range in their work. The objective was to relate specific characteristics of weld fumes and weld spatter to weld quality by analyzing the images regarding the gray levels of spatters. Welding

tests were performed on type 304 stainless steel at three different feed rates. For the characterization of weld spatters, static and dynamic features were defined and combined in a feature vector, including, for example, the radius and the trajectory. An image processing algorithm was developed to track weld spatters detaching from the process zone. It was shown that the detachment of large spatters from the weld pool leads to seam defects. The knowledge gained can be used to implement camera-based quality monitoring. The work of YOU ET AL. (2014) focused on a correlation between weld spatter/vapor and weld quality. A similar objective was pursued by HAUBOLD ET AL. (2017) and HAUBOLD & ZAEH (2019). They were able to detect spatter in the process zone with the aid of a high-speed camera system observing coaxially to the laser beam. The measuring frequency was in the kHz range, enabling spatters to be evaluated in terms of direction and speed based on the gray-scale image data. Significant parameter dependence of the spatter formation was demonstrated.

Welding process monitoring based on the measurement of optical and acoustic emissions in the process zone was investigated by SHEVCHIK ET AL. (2019). For detecting optical emissions and the back reflection of laser radiation, the welding optics were equipped with three photodiodes with different wavelength measuring ranges. The acoustic sensor, sampling at a rate of 10 MHz, was mounted on the workpiece close to the process zone. Welding tests were carried out on samples of Ti6Al4V. Based on metallographic cross-sections, the processed samples were divided into sections without a weld seam, sections with a heat conduction weld, sections with a defect-free deep penetration weld and sections with a porous deep penetration weld. The experimental results were used to label the recorded sensor data for classification. Raw data processing and feature extraction were performed using wavelet analysis. The features were defined as the relative energies of the extracted narrow frequency bands. SHEVCHIK ET AL. trained a Laplacian Graph Support Vector Machine (LapSVM) for the quality assurance in laser beam welding based on multi-sensor inline process monitoring. The classification accuracy of the developed LapSVM was above 85.9 % and decreased with an increase in the weld depth. The overall classification accuracy was improved with sensor data fusion of acoustic and optical measurements. It was also shown that a wavelet transformation of the raw signals offers advantages in data cleansing and transformation by removing noise from the input data and adapting the processing to the given signals. Correlations between the sensor data and the weld depth could not be identified.

YUSOF ET AL. (2020) investigated the determination of the weld depth in pulsed laser beam welding based on airborne noise emission measurements from the process. To generate measurement data as a reference for the studies, 22MnB5 steel sheets were

welded in a butt weld configuration. A microphone placed close to the process zone was utilized to detect acoustic emissions from the process zone, ranging from 20 Hz to 12 kHz. Welding tests were performed using a fiber laser with pulse durations between 2 ms and 6 ms. Stepwise regression analysis was applied to determine relevant features from the acoustic recordings and generate training data for ML-models. YUSOF ET AL. identified, among others, the standard deviation of the acoustic amplitudes, the laser peak power and the pulse duration as relevant features for characterizing the welding process. In particular, the laser peak power and the pulse duration impacted the characteristics of the resulting acoustic emissions. Higher pulse durations induced a more prolonged sound emission due to an extended absorption time of the laser radiation in the workpiece. A multiple linear regression model, accounting for the above-mentioned variables, and an FFNN were trained to predict the weld depth based on the above-mentioned characteristics. The regression model achieved an average accuracy of 92.87 % for the prediction of the weld depth. The FFNN with a hidden layer containing 10 neurons was able to predict the weld depth with an average accuracy of 95.92 %. A measurement of acoustic emissions from the process zone can be classified as an indirect measurement method for determining the weld depth. An inline data analysis was not implemented by the authors.

BOLEY ET AL. (2019a) investigated the observation of the weld depth in DPLW of steel using an X-ray tube and a high-speed camera. The specimens were welded from a top position while the weld was laterally scanned with X-ray radiation. Using a scintillator, the X-rays were converted into visible light and recorded with a high-speed camera at a sampling rate of 1 kHz. The presented experimental set-up allowed to evaluate weld seam features in the dimensional range from 100 µm to 1 mm. Parameter influences of the X-ray transmission on the image quality and the information obtained about the process were investigated. As a result of edge blurring in the images, caused by the set-up of the imaging system, the keyhole walls appeared elongated and the opening on the surface was magnified. A further disturbance factor was added to the images in form of the noise of the image amplifier. Ultimately, an influence of the signal-to-noise ratio on the image quality was determined, concluding that high spatial resolution can only be achieved if the signal can be separated from the noise. The method can be assigned to the direct measurement systems for determining the weld depth in laser beam welding.

Interim conclusion

Various studies on the monitoring of laser material processing have been presented in recent years. In particular, in the field of inline monitoring, a wide variety of

sensors and combinations of sensors have been used to record process conditions. In most cases, indirect measurement methods have been employed, requiring extensive subsequent processing steps to utilize the measurement signals. The dominant goal of the research activities was to increase process understanding by correlating measurement signals with the properties of the manufactured components. Particular attention was paid to the development of data evaluation approaches with the increasing use of ML-methods.

3.3 Optical Coherence Tomography in laser beam welding

OCT is particularly advantageous for process monitoring in close proximity or within the process zone, as the measurement method is not influenced by process emissions and offers high temporal and spatial measurement resolution. The distance information obtained with OCT can be used for various purposes and provides high accuracy information independent of irradiation during laser material processing (FRASER 2011). STADTER ET AL. (2019) used an OCT distance measurement to position the focal point during remote laser beam welding relative to a joining gap detected in the pre-process zone (cf. Figure *7*). Furthermore, STADTER ET AL. (2020b) derived quality predictions for welds from topographic scans of weld surfaces that can be detected in the post-process zone.

OCT also offers a possibility for the direct and inline determination of the keyhole depth in DPLW. One of the first OCT-based process monitoring systems was used to characterize a laser ablation process. The works of WIESNER ET AL. (2010), WEBSTER ET AL. (2010) and WEBSTER ET AL. (2014) focused on inline monitoring of the ablation rate, the surface finish and the quality of processed components.

A comprehensive discussion of the technical implementation of keyhole depth measurement based on OCT was provided by BAUTZE & KOGEL-HOLLACHER (2014), BAUTZE ET AL. (2015), KOGEL-HOLLACHER ET AL. (2014), KOGEL-HOLLACHER ET AL. (2017) and BLECHER ET AL. (2014). Various commercially available sensor systems were described, mostly integrated into fixed optics systems. The potentials of a weld depth control based on an evaluated OCT signal were presented in the context of the studies from JI ET AL. (2015) and KOGEL-HOLLACHER ET AL. (2016).

FETZER ET AL. (2017) used an OCT system with a sampling rate of 70 kHz for process monitoring of a welding process and an arbitrary waveform generator to modulate the laser power. Besides that, a set-up for generating high-speed X-ray images with

an acquisition frequency of 1 kHz, analogous to the experimental set-ups used by ABT ET AL. (2011), HEIDER ET AL. (2013) and BOLEY ET AL. (2019a), was employed. For data generation, FETZER ET AL. produced bead on plate welds on aluminum, copper and mild steel specimens at a constant feed rate. The laser power was sinusoidally modulated. The object of evaluation was the change in the keyhole depth in response to the power input and the keyhole's response to a periodical change of the laser power. As part of the analysis, the recorded data from the OCT system and the X-ray aperture were synchronized and superimposed. An 80th percentile filter was used in a 1 ms time frame after matching the X-ray radiographs to evaluate the OCT signal for the above-described materials. It was obtained that the keyhole depth followed the sinusoidal oscillation of the laser power. At modulation frequencies above 25 Hz, the amplitude of the weld penetration depth response decreased and was out of phase with the power modulation. The keyhole depth's non-linear hysteresis[6] behavior resulted in an abrupt decrease in keyhole depth at a moderate decrease in laser power. In steel and copper welding, the keyhole depth change followed the power modulation less accurately than for the welding of aluminum.

DORSCH ET AL. (2017) investigated the effect of the process parameters laser power, feed rate and focus diameter on the OCT signal during the detection of the keyhole depth based on welding experiments with mild steel, high-alloy steel, duplex steel and aluminum. Longitudinal cross-sections were prepared from the specimens and the weld depth was measured manually using a microscope. The OCT signal for welding duplex steel had the highest signal quality, i.e., low signal noise. The signal was highly scattered for aluminum due to an unstable keyhole behavior. The OCT data deviated within 5 % around the real weld depth for all investigated materials and feed rates except for the measured data at 1 m/min, where significantly more fluctuations occurred. A broad and shallow keyhole was formed for spot diameters of the processing laser above 600 µm. In this case, the OCT signal, which was highly distorted due to multiple reflections, e.g., at the keyhole wall, could not be interpreted. Based on the investigations, an ideal measuring range was found for the employed fixed optics as a function of the laser power, the feed rate and the OCT measuring beam position relative to the keyhole opening. Extending the work of DORSCH ET AL. (2017), BLECHER ET AL. (2014) investigated different materials. Compared to steel and titanium, a significantly higher scattering, i.e., a wider distribution of the measured values in the depth direction, of the OCT signal was found for the keyhole depth measurement during the welding of aluminum. Therefore, it can be concluded

[6] Hysteresis is the dependence of the state of a system on its history. It can be a dynamic lag between an input and an output of a system that depends on the variation frequency of the input. (BROKATE 2012, pp. 1–2).

that the measurements on aluminum require additional effort in the signal interpretation to acquire a precise value for the keyhole depth compared to other materials.

MITTELSTÄDT ET AL. (2019) focused on developing a method for raw data processing of the OCT-based keyhole depth signal and correlating the findings to the welding process parameters. Welding tests were performed with varying laser power on samples of the mild steel 1.0122 and of the aluminum alloy AA5083. The analysis of the recorded OCT data was carried out in offline mode. A 95^{th} percentile filter with a window width of 750 data points was first selected to prefilter the raw depth data. Adjusting the percentile filter parameters to the characteristics of the materials used and the welding process parameters allowed for an increase in the evaluation accuracy of the data for the weld depth. Subsequently, a histogram evaluation[7] was developed for the raw data. The OCT measurement domain was divided into intervals in the first step. A histographic evaluation of the frequency of the depth values within the OCT signal of each interval provided a local maximum, which correlated with the keyhole depth. The histogram evaluation was applied to the aluminum alloy and mild steel welding for the feed rates of 3 – 12 m/min. The deviation from the experimentally determined weld depth, determined by micrographs, was about 10 %. Regarding the robustness of the histogram evaluation, it was found that the accuracy of the depth evaluation correlated with the significance of the maximum in the histogram. The method could only be used for inline data processing to a limited extent and the accuracy was strongly dependent on the OCT signal quality.

BOLEY ET AL. (2019b) developed a statistical data processing method for the OCT signal in keyhole depth measurement. To find a valid and robust filtering method, welding experiments were conducted on mild steel, copper and aluminum. As the first step of data processing, the OCT data was divided into noise and significant measurement points based on a histogram analysis and a *Poisson* probability distribution. For the histographic analysis of the OCT measurement points, a static threshold was found to distinguish noise from valid measurement points. Using a *Poisson* distribution, a probability threshold for noise was identified for the second segmentation approach. OCT measurement points in the range of the expected weld depth or the surface range were assigned a significantly lower probability of belonging to noise than measurement points in other depth ranges. Further investigations were conducted using probability-based segmentation. Welding tests

[7] In the histogram evaluation, the frequency distribution of the measured values is considered in the depth direction. The distribution is discretized in intervals and a depth value is determined by setting a threshold value.

were performed on aluminum and mild steel specimens to confirm the findings. By correlating the OCT data with longitudinal sections from the welding tests, an error smaller than 5 % in comparison to the real weld depth was demonstrated.

SOKOLOV ET AL. (2020) presented an OCT-based weld depth evaluation approach, which was identified as a prerequisite for a subsequent weld depth control in remote laser beam welding. A fillet weld process on aluminum components with variations in the gap size between the joining partners was investigated. The employed optics were equipped with a beam scanning module to superimpose a sinusoidal motion in the sheet plane on the feed motion. As a result, the melt pool could be widened and increased energy input into the upper sheet was achieved with a laser power modulation. A key objective of the work was to find an ideal placement of the OCT measuring-beam relative to the sinusoidally propagating keyhole. For this purpose, various measuring beam positions were tested and evaluated based on characteristic values and as a function of varying gap sizes between the components to be joined. Regarding the process influences on the OCT keyhole depth measurement, it was shown that the OCT signal contained information about the depth of the keyhole and its shape resulting from shape-specific reflections.

HOLLATZ ET AL. (2020b) investigated the keyhole depth measurement using an OCT sensor for laser micro-welding, i.e., welding of thin components with high-brilliance laser radiation. A scanner-based system was employed to deflect the processing beam. Chromatic aberration[8] and the intensity loss of the measurement radiation in the optical set-up posed a challenge for the OCT keyhole depth measurement. HOLLATZ ET AL. (2020b) focused on small focal diameters and shallow penetration depths in stainless steel welding. The OCT data was analyzed for the weld penetration depth using two data processing approaches. A percentile filter, the most common processing method for OCT keyhole depth data, was compared to a *Kalman* filter on the measured data. It was shown that an OCT system combined with scanning optics is capable of measuring the keyhole depth during a laser micro-welding process. The percentile evaluation showed higher average accuracy for the calibrated parameter range, while the *Kalman* approach provided higher robustness against fluctuations. Measurement errors occurred due to the optical set-up of the scanner-based system and the small keyhole diameter.

ALLEN ET AL. (2020) investigated the correlation between the keyhole geometry and laser beam absorption by comparing a keyhole depth measurement based on OCT

[8] Chromatic aberration is an optical effect resulting from the wavelength dependence of the refractive index of optical lenses.

with the reflected power detected by an integrating sphere in the beam path. It was shown that based on these two metrics, the heat conduction and the keyhole regime in laser beam welding were differentiated precisely. The formation of the vapor capillary and the increased weld depth were correlated with a higher absorption of the processing laser beam due to multiple reflections reaching absorption rates greater than 90 %. Similar findings were also obtained by SIMONDS ET AL. (2018). Regarding the behavior of absorption and weld depth with increasing intensity of radiation, the initial rapid growth of depth and absorption was followed by a steady-state behavior of absorption and slow growth of depth. The experimental results allowed quantification of the relationship between the absorption and the keyhole depth. The approach allows to validate the results of ray-tracing simulations, as conducted by STADTER ET AL. (2020a). They can be interpreted in terms of the keyhole geometry and the number of reflections. The results are supported by the findings of CUNNINGHAM ET AL. (2019) on the parameter dependence of the keyhole geometry in DPLW. In summary, it was shown that the energy coupling is very sensitive to the weld pool geometry, especially in the early stages of keyhole formation.

Interim Conclusion

Due to the independence of the measurement of process emissions and due to the high measurement frequencies, Optical Coherence Tomography already is an established method for inline monitoring of laser material processing. The high number of published papers underlines that OCT is of technical relevance, especially for detecting the keyhole depth in laser beam welding. This characteristic significantly influences the quality of welds and cannot be measured directly with other process monitoring methods to date.

Many studies have been published on the advancement of measurement instrumentation and the validation of measurements to qualify industrial production technology. Besides that, some practical approaches have been described to facilitate the applicability of the technology. Commonly, the keyhole depth and the weld depth are considered equivalent, which leads to inaccuracies of measurement results due to the neglect of melt pool influences. The existing approaches have to be adapted and parameterized very precisely to the respective processing task. To date, no flexible and parameter-independent approach exists for determining the weld depth based on an OCT keyhole depth measurement.

3.4 Process control in deep penetration laser beam welding

This section describes the state of the art on the control of the weld depth in DPLW. FRASER (2012) elaborated in his work that a robust and reliable inline measurement of the weld depth forms the basis for controlling the welding process, which is characterized as sensitive to disturbances and stochastically fluctuating. The ability to achieve a constant weld depth according to a preset value is considered an essential requirement to improve the applicability of the DPLW process in a wide range of industrial use cases. ABT (2017) also described the DPLW process as stochastic and non-linear, making robust control of the process essential for an industrial application.

BLUG ET AL. (2012) presented a control strategy for a full penetration hole (FPH) process, i.e., a process in which the keyhole breaks through the lower joining partner's rear side, forming a hole. Using a CNN, a feedback control variable was computed from coaxial inline high-speed camera images of the keyhole opening and the surrounding melt pool. The process control was designed to compensate for stochastically occurring variations of the penetration in aluminum welding. The detection rate of an FPH[9] in a defined time interval was used as the controlled variable. A two-stage control loop was implemented based on the detected signal, combining a fast and a slowly reacting component. The fast component controlled the laser power, as proposed by BLUG ET AL. (2011). If the required FPH occurrence rate was not achieved, the laser power was increased immediately by a fixed correction value. If the FPH rate was too high, the power was reduced. This compensated for variations within the process. Besides that, a limited power range was defined within which the laser power was varied. The slower part in the control loop avoided instabilities due to the dynamic and non-linear process behavior. If the controller tended to exceed or to fall below the defined limits over a longer time interval, the permissible power range was adjusted. An exemplary course of the laser power with the power limits adjusted over time is shown in Figure 18. With the presented approach, an increase of the weld seam quality and a stabilization of the process was achieved.

[9] The detection rate of an FPH is defined as the frequency at which full penetration of the joining partners can be observed over time. Due to the dynamics of the melt pool, no stationary aperture is formed.

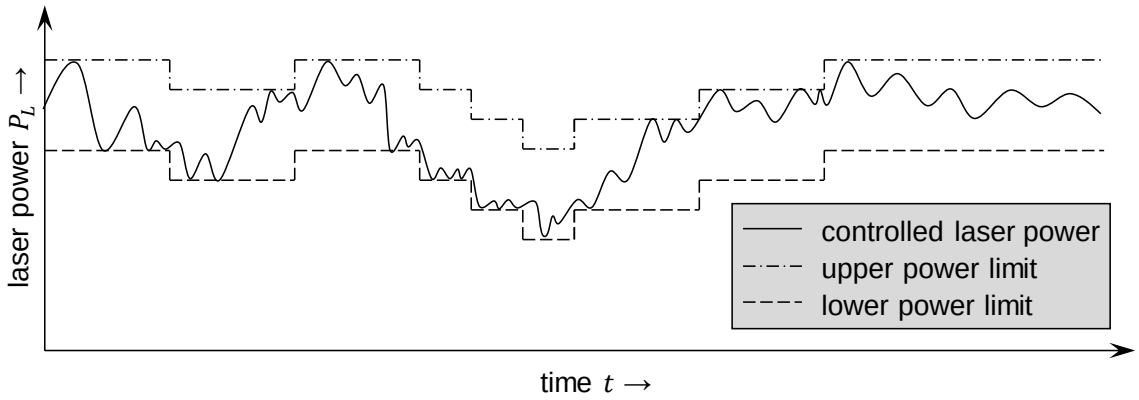

Figure 18: Exemplary representation of the controller reaction of BLUG ET AL. (2012) based on an adaptive limitation of the laser power

BARDIN ET AL. (2005) used a *P*-controller to ensure constant full penetration welding of two sheets in an overlap configuration. Features, e.g., the image brightness, from preprocessed camera images were used as the sensor signals. Based on the image brightness in the keyhole region, a full penetration of the joining partners was detected. The operating point of the controller was quantified experimentally by identifying the difference in brightness between the keyhole and the melt pool for a desired process parameter range. The minimum brightness was found in the keyhole area with complete penetration of the joining partners. In this case, only a small amount of light was reflected due to the backside opening in the keyhole area. The brightness maximum occurred in the melt pool region, where strong reflection appeared at the smooth surface of the molten metal. A linear adjustment of the laser power was performed based on the control deviation of the existing intensity at the minimum from the specified operating point. BARDIN ET AL. (2005) found that the penetration depth and the laser power are not linearly correlated. So a range of validity was defined for the control based on the sheet thicknesses. Linear control of the penetration depth based on the laser power was possible within this range. However, the control is limited to through-welds at stepwise or linearly increasing workpiece cross-sections.

BIRNESSER (2011) used an optical sensor signal for process control. The measuring beam of a spectrometer with a sensitivity in the IR wavelength range was coupled coaxially to a processing beam to observe optical process emissions. A direct correlation of the measurement signals with seam parameters, such as the weld depth, was found. The ranges with a linear relationship between the intensity of the spectrometer signal, the seam characteristics and the laser power were determined experimentally. Digital filtering with infinite impulse response (IIR filter) of the

spectrometer signal was applied to control the weld depth as a function of the laser power. The control deviation was calculated from the filtered value and an externally specified setpoint. The deviation was passed to a proportional-integral-differential-controller (*PID*-controller) with empirically specified control parameters and the laser power as the manipulated variable. However, the procedure description did not clarify which criteria were used to select the control parameters and how they affect the control behavior. The transition from a pilot control to closed-loop control in DPLW resulted in a reduction of the standard deviation of the weld depth by up to 75.3 %. In addition, the focal position and the feed rate were varied experimentally. Using closed-loop control, the detrimental effect of contamination of the optic's protective window could not be corrected, since the contamination influenced the actual laser beam intensity at the workpiece and the detected process emissions.

KONUK ET AL. (2011) focused on the relationship between the keyhole depth and the electron temperature above the process zone to control the weld depth. The depth was determined based on an optical sensor system, detecting spectrally resolved emissions of the process plasma. A constant electron temperature was experimentally identified as the operating point of the controller, which served as a reference point for the control deviation. A proportional-integral-controller (*PI*-controller) was used to regulate the weld depth by adjusting the laser power. However, it was identified that the electron temperature correlated with the weld depth and was also sensitive to the shielding gas composition and the gap between the joining partners in an overlap configuration. For this reason, the relationship between the weld depth and the temperature signal had to be identified and calibrated specifically for the experimental set-up used. The evaluation of the controller was based on the connection of two welded plates with full penetration, while an exact value could not be determined for the weld depth based on the presented method due to the indirect sensor concept.

Comprehensive approaches to process control based on camera images of the process zone in scanner-based laser beam welding were presented by KOS ET AL. (2019) and KOS ET AL. (2020). They illuminated the process zone with laser radiation at a wavelength of 810 nm ± 10 nm and evaluated the images of a camera arranged laterally to the welding optics with regard to differences in brightness caused by the joint geometry. The obtained information on the joint position was used as an input variable for a seam tracking control. Additionally, power control for remote laser welding was introduced. The acquisition of the in-situ variable, i.e., the image brightness, as the basis of the control was founded on the detection of the area of the interaction zone using the above-described camera unit. Based on experimental

investigations, a correlation between the area of the interaction zone and the weld depth was found, showing a linear behavior for a partially penetrating process in the keyhole regime. The laser power, which was calculated using the identified correlation, was used as input to a *PI*-control loop. Furthermore, a descriptive model for the power-area correlation was developed for different feed rates and material thicknesses of the considered AlSi steel. A control deviation of less than 7 % of the target value was achieved during the validation tests.

BOLLIG ET AL. (2005) employed diode-based sensors detecting process emissions in the NIR wavelength range as input for a process control. Based on the signals generated in the course of experimental process investigations, they developed a model-based predictive control for the weld depth in DPLW. An approximation model of the keyhole created by MICHEL (2004) served as a basis, which offered a limited computational efficiency in its original design. Hence, the model was approximated as a time-varying, linear autoregressive-with-exogenous-input (ARX) model for implementation in the model-based control system, allowing a controller frequency of 500 Hz to be achieved. The predictive component of the control was used to generate target values for the laser power to control the weld depth. This resulted in a quality function that weighted the expected control deviation of the estimated output variable as a target value function. The underlying mathematical minimization problem was convex for the selected controller parameterization and provided an explicit solution according to BOLLIG ET AL. (2005). This resulted in a linearly approximated controller validated around an operating point based on the feed rate modulation.

STORK GENANNT WERSBORG (2010) focused on using expert knowledge in manufacturing to deal with high-quality welding tasks. An intelligent process control was presented for an efficient implementation of this knowledge. A sensor data fusion, composed of acoustic signals, photodiode signals and recordings from a coaxial camera, was used as the input variable for the controller. ML-methods, such as a multi-layer FFNN, were employed to implement abstract expert knowledge into a control loop for a steel welding process. The knowledge was then used to control the laser power in situations that were unknown to the controller. In total, sensor signals were recorded for ten welds. These were passed to an FFNN as a training basis with an expert-based visual classification of incorrectly set or suitable laser power for the welding task. In a second step, the learned expert knowledge was used to control the laser power. The output of the FFNN was a quality parameter based on the sensor signals and the expert knowledge. With the help of the control deviation, resulting from the quality parameter and the corresponding target quality value, a

classical *PID*-controller was employed to regulate the laser power. A control frequency of 100 Hz with a transient response within the first 100 cycles was achieved. However, it was found that the use of FFNN is not ideally suited for learning how to perform welds on unknown workpieces from the accumulated expert knowledge.

An advanced approach to an intelligent laser welding architecture using a DNN and reinforcement learning was provided by GÜNTHER ET AL. (2015). A self-learning and self-improving architecture combining two different ML-methods was presented to address the difficulties of non-linearity and stochastic behavior in a laser welding process. A DNN was employed to extract significant characteristics from high-resolution camera data and photodiode signals. The features extracted form sensor data, e.g., the gray value distribution of coaxially captured camera images, were fed to a learning algorithm that predicted process-specific quantities from the signal characteristics. A control strategy was developed based on this prediction and the process characteristics. The authors demonstrated a novel process monitoring and control architecture that combines methods for observing the process, mapping system behavior to a process model and a process control strategy. The authors, however, only presented a methodology whose individual building blocks, such as the control, were tested in offline mode and simulation-based. A real-time capable experimental set-up of the architecture could not be shown.

Interim conclusion

The control of laser welding processes represents a high potential for a wide range of applications. Scrap and rework can be reduced and the quality of the products can be increased. Several approaches have been pursued to control certain process variables based on measurable data and derived information about the process. The non-linearity of the laser welding process poses a challenge, because it causes difficulties in setting up sufficiently accurate models for the controlled systems. As a result, classical control approaches are in many cases only valid for very limited parameter ranges. Increased flexibility is offered by experience-based control methods, which are inspired by the behavior of a human operator and use expert knowledge as the basis for controller interventions. An additional increase in flexibility and accuracy of controlled systems can be achieved by using ML-methods. They can be used, e.g., for the processing and interpretation of sensor signals, which then form the input variables of a controller.

3.5 Conclusions and need for action

Building on the fundamentals described in chapter 2, an overview of the state of the art in process monitoring and process control for laser beam welding was provided in chapter 3. In section 3.2, an overview of approaches for measuring process conditions in laser material processing was given, focusing on inline monitoring of laser beam welding processes. Several works address the enhancement of process knowledge. High-frequency measurement data was used to gain information about parameter influences on the process stability and the process result. Camera-based approaches and methods for acquiring process emissions in discrete wavelength ranges predominate. High-speed cameras attached to the laser processing optics via optical interfaces were employed to capture images from the process zone, e.g., to track the melt pool dynamics or weld spatter formation. Photodiodes were used to measure the process emissions. Thus, metrics such as the back-reflected laser radiation or the process glow were recorded. The data obtained were often related to process instabilities and weld defects by comparing signal values with a reference value thus obtaining deviations. Recent work in the field of process monitoring predominantly focused on improving data evaluation and interpretation approaches as well as on data validation. Furthermore, approaches to combine different sensor systems have been published to improve the robustness of process monitoring systems.

Section 3.3 focused on the application of OCT in laser material processing. Various interferometric distance measurement techniques for process monitoring have been explored in this field, which can be classified according to the evaluation of signals in the time and in the frequency domain. With the availability of robust FD-OCT sensors, this measurement technique was integrated into laser processing optics. Some approaches combined the distance measurement unit with a deflection unit for the measuring beam to acquire surface profiles near the process zone (cf. sub-section 2.3.3). The data could be used, e.g., to track the joint gap during welding or the weld surface in the post-process zone. Since process emissions do not influence OCT measurements in the laser processing of metals, the detection of quantities such as the keyhole depth in DPLW was enabled. Several studies have focused on the increase in signal understanding. Process parameter influences on the OCT signal in keyhole depth measurement were identified and quantified. Further work focused on interpreting the signal for the weld depth using statistical methods and signal filters, e.g., percentile filters. However, no published research approach accounts for the dependence of the keyhole depth measurement signal on process parameters and boundary conditions when interpreting the signal in terms of the weld depth. A

challenge in the parameterization of weld depth evaluation methods is the high effort for obtaining reference data. Hence, within the framework of the existing approaches for inline weld depth evaluation, only solutions with a limited range of validity, i.e., restricted adaptability to process parameter variations, were developed.

An overview of control approaches to laser beam welding was given in section 3.4. Considerable work has been devoted to the full penetration process, in which the aim is to achieve a full penetration weld of two joining partners in an overlap configuration. In all existing approaches, the weld depth control is mainly based on the acquisition of indirect process variables. Correlations between the weld depth and indirect process variables such as process light or acoustic process emissions were used as input variables for controllers. Some published works describe the application of linear controllers. Since no universal physical model of the laser welding process has been established to date, existing control approaches have limited validity and can only be used for specific applications. Additionally, the interpretation of indirect measurement variables often led to reduced precision. The potential of ML-methods to obtain a controlled variable has been shown in few works so far. Nevertheless, the validity ranges of the developed methods have been extended compared to classical control approaches. A closed-loop control system based on OCT keyhole depth measurement has not been described in the literature to date. Fuzzy control (cf. sub-section 2.5.2) of the weld depth has also not been considered so far and its applicability has only been demonstrated for the full penetration welding process.

In the following, the identified research deficit is summarized. The remarks refer to the state of the art at the respective time of publication of the scientific results as described in chapter 5 of this dissertation.

- Few studies describe the signal characteristics of OCT-based keyhole depth measurement. It is known that process parameters and process boundary conditions influence the signal. However, these influences have not yet been quantified nor implemented within the signal interpretation. The weld depth evaluation is currently based on keyhole depth measurements and is subject to complex and time-consuming parametrization for specific applications. It is only valid for the calibrated processing range.
- In existing approaches for determining the weld depth based on keyhole depth measurements, the melt layer surrounding the keyhole during the welding process is not considered. The melt layer thickness depends on a parameter-specific offset between the measurable keyhole depth and the weld depth, which cannot be detected with OCT.

- Existing control approaches predominantly apply physical or analytical models of the laser beam welding process. The validity of these approaches is typically limited to linear relationships between the process parameters and the responses, available only for small ranges with linear behavior. A method for describing a large-scale parameter range for a heavily non-linear system has not yet been established in the field of laser beam welding.
- No weld depth control is available for DPLW, which features simple adaptability to changing processing conditions.

The identified research deficits substantiate the need for action and motivate the foundation of the research approach presented in chapter 4.

4 Research Approach

4.1 Chapter overview

This chapter presents the scientific objectives and the research approach of this thesis. The state of the art, described in chapter 3, serves as a fundamental basis. In section 4.2, the overall objective is outlined, which provides the framework for the derivation of the sub-objectives. These sub-objectives (SO) are embedded into a methodology in section 4.3. The integration of the five publications, representing the scientific content of this thesis, is also illustrated in section 4.3. The experimental set-up used to generate the scientific results is described in section 4.4.

4.2 Scientific objectives

This thesis focuses on the overall objective to enable the control of the weld depth in DPLW based on the inline measurement of the keyhole depth. For this purpose, a method for interpreting the OCT keyhole depth measurement signal for the actual weld depth is developed, supported by a numerical weld pool simulation. A high quality of laser welds must be ensured and scrap and rework due to a weld depth deviating from a target value need to be reduced. It was essential to investigate and quantify the process influences on the OCT signal using statistical approaches. In addition, the real-time evaluation of the measurement signal had to be investigated, which can be executed on an industrial control system. The execution sequence of the program had to be optimized in order to ensure a quick response of the process control. From these requirements, a total of six sub-objectives can be derived, which are listed in the following.

SO1: Characterization of the process influences on the OCT signal

The influences of the process parameters on the OCT signal had to be quantified and conditioned for subsequent use in OCT data interpretation. Thereby, the general applicability of OCT for the measurement of the keyhole depth in DPLW over a wide parameter range and especially for challenging process conditions had to be proven.

SO2: Quantification of the melt layer thickness

An OCT sensor allows to determine the *keyhole depth* during DPLW. However, the *weld depth* is relevant for the process design. Consequently, the geometric correlation between the two quantities, characterized by a melt layer below the keyhole, had to be investigated.

SO3: Acquisition method for training and test data for the weld depth evaluation

A method for acquiring the weld depth along weld samples had to be developed. In addition, a method for the temporal and spatial correlation of the real weld depth with the OCT measurement signal and the processing parameters was to be found. Based on this, reference data-sets were to be created, showing the correlation between the OCT signal and the weld depth.

SO4: Evaluation of the weld depth as a function of the processing conditions

A method was to be found to determine the weld depth from an OCT keyhole signal. Process parameters, signal characteristics and the melt layer thickness had to be considered.

SO5: Identification and specification of the process behavior as a function of the process parameters

The influence of the process parameters, i.e., laser power and feed rate, on the weld depth had to be investigated. Thereby, also the fluctuation of the weld depth was to be statistically examined. The results were to be incorporated into a process model describing the welding process in terms of depth and stability.

SO6: Development of a weld depth control

A weld depth control was to be implemented, selecting a set of start parameters with high stability based on the target depth. The aim was a dynamic adjustment of the parameters during the welding process in order to keep the weld depth within a defined tolerance range.

4.3 Methodology and integration of the publications

This section describes the methodology for addressing the scientific objectives outlined in section 4.2. According to the individual scientific focus, the author's publications are assigned to the fields of action within the methodology. Figure 19 summarizes the methodology and the association of the publications (P), while a detailed discussion of the scientific results is provided in section 5.2.

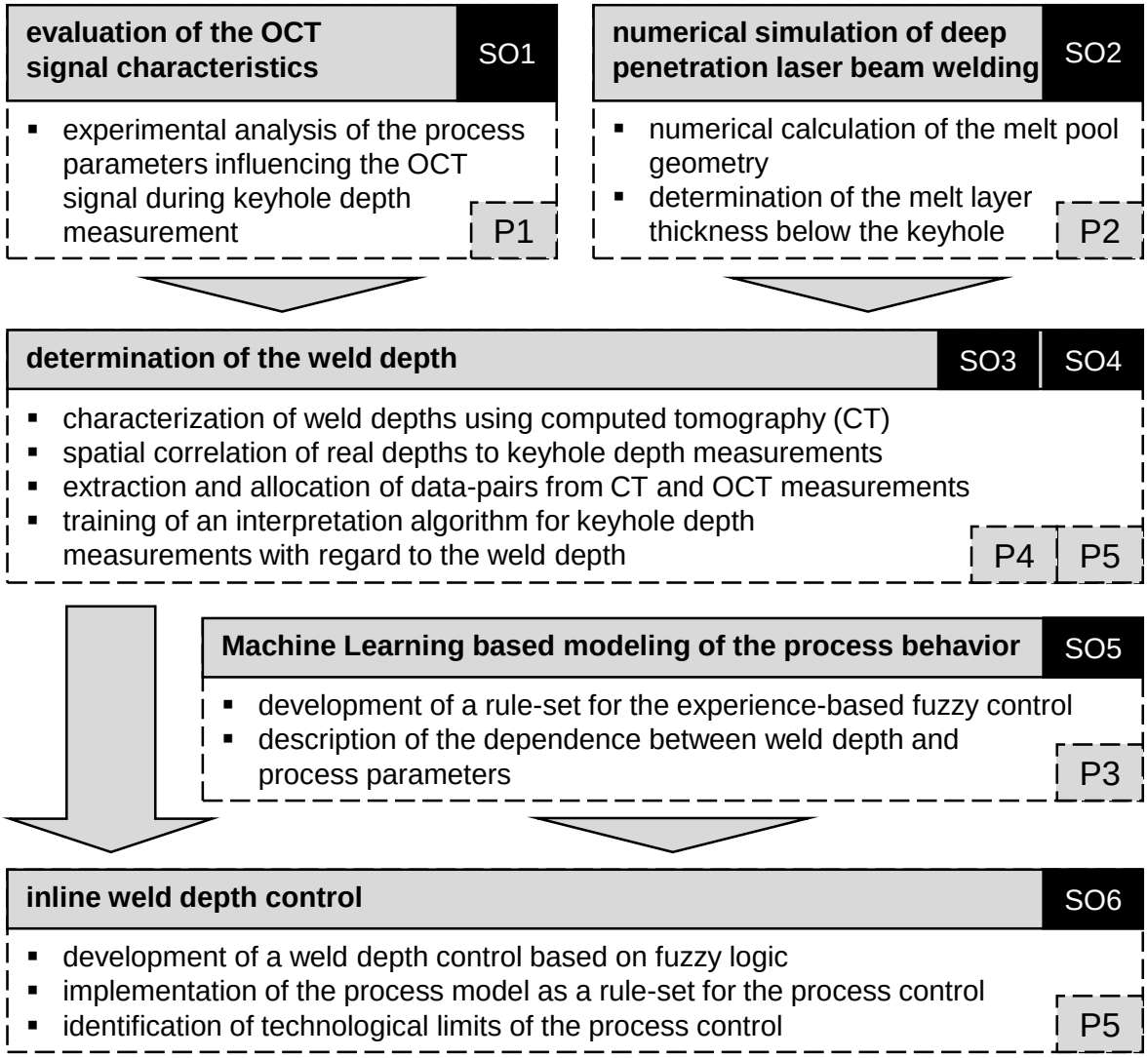

Figure 19: Methodical approach and thematic classification of publications P1 to P5 regarding the sub-objectives (SO) defined in section 4.2

Evaluation of the keyhole depth signal characteristics

A comprehensive understanding of the measurement signal represents the basis for determining the weld depth using an OCT-based keyhole depth measurement. For

this reason, it is necessary to investigate the influences of process parameters and boundary conditions on the characteristics of the keyhole depth signal within the scope of an experimental study. In particular, process parameters that have a direct influence on the stability and geometry of the keyhole are to be varied. These include the line energy[10], the focus diameter, the angle of incidence of the processing laser beam relative to the workpiece surface and the material of the workpiece. Following the investigations of DORSCH ET AL. (2016) and DORSCH ET AL. (2017), keyhole depth measurement signals are to be recorded under variation of the specified parameters and evaluated by statistical methods. A model of the characteristics of the OCT signal is to be derived from this. The OCT signal characterization results are presented in publication P1 and address SO1 as outlined in the methodical approach.

Numerical simulation of deep penetration laser beam welding

In addition to the understanding of the signal, the description of the physical relationship between the observable *keyhole depth* and the resulting *weld depth* represents an essential aspect of the inline weld depth evaluation. For this reason, the thickness of the melt layer surrounding the keyhole during the welding process must be determined. Since an inline measurement of the keyhole and melt pool geometry demands considerable experimental effort (VÄNSKÄ ET AL. 2013), a 3D-FEM model is required to calculate the weld pool geometry. Process variables that are difficult to measure need to be calculated, taking physical boundary conditions into account. An overview of existing simulation approaches is given by SVENUNGSSON ET AL. (2015). The simulation model should be embedded in an optimization loop to derive the keyhole geometry based on metallographic sections. In the optimization loop, a reduction of the deviations between the metallographically determined and the calculated melt pool geometry should be achieved by an iterative adjustment of the modeled heat source geometry. A correlation between the process parameters and the melt layer thickness below the keyhole needs to be found from the calculation results. The results of the numerical study are presented in publication P2 and refer to SO2.

Determination of the weld depth

Building on the results of the publications P1 and P2, the keyhole signal of the OCT-based keyhole depth measurement is to be evaluated in inline mode regarding the weld depth. First, suitable data processing methods have to be identified that meet the requirements of the process and the laser welding system employed. Subsequently,

[10] Line energy is defined as the ratio of laser power to feed rate, describing the energy input per length unit into the weld seam.

evaluation algorithms need to be developed, parameterized and implemented on a real-time data processing system. In addition, interfaces should be provided, by means of which both the signal characteristics (P1) and the melt layer thickness (P2) can be considered to evaluate the weld depth. The research results are summarized in publication P5 and address SO4. Since typically large amounts of reference data are required for robust parameterization of process monitoring systems, a method should be found to generate high-quality reference data. It is necessary to correlate the data with the position along a weld sample in order to investigate the relationship between the process result and the measurement signals at selected positions. This method represents the achievement of SO3 and is the main content of publication P4.

Modeling of the process behavior

To define reaction options in the process for controlling the weld depth, the dependence of the weld depth on the process parameters must be quantified. In the first step, the process parameters that significantly influence the weld depth and that are suitable for the integration into a control loop must be evaluated. Based on these findings, the effects of the parameters on the weld depth and its variance are to be evaluated in experimental investigations. On this basis, a method for a significant reduction of the experimental effort in the evaluation of the process behavior is to be developed. The established method will be used to create a process model for the DPLW process. This work addresses SO5 and is summarized in publication P3.

Inline weld depth control

As described in SO4 (section 4.2), the weld depth evaluated in inline mode is to be embedded in a closed-loop control system. The first step is to identify a suitable controller architecture. It is essential that a low effort is required for the controller parameterization and that the non-linear behavior of the laser beam welding process can be compensated robustly. In addition, a fast response to process fluctuations must be ensured. Therefore, reaction times must be considered when changing the laser power P_L and the feed rate v_w. The selected controller architecture should then be implemented on a demonstrator system and tested with a focus on robustness and reaction time. The results, which address SO6, are presented in P5. In the control loop, which is schematically outlined in Figure 20, all SOs are incorporated. Thus, the results of the publications P1 to P5 are combined into an overall methodology.

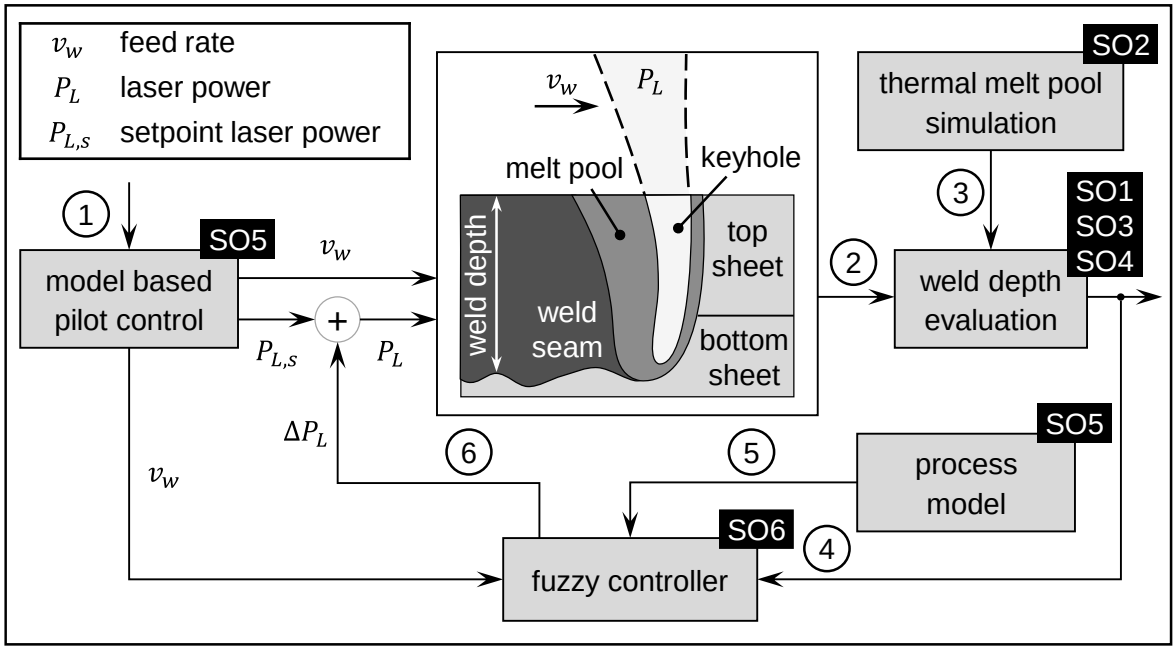

1	desired weld depth	2	keyhole depth measurement signal
3	melt layer thickness	4	current weld depth
5	fuzzy rules / control reactions	6	power correction value

Figure 20: Structure of the weld depth control loop and assignment of the Sos to the individual modules

4.4 Experimental set-up

Within the scope of the experimental investigations in this work, a laser beam welding system was used, which was developed for the specific purpose of inline weld depth control. The system is characterized by a full-time synchronization between signals of a process monitoring system and the control signals of the significant influencing components. The core of the set-up is the programmable logic controller (PLC), which processes all measurement and control signals and provides them with a time stamp. The process control system is implemented within the PLC, which allows the process parameters to be adapted to the measured control variables. A fixed optics (YW52, Precitec GmbH, Germany) is used. A 3-axis computerized numerical control (CNC[11]) system controls the component movement and the positioning of the welding optics at a maximum speed of 12 m/min (cf. Figure 21). It serves to adjust the distance between the focal point and the component and to move the component relative to

[11] CNC refers to an approach for controlling machine tools with multiple axes that simultaneously perform interpolated movements.

the fixed operating point of the optics. Three synchronous servo motors are used for the axis movements, which return their respective positions to the controller in real-time. The data obtained can be used, for example, to determine the actual feed rate of the component in the x-y-plane, which may deviate slightly from the specified value due to external influences. A continuous-wave (cw) multi-mode fiber laser (FL080, ROFIN-SINAR Laser GmbH, Germany) provides the laser radiation for the processing and is guided to the optics by an optical fiber. The laser beam source is also integrated into a control loop, in which it receives a power setpoint from the control system and returns the actual value. In addition, an OCT-based inline process monitoring system (IDM 1.1, Precitec GmbH, Germany) is integrated into the welding system. It measures the distance between the processing optics and a specific point on the component. The principle of OCT and the integration into the welding optics were explained in detail in sub-section 2.3.3. The OCT sensor transmits distance values in the form of an analog signal to the PLC (Beckhoff Automation GmbH, Germany), which records the process monitoring signals and synchronizes them with an internal clock to all other recorded process variables. Figure 21 shows the schematic structure of the laser beam welding system and the information flows transmitted in the form of light, digital signals or analog signals.

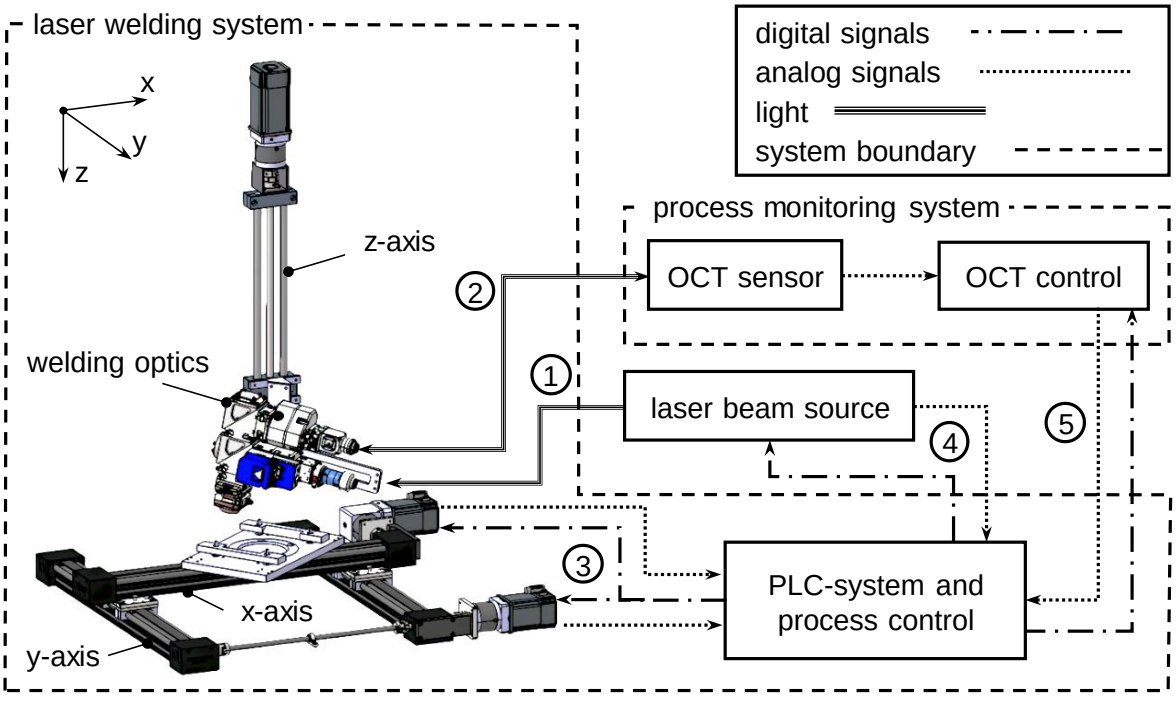

1 processing laser radiation 2 OCT measurement radiation 3 axis drive signals
4 laser beam source signals 5 OCT signals and control

Figure 21: Experimental set-up used in this work with the signal flows between the individual components

The technical data of the laser beam source, the laser processing optics, the OCT sensor and the PLC are summarized in Table 4-1.

For the radiographic inspection of the weld specimens, a microfocus X-ray computed tomography (µCT) system was used. The system features the ability to acquire three-dimensional images of a specimen with a voxel resolution, the three-dimensional equivalent of the image pixel resolution, in the range of 10 µm. The sample, which is mounted on a rotatable fixture, is rotated 360 degrees in fine angular increments during measurement. The rotation is interrupted at each angular position and an image of the sample is recorded. The individual images are referred to as projections and their reconstruction generates a three-dimensional data-set. The voxel resolution is determined by the distance of the sample l_s and by the distance of the detector screen l_d to the radiation source. For the analysis of metal samples, the measuring radiation is generated in the CT tube and guided towards the sample with the accelerating voltage. As the radiation passes through the sample, it is attenuated and the resistance of a sample determines the degree of attenuation. Using a weld seam specimen as an example, the X-rays are attenuated less when passing through a porous area in the weld seam sample than when passing through a fully solid metal body. After passing through the sample, the partially attenuated radiation is converted into visible light when it hits the detector screen. The light pattern at the screen is captured by a camera, with the images forming the basis for reconstructing the 3D-data. Figure 22 shows the basic set-up of a µCT system and the parameters of the system used.

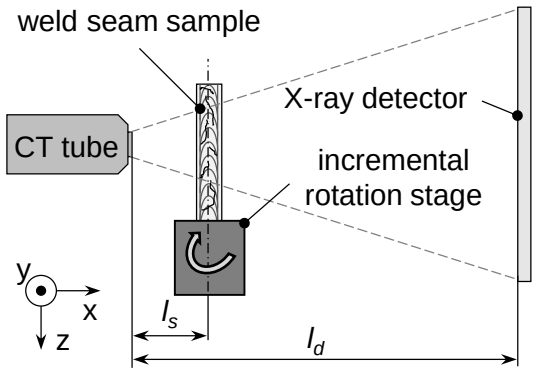

acceleration voltage	110 kV
projections	1801
measurement time per projection	5 s
sample size (x-direction)	4 mm
sample size (y-direction)	4 mm
minimum voxel size	7.7 µm
maximum voxel size	17.5 µm

Figure 22: Schematic set-up of a microfocus X-ray computed tomography system (µCT) and measurement parameters for the radiographic inspection of weld samples

Laser beam source (FL080, ROFIN-SINAR Laser GmbH, Germany)	
operating mode	continuous-wave
max. output power	8 kW
fiber core diameter	100 µm
wavelength	1070 ± 10 nm
beam parameter product (BPP)	≤ 4 mm · mrad (multi-mode)
Processing optics (YW52, Precitec GmbH, Germany)	
image ratio	1:1
focal diameter of the processing beam	100 µm
OCT sensor (IDM 1.1, Precitec GmbH, Germany)	
max. measurement frequency	70 kHz
wavelength	1550 ± 20 nm
focal diameter of the measurement beam	50 µm
max. power	20 mW
PLC system (CP3219-0020, Beckhoff Automation GmbH, Germany)	
processing frequency	3.4 GHz
number of processor cores	2
automation software	TwinCat 3, Beckhoff

Table 4-1: Technical data of the laser beam source, the laser processing optics, the OCT sensor and the PLC

5 Research Findings

5.1 Chapter overview

Based on the methodological approach presented in section 4.3, this chapter outlines the scientific results obtained in the context of this work. The results are described in the form of short recapitulations of the author's publications in section 5.2. Following the summary of each publication, a brief review of the individual author's contributions to the scientific result is provided. Section 5.3 presents a review of the scientific results with reference to the state of the art.

5.2 Recapitulation of the embedded publications

5.2.1 P1: “Inline Weld Depth Measurement for High Brilliance Laser Beam Sources Using Optical Coherence Tomography”

Publication P1 “Inline Weld Depth Measurement for High Brilliance Laser Beam Sources Using Optical Coherence Tomography” (SCHMOELLER ET AL. 2019) describes the fundamental influences on the measurement signal when acquiring the keyhole depth by Optical Coherence Tomography. A MM fiber laser and a SM fiber laser were used for the investigations. The fixed optics employed were equipped with a coaxial OCT sensor. A beam splitter was used to direct one fraction of the OCT radiation into the keyhole and another fraction onto the component surface adjacent to the process zone. The keyhole depth was determined from the differences between the two lengths (cf. Figure 8). The work described in P1 was focused on the characterization of the signal component recorded from the keyhole. The results presented for the keyhole depth measurements were compared to metallographic cross-sections from which the corresponding weld depth was measured by using a microscope. The characteristics of the OCT signal were evaluated using statistical

parameters, e.g., the variance and the relative frequency of the measurements in the depth direction (cf. Figure 23), i.e., the normalized frequency of occurring weld depth values along each of the examined weld seams in the labeled areas.

In an experimental study, the influences of the angle of incidence, the sample material and the weld geometry on the quality of the sensor signal were investigated. When using a multi-mode fiber laser beam source with a focal diameter of 320 µm, the measurements showed a strong material-dependent behavior. For the copper alloy C10200, a signal with low scattering and a high signal density in the weld depth range was detected. Measurements on the aluminum alloy AA6082 showed a much more pronounced scattering of the OCT signal in the depth direction (cf. Figure 23). In addition, the position of the signal region with the highest relative frequency of depth measurement points was shifted towards the component surface. Regarding the angle of incidence, it was shown that a more stable measurement signal was obtained for a piercing[12] process configuration than for a dragging[13] configuration. By varying the feed rate and the laser power, it was possible to investigate the influence of the weld depth on the measurement signal for otherwise identical process boundary conditions. It was shown that an increase of the weld depth led to an approximately linear increase in signal noise. The knowledge of the measurement signal properties gained in the study was then applied to laser beam welding using a single-mode fiber laser with a spot diameter of 55 µm. With about 50 µm, the OCT measurement beam diameter was only slightly smaller than that of the single-mode processing beam, leading to increased requirements on the positioning accuracy of the measurement beam and the signal evaluation. A wide variety of tests were performed to determine the limits of the measurement method. An approximately linear increase in signal noise over the weld depth was also demonstrated for the single-mode process for copper and aluminum. The deviation of the detectable keyhole depth to the real weld depth increased with the weld depth.

The results showed that the application of OCT enables the inline monitoring of the weld depth with multi-mode and single-mode laser beams. In addition, process influences on the signal were identified, such as material-specific weld pool dynamics and characteristic reflection and absorption properties. The publication contributed to a fundamental understanding of the OCT-signal during the keyhole depth measurement, which is the foundation for a reliable signal interpretation.

[12] In a *piercing* welding configuration, the welding optics are tilted against the feed direction. As a result, the laser beam predominantly interacts with the non-melted material.
[13] In a *dragging* welding configuration, the welding optics are tilted in the feed direction. As a result, the laser beam predominantly impinges the melt pool.

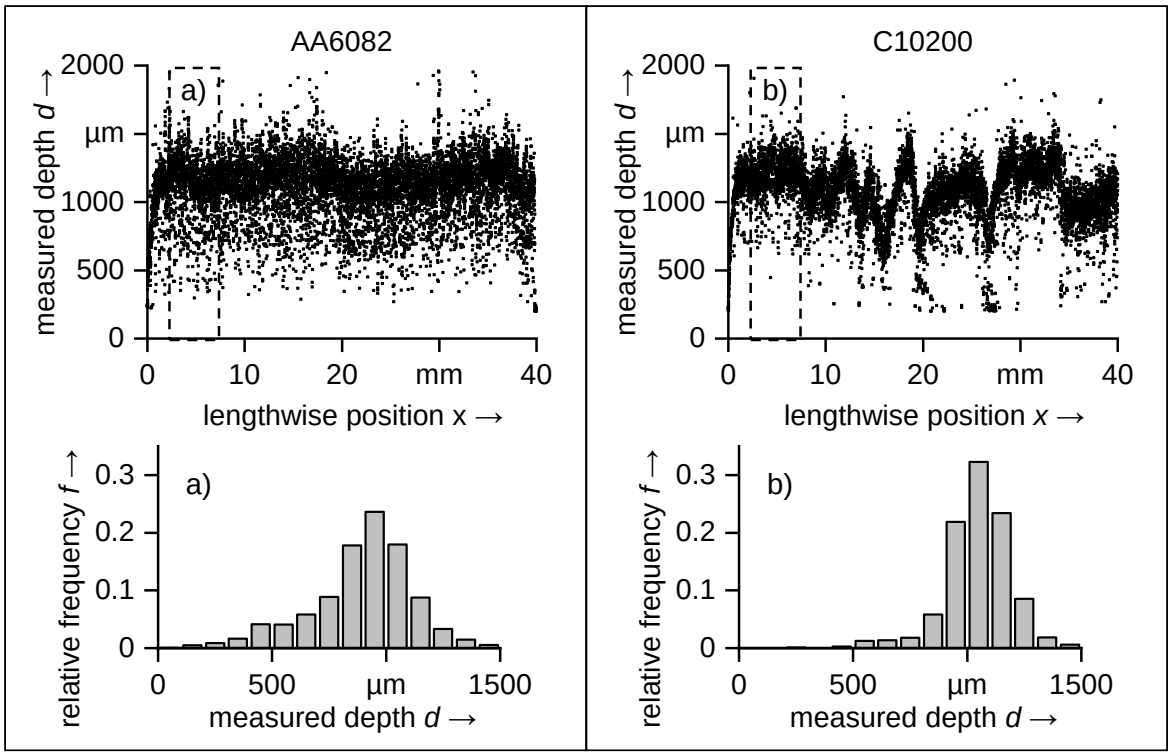

Figure 23: OCT-based keyhole depth measurement signals for the aluminum alloy AA6082 (left) and the copper alloy C10200 (right) with histographic evaluation of the signal distribution in the depth direction in the areas a) and b); based on SCHMOELLER ET AL. (2019)

Author's contribution

Maximilian Schmoeller and Christian Stadter collaborated on developing the idea for OCT signal characterization as a function of the process boundary conditions. Maximilian Schmoeller performed the analysis and interpretation of the data. The manuscript was written by Maximilian Schmoeller and edited by Christian Stadter, Stefan Liebl and Michael F. Zaeh. All authors discussed and commented on the scientific approach and the results during the preparation of the publication. Maximilian Schmoeller presented the results in a lecture at the International Congress on Applications of Lasers and Electro-Optics (ICALEO) in Orlando, FL, USA in 2018. Table 5-1 lists the contributions of the author of this dissertation to publication P1.

	concept	content	manuscript	**total**
M. Schmoeller	90 %	70 %	80 %	**80 %**

Table 5-1: Contributions of the author to the conception, the development of the contents and the manuscript of publication P1

5.2.2 P2: “Numerical Weld Pool Simulation for the Accuracy Improvement of Inline Weld Depth Measurement Based on Optical Coherence Tomography”

Publication P2 "Numerical Weld Pool Simulation for the Accuracy Improvement of Inline Weld Depth Measurement Based on Optical Coherence Tomography" (SCHMOELLER ET AL. 2020b) presented a numerical simulation model for the calculation of the melt pool geometry in DPLW.

A calibrated numerical simulation model was employed to describe the geometry of the melt pool as a function of the process parameters. The melt layer thickness below the keyhole was determined from the calculation results. This dimension represents the geometric difference between the weld depth and the keyhole depth, measured using Optical Coherence Tomography. The model presented was based on LIEBL ET AL. (2017). The heat source was modeled by a geometric approximation of the keyhole geometry and by applying the evaporation temperature to the capillary wall. The feed rate was implemented by a material flow with a constant velocity around the stationary keyhole geometry. The material parameters mass density ρ_m, specific isobaric heat capacity c_p, thermal conductivity λ_{th} and dynamic viscosity μ_{dyn} were formulated as a function of temperature. In the approximation of the temperature functions, special consideration was given to numerical stability to achieve high computational efficiency of the model.

The geometrical parameters of the heat source shape, i.e., the keyhole shape, were adjusted using a genetic algorithm (GA) in several successive computational runs. The goal of the GA was to minimize the deviation between the simulated melt pool geometry and the corresponding metallographic cross-sections. When reaching a termination criterion, i.e., a maximum permissible deviation between simulation and reality, the optimization was terminated. By this approach, the keyhole geometry, which is difficult to measure experimentally, was calculated based on the metallographically determined melt pool contour. The laser power as the governing measure for the weld depth was indirectly considered, since the heat source only incorporates the evaporation temperature and the keyhole geometry (cf. Figure 24). The main advantage of that approach lies in its flexible applicability in the case of an adjustment of the process parameters due to a calculation and optimization time of approx. 3 h under the given boundary conditions (i.e., available computing resources[14]). Usually, within the genetic optimization by applying the GA, at least

[14] Technical data of the simulation computer used: CPU: INTEL® Xeon® CPU E5-1650 v4 with 6 cores at 3.60 GHz each; RAM: 64 Gb; Operating system: Windows® Server 2012 R2 Standard (64 Bit)

five epochs with ten individuals each, i.e., at least 50 models, were calculated. The procedure of the genetic adaptation of the keyhole geometry is shown in Figure 24.

The experimental investigations for the generation of metallographic cross-sections as an optimization and validation basis were carried out for the presented results with a fixed optics welding system combined with a multi-mode fiber laser. The focal diameter of the laser beam was about 320 µm at a wavelength of 1070 nm. Within a parameter range suitable for welding the aluminum alloy AA6082, the influences of the feed rate and the laser power on the melt layer thickness were investigated.

A small parameter dependence of the calculated melt layer thickness was found for the evaluated process parameter range. The correlation between the keyhole depth and the melt pool depth was used as an input variable for interpreting the keyhole depth measurement for the weld depth. Thus, the accuracy of the evaluation algorithms could be increased, since an uncertainty in the measurement caused by the melt layer thickness was considered. The results showed that a layer thickness of about 300 µm had to be considered for the investigated parameter range, which corresponded to a high multiple of the absolute accuracy of an OCT-based measurement system. Furthermore, it was shown that the melt layer thickness corresponded approximately to the focus diameter of the processing laser beam. Expanding on these relationships provides room for further research.

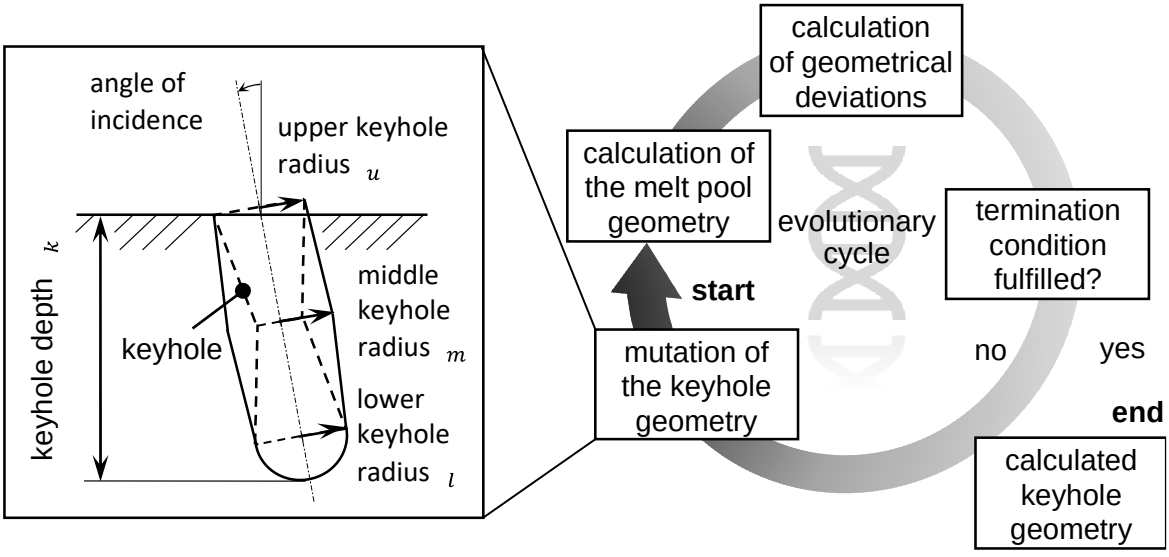

Figure 24: Procedure of the genetic variation of the keyhole geometry in the 3D-FEM model to minimize the deviation between the calculated and the actual melt pool cross-section; based on SCHMOELLER ET AL. (2020b)

Author's contribution

Maximilian Schmoeller developed the idea of the numerical simulation of the melt pool to characterize the melt layer thickness. Maximilian Neureiter supported the development of the simulation model and the optimization algorithm in the framework of a student project, which was supervised and guided by Maximilian Schmoeller. The manuscript was written by Maximilian Schmoeller and edited by Maximilian Neureiter, Christian Stadter and Michael F. Zaeh. All authors commented on the results of the publication. Maximilian Schmoeller presented the results in a lecture at the International Congress on Applications of Lasers and Electro-Optics (ICALEO) in Orlando, FL, USA in 2019. The contributions of the author of this dissertation to publication P2 are listed in Table 5-2.

	concept	content	manuscript	**total**
M. Schmoeller	80 %	60 %	70 %	**70 %**

Table 5-2: Contributions of the author to the conception, the development of the contents and the manuscript of publication P2

5.2.3 P3: "Investigation of the Influences of the Process Parameters on the Weld Depth in Laser Beam Welding of AA6082 Using Machine Learning Methods"

In the publication P3 "Investigation of the Influences of the Process Parameters on the Weld Depth in Laser Beam Welding of AA6082 Using Machine Learning Methods" (SCHMOELLER ET AL. 2020a), a process model for laser beam welding of the aluminum alloy AA6082 was presented. The objective was to efficiently model the process behavior to correlate the process-determining parameters *laser power* and *feed rate* with the weld depth based on ML. A Variational Autoencoder (VAE) combining a neural encoder with a neural decoder served as the basis for the process model. From observations consisting of metallographically determined weld depths and the corresponding process parameters, the encoder network calculated a set of latent[15] factors that were completely independent of each other. The latent factors are equivalent to the knowledge gained from the observations made by the encoder network. HIGGINS ET AL. (2017) proposed adding a hyperparameter β to the cost function of a VAE. It supports the learning with greater independence of the probability distributions in the latent factors. As a result, each latent factor represents a unique input data aspect.

For predicting the weld penetration depth as a function of the process parameters, the strictly forward-directed architecture of a Beta-Variational Autoencoder (β-VAE) proposed by ITEN ET AL. (2020) and building on the results of HIGGINS ET AL. (2017) is well applicable. In P3, this architecture was extended to include an additional input layer of the decoder. It allowed for generating a generative response for a predicted weld depth d_w in the output layer. In the chosen architecture, the input layer was a vector $[\boldsymbol{d}_w^k]_{k\in\{1,\dots,N\}} = [\vdots]$ of N experimentally determined weld depths generated with the parameters P_L and v_w. The parameter layer consisted of the process parameters for which the weld penetration depth is to be predicted. The input vector $\boldsymbol{d_w}$ was required to contain statistically validated information about the weld penetration depth within a parameter range for the training of the β-VAE. For instance, the information on the real weld depth can be obtained from longitudinal metallographic sections or from multiple metallographic cross-sections along the welding direction.

A total of 63 parameter combinations were used to verify the methodology. The laser power P_L was set between 400 W and 1400 W and the feed rate v_w was set between

[15] A latent factor cannot be measured directly. However, one or more latent factors described by the test results can be extracted from a variety of test results, i.e., the observable factors.

4 m/min and 10 m/min including the limits in both cases. The parameter combinations with a laser power of 400 W and 1400 W, i.e., the outlying domains, were not used for training but served to verify the extrapolation validity of the approach. For each parameter combination, the weld depths were determined using 30 cross-sections. Since no equivocal position along the weld seam was assignable to the cross-sections, a parameter vector without time dependence had to be used. This precluded any parameter variation during the welding process aiming at an increase in efficiency, since otherwise a geometric relation would have to be established between the measurement data and their recording position along the weld seam. For the prediction of the weld depths, the β-VAE was activated with a random series of 40 out of 49 test points from the training domain and with the corresponding parameter combinations. The remaining 9 points were used as test data set, which was expanded with the outlying domains at 400 W and 1400 W laser power. The weld depth prediction results for the considered parameter range are shown in Figure 25(a). Figure 25(b) depicts the corresponding prediction accuracies based on the root mean square error (RMSE) associated with the respective test points.

An extensive database enabled the training of a β-VAE and the interpretation of the learned generative factors for the weld depth. The transient process behavior during laser deep penetration welding could be modeled with high accuracy (cf. Figure 25 (b)) using the β-VAE. Based on the trained network, a prediction of the weld depth was performed for test parameter sets thus far unknown to the network. Consequently, the results were used as a basis for experience-based process control, which can be realized by OCT-based keyhole depth measurement.

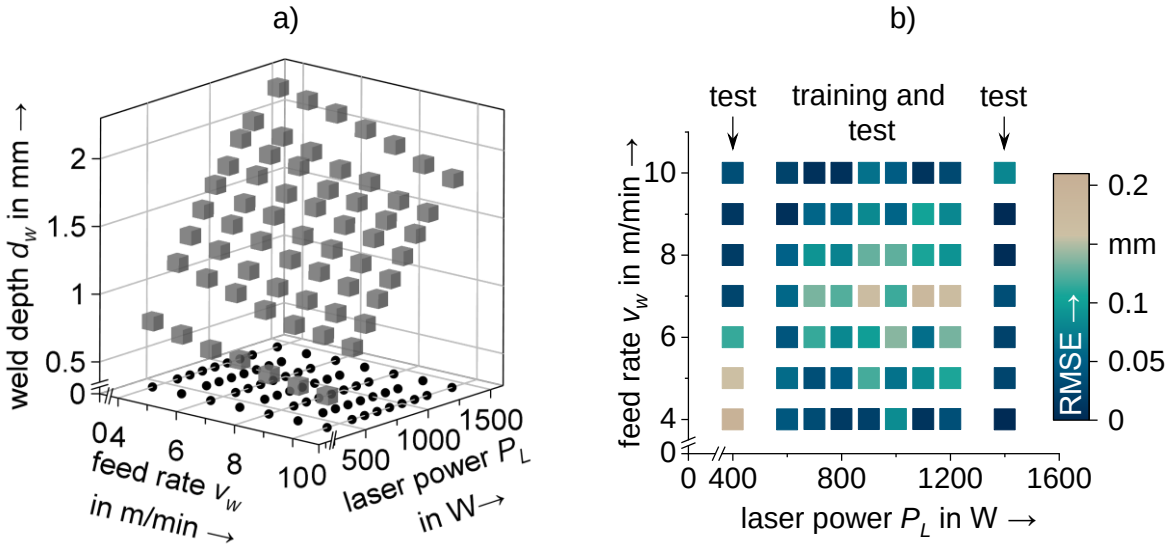

Figure 25: Results of the weld depth prediction using a β-VAE; mean values of predictions for 400 W – 1400 W laser power and 4 m/min – 10 m/min feed rate; corresponding deviations of predictions from test data represented by the root mean square error (RMSE); based on SCHMOELLER ET AL. *(2020a)*

Author's contribution

As part of his scientific work, Maximilian Schmoeller defined the requirements for the model to describe the behavior of the DPLW process. In the development of the model architecture based on ML, Maximilian Schmoeller was supported by Markus Wagner as part of a student project. Christian Stadter supported the model development and the planning and execution of experiments. Maximilian Schmoeller wrote the manuscript, which was then edited by Markus Wagner, Christian Stadter and Michael F. Zaeh. All authors discussed and commented on the results. Maximilian Schmoeller presented the results in an online lecture at the 11th CIRP Conference on Photonic Technologies (LANE) in 2020. The contributions of the author of this dissertation to publication P3 are listed in Table 5-3.

	Concept	content	manuscript	**total**
M. Schmoeller	80 %	60 %	70 %	**70 %**

Table 5-3: Contributions of the author to the conception, the development of the contents and the manuscript of publication P3

5.2.4 P4: "A Novel Approach for the Holistic 3D-Characterization of Weld Seams – Paving the Way for Deep Learning Based Process Monitoring"

The challenges in obtaining high-quality and comprehensive training data for ML approaches in laser beam welding process monitoring are addressed in the publication P4 "A Novel Approach for the Holistic 3D-Characterization of Weld Seams – Paving the Way for Deep Learning Based Process Monitoring" (SCHMOELLER ET AL. 2021). Based on a microfocus X-ray computed tomography set-up (µCT) to inspect metallic samples, a method to evaluate three-dimensional (3D) measurements of an internal weld seam geometry for the aluminum alloy AA2219 was developed. From the scans, extensive information was obtained on the weld geometry, on internal defects and on the relationships between the process parameters and the weld properties. The evaluation procedure is illustrated in Figure 26.

The methodology for 3D weld characterization was composed of three consecutive operations. An X-ray-based measurement method was qualified to acquire raw data in the first step. Subsequently, the results were used to develop an evaluation routine for the 3D-assessment of the geometric characteristics of welds. The acquired geometric features were evaluated in the third step for their dependence on the process parameters and correlated with sensor signals from inline process monitoring systems, e.g., OCT keyhole depth measurements.

To qualify the measurement system, welding tests were carried out on aluminum alloys with different microstructures, material compositions and manufacturing methods. Based on SCHAFF ET AL. (2017), it was presumed that a significant change in microstructure due to the welding process could result in a detectable change in the attenuation of X-rays passing through a specimen. Measurements on the aluminum alloy AA2219 allowed a complete visualization of the weld geometry inside the specimen. The acquisition parameters of the µCT system were evaluated for the measurement resolution. With a voxel size of 7.7 µm edge length, a high contrast of the molten and resolidified material compared to the base material and a good detectability of seam defects such as cracks was achieved.

In an extensive series of tests based on the design of the experiments of publication P3, the weld defects, classified as pores and cracks, were studied and the three-dimensional weld contour over a length of 12 mm per specimen was evaluated. Referenced to the specimen surface, the weld penetration depth was determined. Since the maximum weld penetration depth was not always located in the center of the weld,

the three-dimensional characterization offers the advantage over longitudinal cross-sections that measurement errors due to those characteristics can be avoided.

Based on the three-dimensional weld characterization results, a method was developed for the local and temporal correlation of geometric weld features with the measurement signals from inline process monitoring systems such as an OCT sensor. For this purpose, the weld specimens were provided with a reference notch before the test execution. In the keyhole depth measurement signal from the OCT sensor, the notch resulted in a characteristic pattern. Due to the complete and temporally correlated closed-loop acquisition of all sensor signals, axis positions and velocities, the notch, which was detectable in the OCT signal and the µCT images, was used as a reference. Thus, comprehensive comparative data, i.e., experimental reference date, for the weld penetration depth and other weld properties were made available for the sensor signals.

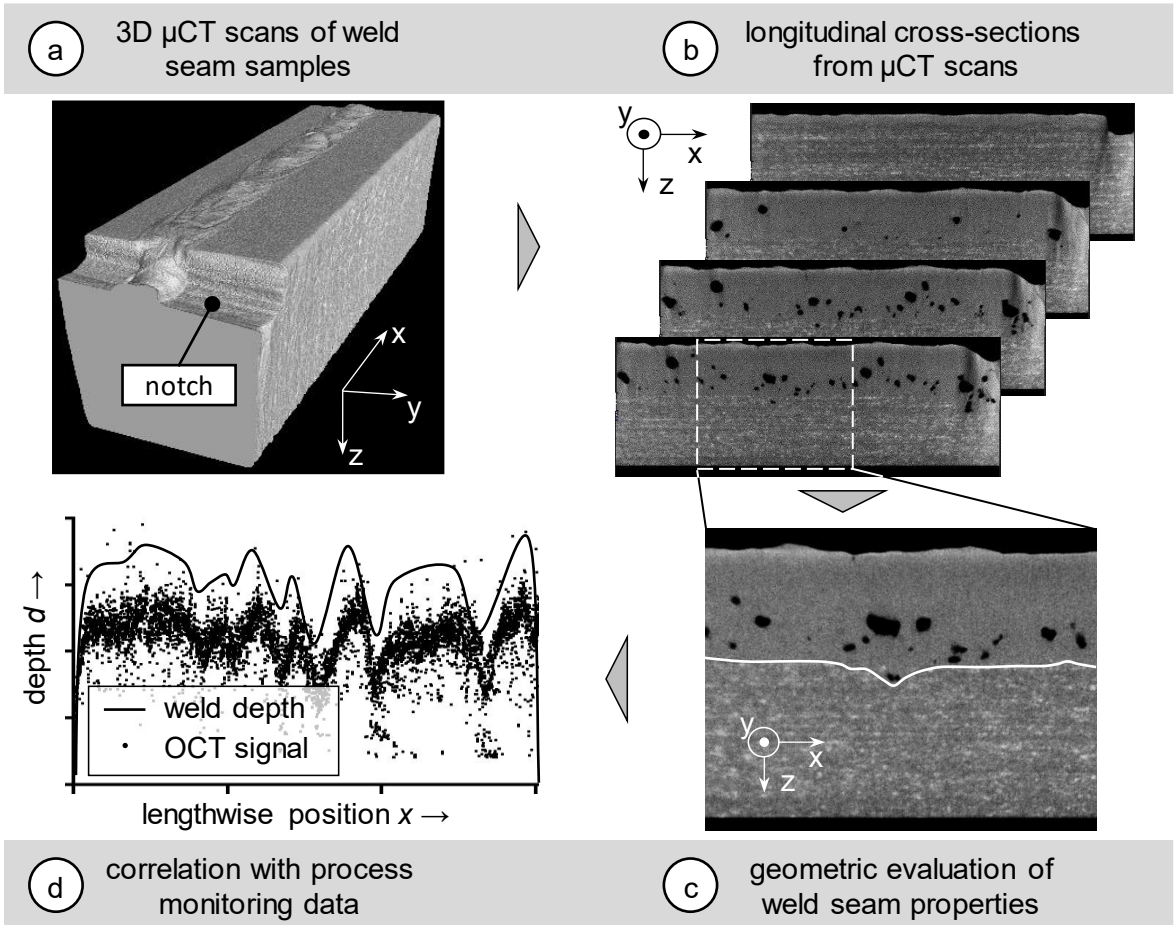

Figure 26: Procedure for the 3D weld seam characterization based on microfocus X-ray computed tomography (µCT) with a focus on the determination of the weld depth values over the feed direction; based on SCHMOELLER ET AL. *(2021)*

The overall goal of publication P4 was to obtain a detailed database of weld characteristics that can significantly improve the evaluation accuracy of inline process monitoring systems. By reliably correlating sensor signals with process results, the data obtained could be used to train different models based on various ML approaches. With the help of extensive data-sets, it is also possible to use DNN architectures that require substantial amounts of training data. These are available, as the result of the measurements is a quasi-continuous course with a high temporal and local resolution of the weld depth with a voxel size of 7.7 µm.

Author's contribution

Maximilian Schmoeller and Christian Stadter collaborated on developing the idea for the three-dimensional characterization of welds using microfocus X-ray computed tomography. Both authors planned and performed the experiments and analyzed and interpreted the data together. Christian Stadter and Maximilian Schmoeller prepared the manuscript, which was edited by Michael Kick, Christian Geiger and Michael F. Zaeh. All authors commented on the results. Table 5-4 summarizes the contributions of the author of this dissertation to publication P4.

	concept	content	manuscript	**total**
M. Schmoeller	50 %	40 %	40 %	**40 %**

Table 5-4: Contributions of the author to the conception, the development of the contents and the manuscript of publication P4

5.2.5 P5: “Inline Weld Depth Evaluation and Control Based on OCT Keyhole Depth Measurement and Fuzzy Control”

Publication P5 "Inline Weld Depth Evaluation and Control Based on OCT Keyhole Depth Measurement and Fuzzy Control" (SCHMOELLER ET AL. 2022) describes the inline evaluation of keyhole depth measurement signals obtained from an OCT sensor based on ML and the fuzzy-based control of the weld depth. The foundation for the weld penetration depth evaluation, which provides the input signal for the control, was described in publications P1, P2 and P4. The fuzzy controller is based on the process model from publication P3. The focus of P5 was on the compensation of weld penetration depth changes as a result of changing process boundary conditions.

The basis of the process control is a precise evaluation of the weld depth. For this purpose, the raw signal of the OCT keyhole depth measurement was interpreted to

gain the weld depth based on an FFNN. The input variables considered in the evaluation were:

- The OCT signal from the keyhole,
- the OCT signal from the component surface as a reference,
- the OCT signal characteristics,
- the process parameters laser power, feed rate, focus diameter and angle of incidence of the laser beam,
- the material of the joining partners and
- the melt layer thickness for the corresponding process parameters.

The reference data from publication P4 formed the basis for the training. To ensure a small time offset between the signal detection and the controller response, both the data evaluation and the process control were implemented on a real-time capable industrial PLC system. The corresponding time delays of all the data processing and control loop components were characterized in publication P5. The reaction of the process controller to a deviation of the actual value took three calculation cycles in the control system used, which corresponds to a delay time of 3 ms. This temporal component included the acquisition and processing of the OCT data. As a result, the reaction time of the controller was negligible compared to the reaction time of the laser beam source to a change in the target power, which is approx. 20 ms.

The process control was validated for an overlap joint. A disturbance to the process was applied by a sudden change of the upper joining partner's thickness. This allowed for a defined change in the weld depth to be caused externally, which was compensated for by the controller for all investigated parameter combinations. The controller intervention was considered successful if the desired weld depth could be reattained within a length of 5 mm in the lower joint partner. An exemplary data-set with the progressions of the inline-evaluated weld depth used as the controlled variable as well as the desired and the actual laser power are shown in Figure 27. The deviation of the actual laser power from the desired laser power results from a delay caused by the laser beam source response.

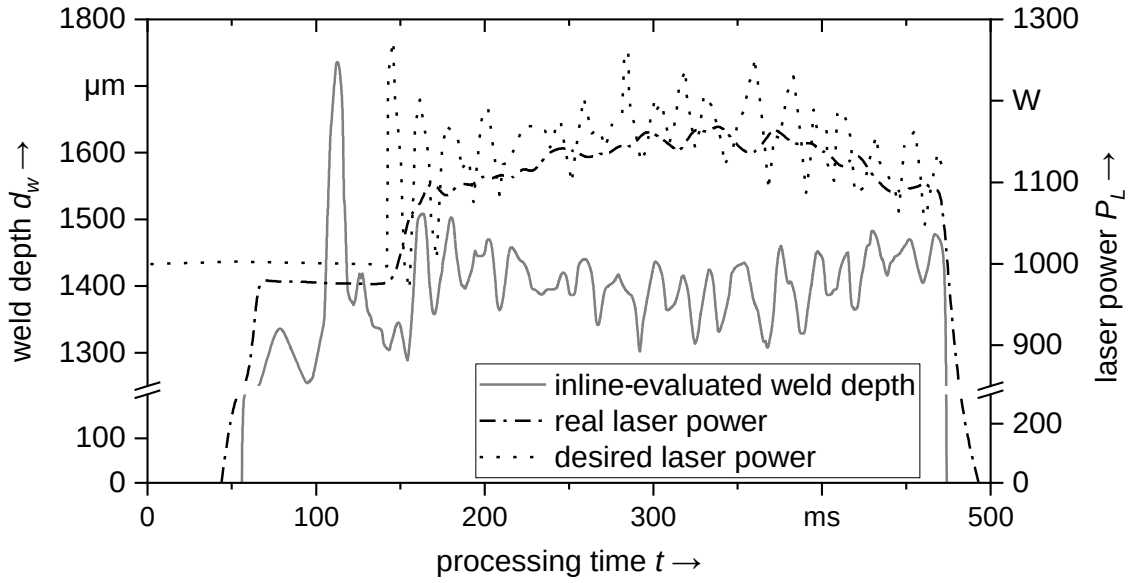

Figure 27: Exemplary illustration of a controlled process with a comparison of the inline-determined weld depth, as well as the target (desired) and actual laser power; based on SCHMOELLER ET AL. (2022)

Author's contribution

Maximilian Schmoeller developed the idea of an inline weld depth determination based on ML and the concept of a fuzzy control of the weld depth. Tony Weiss contributed to developing the data processing method as part of his student project. Korbinian Goetz and Christian Bernauer supported the development of the process control. Christian Stadter advised on the implementation of the OCT data analysis. The manuscript was written by Maximilian Schmoeller and reviewed by Christian Stadter and Michael F. Zaeh. All authors commented on the results. The contributions of the author of this dissertation to publication P5 are listed in Table 5-5.

	concept	content	manuscript	**total**
M. Schmoeller	80 %	60 %	50 %	**65 %**

Table 5-5: Contributions of the author to the conception, the development of the contents and the manuscript of publication P5

5.3 Discussion of the findings

This section briefly discusses the results of publications P1 to P5. The knowledge gained in each of these publications is compared with exemplary work from the state of the art. As shown in Figure 28, the work within this dissertation can be assigned to the three central research areas *process characterization*, *process monitoring* and *process control*.

Process characterization in this context describes the process behavior analysis in DPLW. A distinction can be made between experimental and model-based methods. The aim is to determine the relationship between the weld pool or the weld seam geometry and the process parameters. *Process monitoring* includes the inline acquisition and interpretation of information about the weld depth. Indirect and direct sensor approaches can be distinguished for the acquisition of measurement data. With indirect methods, a correlation is established between a measurable process variable and a non-measurable target variable. Direct measurement methods such as OCT for keyhole depth measurement can detect the target variable. A differentiation in filter methods and interpretation approaches can be made regarding the evaluation of process monitoring signals. *Process control* describes the weld depth control based on inline measurements of process variables. Here, classical controller architectures, i.e., linear controllers, contrast with fuzzy controllers. In addition, three target variables can be identified. Some research approaches deal with controlling the stability of a full penetration process and others try to control the weld depth or the process stability in a partial penetration process.

The publication P1 of this dissertation can be assigned to the category process monitoring. It describes the dependence of the OCT signal during the keyhole depth measurement on process parameters and boundary conditions. As shown in section 3.3, a basic understanding of the influences of the observed process on the appearance of the keyhole depth measurement signal was not available prior to this thesis. The works of DORSCH ET AL. (2017) and BOLEY ET AL. (2019b) consider similar aspects but with specific objectives for the application of the OCT sensor technology and with limited ranges of applicability. Their works aim to describe the influence of individual aspects on the signal. Thus, they underline the importance of a detailed investigation of the influencing factors as a basis for a precise inline determination of the weld depth using an OCT-based keyhole depth measurement. In particular, the systematic variation of essential process parameters and the subsequent stochastic description of the OCT signal in P1 go beyond the state of the art.

process characterization	model-based	experimental
melt pool geometry	SCHMOELLER ET AL. (2020a) P2 LIEBL ET AL. (2017)	
weld seam geometry	SCHMOELLER ET AL. (2020b) P3 STADTER ET AL. (2021)	SCHMOELLER ET AL. (2021) P4

process monitoring	indirect measurement	direct measurement
signal filter / threshold	YUSOF ET AL. (2020)	SCHMOELLER ET AL. (2019) P1 BOLEY ET AL. (2019b)
signal interpretation	STORK-WERSBORG (2010) GÜNTHER ET AL. (2015)	SCHMOELLER ET AL. (2022) P5 STADTER ET AL. (2019a)

process control	linear control	fuzzy control
full penetration control	BARDIN ET AL. (2005)	BLUG ET AL. (2012)
stability control	BIRNESSER (2011)	GÜNTHER ET AL. (2015)
weld depth control	KOS ET AL. (2020) STORK-WERSBORG (2010)	SCHMOELLER ET AL. (2022) P5

Figure 28: Classification of the publications P1 to P5 of this dissertation relative to the state of the art and assignment to the research categories process characterization, process monitoring and process control

Furthermore, it was shown in P1 that even for small focal diameters of the laser beam, resulting in small vapor capillary diameters, measurements of the keyhole depth are possible. In the measurements, the focal diameter was approx. 10 % larger than the diameter of the OCT measurement spot. Building on publication P1, SOKOLOV ET AL. (2020) were able to show a significant dependence of the OCT signal on the position of the measuring beam relative to the keyhole opening. By describing and quantifying influences on the keyhole depth measurement signal, publication P1 meets SO1, defined in section 4.2.

Publication P2, which can be assigned to the field of *process characterization* (cf. Figure 28), significantly helped to increase the accuracy of weld penetration depth determination based on a keyhole depth measurement. For this purpose, the physical relationship between the measurable depth of the keyhole and the melt pool depth, i.e., the resulting weld depth, was established. The depth difference, which results from a melt layer around the keyhole during welding, has only been indirectly accounted for in existing approaches of inline weld depth determination within the calibration of the signal evaluation. In P2, however, it was shown that the melt layer thickness has dimensions in the range of the processing laser's focal diameter. Therefore, taking it into account when interpreting the keyhole depth signal with respect to the weld depth can contribute to a significant increase in accuracy and robustness. The basic structure of the numerical model was developed by LIEBL ET AL. (2017), who performed an FEM simulation of a double-focus welding process. In particular, modeling the heat source as a geometric imitation of a keyhole with an evaporation temperature boundary condition on the capillary wall was well suited for calculating the melt layer thickness. The genetic optimization of the keyhole geometry proposed in P2 has not been considered in the literature prior to this thesis work. It was possible to prove the applicability of such an approach to the geometry of a keyhole. Thus, P2 contributed to the fulfillment of SO2 (cf. section 4.2).

Building on an experimental study, the modeling of process behavior in DPLW was investigated as part of P3. A method for *process characterization* (cf. Figure 28) was developed to determine the dependence of the weld depth and its stability on the laser power and the feed rate. A similar objective was pursued by CASALINO ET AL. (2016), who used an FFNN to evaluate the influences of shielding gas and feed rate on the pore formation and the weld geometry. LUO & SHIN (2015) also considered the parameter dependence of the weld depth in laser beam welding of steel and applied an FFNN and an RNN for the evaluation. The described approaches were well suited to represent the process behavior as a mathematical function with validity in the trained parameter range. The method based on ML in P3 goes beyond the state of the art, as a high accuracy and extrapolation capability of the weld penetration depth prediction can be achieved with reduced experimental effort. Thus, P3 represents a solution for SO5.

The accuracy of a weld depth evaluation based on the OCT keyhole depth measurement strongly depends on the available reference data. In particular, if ML-methods are used, an extensive training database must be at hand. P4 represents a method for obtaining extensive and precise reference information about the weld depth in laser welding of aluminum. A non-destructive method using microfocus X-

ray computed tomography was developed that allowed for a three-dimensional acquisition of the weld depth geometry inside a specimen. Available literature was limited to 3D-characterization of defects such as pores and cracks in welds on a microscopic scale (HAMADE & BAYDOUN 2019; EARL ET AL. 2019). SCHAFF ET AL. (2017) performed a 3D-characterization of the microstructure of the joining partners in friction stir welding. However, the measurements were allocated to the macroscopic range due to a limited measurement resolution of the X-ray dark field CT. The method in P4 represents an advancement relative to the state of the art, as it enables a precise 3D-measurement of welds without destructive testing for the first time. Hence, the requirements from SO3 were fulfilled within the scope of P4.

The results of P5 can be assigned to the areas of *process monitoring* and *process control*. A closed-loop weld penetration depth determination and control was presented. For determining the weld depth from the OCT data, the signal characteristics (P1) and the melt layer thickness (P2) were considered. The depth was calculated based on an RNN with the training data from P4. A related approach to inline data evaluation was presented by GÜNTHER ET AL. (2015). They recorded camera and diode data during the process and used it for downstream process control. The weld depth control presented in P5 is fuzzy-based. Other control approaches used classical linear controllers, which have limited validity ranges due to the non-linearity of most of the dependencies of the laser welding process (BARDIN ET AL. 2005; BIRNESSER 2011; STORK GENANNT WERSBORG 2010; KOS ET AL. 2020). By combining inline evaluation of OCT signals with a weld depth control, P5 addressed SO4 and SO6.

6 Summary and Outlook

6.1 Summary

Laser beam welding is a suitable joining process for applications with high demands on mechanical stability and seam quality. It is mainly used in applications requiring a low heat input by the welding process into the components to be joined. One application example of laser beam welding is contacting battery cells to produce electrical energy storage modules. For this application, the welding process has to be carried out in an overlap configuration with only one-sided accessibility of the joining area. A reliable joining operation must be ensured to enable an automated production process. On the one hand, the joints must have a sufficient connection interface, which is decisive for the mechanical strength and the electrical conductivity. On the other hand, the permissible weld depth must not be exceeded to avoid damaging the joining partners and underlying components.

One way to achieve the desired weld seam properties in DPLW is the inline control of the weld depth. Thereby, a non-conforming process can be excluded while quality documentation can be carried out in real-time. Various measuring systems can obtain information about the process state during laser beam welding. For example, camera systems are used to acquire images of the process zone. Systems for detecting process emissions, i.e., the characteristic radiation of a process or the back reflection of laser radiation from the processing zone, can also provide information on the processing conditions. To determine the weld depth from the acquired signals, correlations between the measured data and the corresponding depth must be found. Hence, such methods are referred to as indirect measurement systems. In contrast, the keyhole depth can be directly measured during welding based on an interferometric measurement, called Optical Coherence Tomography. The measurement radiation is guided coaxially through the welding optics into the process zone, i.e., the keyhole, where it is reflected. A length difference is determined between the reflected measuring radiation and a reference signal from the component surface. The result is

distance information at measurement frequencies in the kilohertz range. The acquired signal is strongly dependent on the process boundary conditions and parameters. In addition, a difference between the keyhole and the weld depth results from a melt layer below the keyhole. Its thickness can be calculated numerically. After the keyhole depth signal has been interpreted in terms of the weld depth, considering the melt layer thickness, it can be used as an absolute value for process control.

The chapter on the state of the art in this thesis covers approaches in the field of laser material processing, with a detailed discussion of process monitoring (cf. section 3.2), the application of Optical Coherence Tomography (cf. section 3.3) and process control (cf. section 3.4). The identified need for action can be summarized as follows:

- The influences of the process parameters on the OCT keyhole depth measurement signal are commonly neglected when determining the weld depth. In that case, the determination was only valid for a limited range of process parameters. Hence, a quantitative model of the influencing variables on the OCT keyhole depth signal as a function of process parameters and boundary conditions needed to be derived.
- The melt layer enclosing the keyhole during DPLW leads to an offset between the measurable keyhole depth and the weld depth. This deviation must be considered when determining the weld depth based on keyhole depth measurements.
- The basis of flexible process control for laser beam welding is a description of the process behavior with a wide range of validity. An efficient and real-time capable prediction model for the weld depth as a function of process parameters needed to be determined from this.
- A weld depth control for DPLW needed to be developed based on the keyhole depth measurement. It is characterized by simple parameterization and flexible adaptability to changing process boundary conditions.

The scientific approach of this work includes the quantitative description of the OCT keyhole depth signal as a function of the process parameters (cf. sub-section 5.2.1) and the FEM-based determination of the melt layer thickness around the keyhole (cf. sub-section 5.2.2). Furthermore, the process behavior during DPLW (cf. sub-section 5.2.3) as well as a method for the comprehensive three-dimensional characterization of the weld seam geometry in the inner area of weld seam samples (cf. sub-section 5.2.4) is described. These individual aspects of the research approach are combined in an inline weld depth control loop (cf. sub-section 5.2.5). For each considered aspect, an enhancement compared to the state of the art was achieved (cf. section 5.3).

Of particular importance is the method for three-dimensional characterization of weld geometries inside the component, based on microfocus X-ray computed tomography. The high-resolution data-sets can provide information about the relationship between the process dynamics and resulting quality characteristics of welds, such as weld defects or penetration depth variations. In addition, the availability of reference data for welding processes, which was previously difficult to generate, is the basis for significant improvements in the accuracy of process monitoring systems, as demonstrated by the OCT data evaluation in sub-section 5.2.5.

6.2 Outlook

Based on the findings within the framework of this thesis, several advancement potentials can be identified, which are described in the following.

Joint geometry of the components

The experimental investigations in the publications, presented in the sub-sections 5.2.1 to 5.2.5, were performed using bead on plate welds. This simplification was made to avoid interference of the OCT signal with the joint geometry and to investigate the keyhole depth measurement signal systematically. One way to extend the applicability of weld depth control to the reliable and flexible welding of two components is to consider the joint geometry when determining the weld depth. For this purpose, the algorithm for interpreting the OCT signal must be modified and extended to include the joint geometry as an input variable. This step also includes investigating the geometric influences on the signal characteristics as described in sub-section 5.2.1, without considering the joint geometry. Another aspect to be examined for this purpose is the influence of the position of the OCT measurement spot relative to the opening of the keyhole. The dedicated characterization and consideration of this influencing variable have already been shown by SOKOLOV ET AL. (2020) and SOKOLOV ET AL. (2021) to join two sheet metal components in a fillet weld configuration. The approach can be extended to other joint geometries in further studies.

Material adaptability

In publication P1 (cf. sub-section 5.2.1), the influence of the material on the OCT signal characteristics during keyhole depth measurement was investigated. However, the subsequent publications focused on the aluminum alloys AA6082 (cf. sub-

sections 5.2.2, 0 and 5.2.5) and AA2219 (cf. sub-section 5.2.4). This limitation was introduced based on the results of sub-section 5.2.1. The measurement of the keyhole depth in aluminum, compared to copper, presents a greater challenge due to the high scattering of the OCT signal within the keyhole. Future studies may enable OCT-based weld penetration depth evaluation and control for other materials such as steel or copper. In addition, the weld depth is an important process variable for manufacturing components with dissimilar metals to be joined. For example, aluminum and copper components are typically welded in an overlap configuration, with laser radiation coupled to the aluminum component. High joint-strengths can be achieved if a low degree of intermixing of the materials is achieved, as this avoids the formation of brittle intermetallic phases (HOLLATZ ET AL. 2020a). The targeted penetration into the overlying aluminum component can be ensured with weld depth control. An indication of the correct penetration depth may also be provided by the change in OCT signal characteristics induced by the keyhole reaching the copper component.

Technology integration

The technological platform for the introduced weld depth control is a fixed optics system with an integrated OCT sensor system. In industrial applications like car-body or battery-storage production, fixed-optics are widely used. However, for brilliant laser radiation with small focal diameters and high intensity, galvanometer scanning optics are preferred for industrial applications, since they allow for a highly dynamic deflection of a laser beam. To achieve a widening of the weld seam in a stable processing regime, additional oscillation trajectories of the focal point can be superimposed on the feed motion along the weld seam (SCHWEIER ET AL. 2016). Various technical enhancements are necessary to employ weld depth control in a scanner welding system. In particular, a highly dynamic positioning of the OCT measurement spot relative to the focal point of the processing laser is required, since the relative positioning accuracy of the measurement and the processing spot depends on the accuracy of the scanner system. Consequently, a calibration method for the measuring system must be provided to position the OCT focal point over the entire processing field of the scanning optics.

7 References[16]

AALDERINK ET AL. 2007

Aalderink, B. J.; Lange, D. F.; Aarts, R. G.; Meijer, J.: Keyhole shapes during laser welding of thin metal sheets. Journal of Physics D: Applied Physics 40 (2007) 17, pp. 5388–5393.

ABT ET AL. 2011

Abt, F.; Boley, M.; Weber, R.; Graf, T.: X-ray videography for investigation of capillary and melt pool dynamics in different materials. ICALEO Conference Proceedings. Orlando, USA, 23.10.–27.10.: Laser Institute of America 2011, pp. 179–186. ISBN: 978-0-912035-94-9.

ABT 2017

Abt, F.: Bildbasierte Charakterisierung und Regelung von Laserschweißprozessen. Diss. Universität Stuttgart. Munich, Germany: Utz 2017. ISBN: 978-3-8316-4691-3.

ALLEN ET AL. 2020

Allen, T. R.; Huang, W.; Tanner, J. R.; Tan, W.; Fraser, J. M.; Simonds, B. J.: Energy-Coupling Mechanisms Revealed through Simultaneous Keyhole Depth and Absorptance Measurements during Laser-Metal Processing. Physical review applied 13 (2020) 6.

ALLMEN & BLATTER 1995

Allmen, M.; Blatter, A.: Laser-Beam Interactions with Materials. Berlin, Germany: Springer 1995. ISBN: 978-3-540-59401-7.

[16] Wherever no bibliographic indices are given, the information is not available or not known to the author.

BARDIN ET AL. 2005
Bardin, F.; Cobo, A.; Lopez-Higuera, J. M.; Collin, O.; Aubry, P.; Dubois, T.; Högström, M.; Nylen, P.;Jonsson, P.; Jones, J. D. C.; Hand, D. P.: Closed-loop power and focus control of laser welding for full-penetration monitoring. Applied optics 44 (2005) 1, pp. 13–21.

BAUTZE ET AL. 2015
Bautze, T.; Moser, R.; Strebel, M.; Kogel-Hollacher, M.: Use of inline coherent imaging for laser welding processes: Process control and beyond. Lasers in Manufacturing. Munich, Germany, 22.06.–25.06. 2015.

BAUTZE & KOGEL-HOLLACHER 2014
Bautze, T.; Kogel-Hollacher, M.: Keyhole Depth is just a Distance. Laser Technik Journal 11 (2014) 4, pp. 39–43.

BENGIO ET AL. 1994
Bengio, Y.; Simard, P.; Frasconi, P.: Learning long-term dependencies with gradient descent is difficult. IEEE transactions on neural networks 5 (1994) 2, pp. 157–166.

BEYER 1995
Beyer, E.: Schweißen mit Laser. Berlin, Germany: Springer 1995. ISBN: 978-3-642-75760-0.

BIRNESSER 2011
Birnesser, A. J.: Prozessregelung beim Laserstrahlschweißen. Diss. Universität Stuttgart. Munich, Germany: Utz 2011. ISBN: 978-3-8316-4133-8.

BLECHER ET AL. 2014
Blecher, J. J.; Galbraith, C. M.; van Vlack, C.; Palmer, T. A.; Fraser, J. M.; Webster, P. J.; DebRoy, T.: Real time monitoring of laser beam welding keyhole depth by laser interferometry. Science and Technology of Welding and Joining 19 (2014) 7, pp. 560–564.

BLIEDTNER ET AL. 2013
Bliedtner, J.; Müller, H.; Barz, A.: Lasermaterialbearbeitung. Grundlagen, Verfahren, Anwendungen, Beispiele. Munich, Germany: Hanser-Verlag 2013. ISBN: 978-3-446-42168-4.

BLUG ET AL. 2011

Blug, A.; Carl, D.; Höfler, H.; Abt, F.; Heider, A.; Weber, R.; Nicolosi, L.; Tetzlaff, R.: Closed-loop Control of Laser Power using the Full Penetration Hole Image Feature in Aluminum Welding Processes. Physics Procedia 12 (2011), pp. 720–729.

BLUG ET AL. 2012

Blug, A.; Abt, F.; Nicolosi, L.; Heider, A.; Weber, R.; Carl, D.; Höfler, H.; Tetzlaff, R.: The full penetration hole as a stochastic process. Controlling penetration depth in keyhole laser-welding processes. Applied Physics B 108 (2012) 1, pp. 97–107.

BÖCKH & WETZEL 2014

Böckh, P.; Wetzel, T.: Wärmeübertragung. Grundlagen und Praxis. Berlin, Germany: Springer 2014. ISBN: 978-3-642-37730-3.

BOHN & UNBEHAUEN 2016

Bohn, C.; Unbehauen, H.: Identifikation dynamischer Systeme. Methoden zur experimentellen Modellbildung aus Messdaten. Wiesbaden, Germany: Springer 2016. ISBN: 978-3-8348-1755-6.

BOLEY ET AL. 2019a

Boley, M.; Fetzer, F.; Weber, R.; Graf, T.: High-speed x-ray imaging system for the investigation of laser welding processes. Journal of Laser Applications 31 (2019) 4.

BOLEY ET AL. 2019b

Boley, M.; Fetzer, F.; Weber, R.; Graf, T.: Statistical evaluation method to determine the laser welding depth by optical coherence tomography. Optics and Lasers in Engineering 119 (2019), pp. 56–64.

BOLLIG ET AL. 2005

Bollig, A.; Mann, S.; Beck, R.; Kaierle, S.: Einsatz optischer Technologien zur Regelung des Laserstrahlschweißprozesses. at - Automatisierungstechnik 53 (2005) 10/2005.

BROKATE 2012

Brokate, M.: Hysteresis and phase transitions. New York, USA: Springer 2012. ISBN: 978-1-4612-8478-9.

CARNEIRO ET AL. 2007
Carneiro, G.; Chan, A. B.; Moreno, P. J.; Vasconcelos, N.: Supervised learning of semantic classes for image annotation and retrieval. IEEE transactions on pattern analysis and machine intelligence 29 (2007) 3, pp. 394–410.

CASALINO ET AL. 2016
Casalino, G.; Facchini, F.; Mortello, M.; Mummolo, G.: ANN modelling to optimize manufacturing processes: the case of laser welding. IFAC 49 (2016) 12, pp. 378–383.

CHINN ET AL. 1997
Chinn, S. R.; Swanson, E. A.; Fujimoto, J. G.: Optical coherence tomography using a frequency-tunable optical source. Optics letters 22 (1997) 5, pp. 340–342.

CONNOR ET AL. 1994
Connor, J. T.; Martin, R. D.; Atlas, L. E.: Recurrent neural networks and robust time series prediction. IEEE transactions on neural networks 5 (1994) 2, pp. 240–254.

CUNNINGHAM ET AL. 2019
Cunningham, R.; Zhao, C.; Parab, N.; Kantzos, C.; Pauza, J.; Fezzaa, K.; Sun, T.; Rollett, A. D.: Keyhole threshold and morphology in laser melting revealed by ultrahigh-speed x-ray imaging. Science 363 (2019) 6429, pp. 849–852.

DAGGE ET AL. 2009
Dagge, L.; Harr, K.; Paul, M.; Schnedl, G.: Classification of process analysis: offline, atline, online, inline. Cement International 7 (2009) 5, pp. 72–81.

DAHOTRE & HARIMKAR 2008
Dahotre, N. B.; Harimkar, S. P.: Laser Fabrication and Machining of Materials. New York, USA: Springer 2008. ISBN: 978-0-387-72343-3.

DIMITROVA & WEIS 2008
Dimitrova, T. L.; Weis, A.: The wave-particle duality of light: A demonstration experiment. American Journal of Physics 76 (2008) 2, pp. 137–142.

DONGES & NOLL 2015
Donges, A.; Noll, R.: Laser measurement technology. Fundamentals and applications. Berlin, Germany: Springer 2015. ISBN: 978-3-662-43633-2.

DÖRN 2018
Dörn, S.: Programmieren für Ingenieure und Naturwissenschaftler. Berlin, Germany: Springer 2018. ISBN: 978-3-662-54303-0.

DORSCH ET AL. 2016
Dorsch, F.; Harrer, T.; Haug, P.; Plasswich, S.: Process control using capillary depth measurement. ICALEO Conference Proceedings. San Diego, USA, 16.10.–20.10.: Laser Institute of America 2016, p. 1505–1505. ISBN: 978-1-940168-17-3.

DORSCH ET AL. 2017
Dorsch, F.; Dubitzky, W.; Effing, L.; Haug, P.; Hermani, J.-P.; Plasswich, S.: Capillary depth measurement for process control. In: Kaierle, S. et al. (Eds.): High-Power Laser Materials Processing: Applications, Diagnostics, and Systems VI, SPIE LASE. San Francisco, USA, 28.01.: SPIE 2017.

DREXLER & FUJIMOTO 2015. Drexler, W.; Fujimoto, J. G.: Optical coherence tomography. Technology and applications. Cham, Switzerland: Springer 2015. ISBN: 978-3-319-06418-5.

EARL ET AL. 2019
Earl, S.; Rankin, K. E.; Lewis, R.; Smith, L.; Rainforth, W. M.: Verification of the use of Micro-CT scanning to assess the features of entire squat type defects. Wear 438-439 (2019) 1, pp. 203074–203074.

EICHLER & EICHLER 2010
Eichler, J.; Eichler, H.: Laser. Bauformen, Strahlführung, Anwendungen. Berlin, Germany: Springer 2010. ISBN: 978-3-642-10462-6.

ERTEL 2016
Ertel, W.: Grundkurs Künstliche Intelligenz. Eine praxisorientierte Einführung. Wiesbaden, Germany: Springer 2016. ISBN: 978-3-658-13548-5.

FETZER ET AL. 2017
Fetzer, F.; Boley, M.; Weber, R.; Graf, T.: Comprehensive analysis of the capillary depth in deep penetration laser welding. In: Kaierle, S. et al. (Eds.): High-Power Laser Materials Processing: Applications, Diagnostics, and Systems VI, SPIE LASE. San Francisco, USA, 28.01.: SPIE 2017, pp. 1009709–1009709.

FÖLLINGER ET AL. 2013
Föllinger, O.; Konigorski, U.; Lohmann, B.; Roppenecker, G.; Trächtler, A.: Regelungstechnik. Einführung in die Methoden und ihre Anwendung. Berlin, Germany: VDE-Verlag 2013. ISBN: 978-3-8007-3231-9.

FRASER 2011
Fraser, J. M.: Inline coherent imaging of laser processing. In: Heisterkamp, A. et al. (Eds.): Frontiers in Ultrafast Optics: Biomedical, Scientific, and Industrial Applications XI, SPIE LASE. San Francisco, USA, 22.01.: SPIE 2011, p. 792516–792516.

FRASER 2012
Fraser, J. M.: Laser process monitoring and automatic control at kHz rates through inline coherent imaging. In: Phipps, C. (Eds.): International Symposium on High Power Laser Ablation 2012. New Mexico, USA, 30.04.–03.05.: American Institute of Physics 2012, pp. 492–496. ISBN: 978-0-7354-1068-8.

GERS ET AL. 2000
Gers, F. A.; Schmidhuber, J.; Cummins, F.: Learning to forget: continual prediction with LSTM. Neural Computation 12 (2000) 10, pp. 2451–2471.

GOODFELLOW ET AL. 2016
Goodfellow, I.; Bengio, Y.; Courville, A.: Deep learning. Cambridge, USA: MIT Press 2016. ISBN: 978-0-26203-561-3.

GRAF 2015
Graf, T.: Laser. Grundlagen der Laserstrahlerzeugung. Wiesbaden, Germany: Springer 2015. ISBN: 978-3-658-07953-6.

GÜNTHER ET AL. 2015
Günther, J.; Pilarski, P. M.; Helfrich, G.; Shen, H.; Diepold, K.: Intelligent laser welding through representation, prediction, and control learning: An architecture with deep neural networks and reinforcement learning. Mechatronics 34 (2015), pp. 1–11.

HAMADE & BAYDOUN 2019

Hamade, R. F.; Baydoun, A. M.: Nondestructive detection of defects in friction stir welded lap joints using computed tomography. Materials and Design 162 (2019), pp. 10–23.

HAUBOLD ET AL. 2017

Haubold, M. W.; Wulf, L.; Zaeh, M. F.: Validation of a spatter detection algorithm for remote laser welding applications. Journal of Laser Applications 29 (2017) 2, pp. 22011–22011.

HAUBOLD & ZAEH 2019

Haubold, M. W.; Zaeh, M. F.: Real-time spatter detection in laser welding with beam oscillation. Procedia CIRP 79 (2019), pp. 159–164.

HEBER ET AL. 2013

Heber, M.; Lenz, M.; Rüther, M.; Bischof, H.; Fronthaler, H.; Croonen, G.: Weld seam tracking and panorama image generation for on-line quality assurance. International Journal of Advanced Manufacturing Technology 65 (2013) 9-12, pp. 1371–1382.

HEIDER ET AL. 2013

Heider, A.; Sollinger, J.; Abt, F.; Boley, M.; Weber, R.; Graf, T.: High-Speed X-Ray Analysis of Spatter Formation in Laser Welding of Copper. Physics Procedia 41 (2013), pp. 112–118.

HIGGINS ET AL. 2017

Higgins, I.; Matthey, L.; Pal, A.; Burgess, C.; Glorot, X.; Botvinick, M.: beta-VAE: Learning Basic Visual Concepts with a Constrained Variational Framework. 5th International Conference on Learning Representations. Toulon, France, 24.–26.04. 2017.

HOCHREITER & SCHMIDHUBER 1997

Hochreiter, S.; Schmidhuber, J.: Long Short-Term Memory. Neural Computation 9 (1997) 8, pp. 1735–1780.

HOLLATZ ET AL. 2020a

Hollatz, S.; Heinen, P.; Limpert, E.; Olowinsky, A.; Gillner, A.: Overlap joining of aluminium and copper using laser micro welding with spatial power modulation. Welding in the World 64 (2020) 3, pp. 513–522.

HOLLATZ ET AL. 2020b
Hollatz, S.; Hummel, M.; Jaklen, L.; Lipnicki, W.; Olowinsky, A.; Gillner, A.: Processing of Keyhole Depth Measurement Data during Laser Beam Micro Welding. Journal of Materials: Design and Applications 234 (2020) 5, pp. 722–731.

HUANG ET AL. 1991
Huang, D.; Swanson, E. A.; Lin, C. P.; Schuman, J. S.; Stinson, W. G.; Chang, W.; Hee, M. R.; Flotte, T.;Gregory, K.; Puliafito, C. A.: Optical coherence tomography. Science 254 (1991) 5035, pp. 1178–1181.

HÜGEL & GRAF 2009
Hügel, H.; Graf, T.: Laser in der Fertigung. Strahlquellen, Systeme, Fertigungsverfahren. Wiesbaden, Germany: Vieweg 2009. ISBN: 978-3-8351-0005-3.

ITEN ET AL. 2020
Iten, R.; Metger, T.; Wilming, H.; Del Rio, L.; Renner, R.: Discovering Physical Concepts with Neural Networks. Physical Review Letters 124 (2020) 1, pp. 10508–10508.

JAIN ET AL. 1999
Jain, A. K.; Murty, M. N.; Flynn, P. J.: Data clustering. ACM Computing Surveys 31 (1999) 3, pp. 264–323.

JI ET AL. 2015
Ji, Y.; Grindal, A. W.; Webster, P. J.; Fraser, J. M.: Real-time depth monitoring and control of laser machining through scanning beam delivery system. Journal of Physics D: Applied Physics 48 (2015) 15, pp. 155301–155301.

KAMPKER & NOWACKI 2014
Kampker, A.; Nowacki, C.: Elektromobilproduktion. Berlin, Germany: Springer 2014. ISBN: 978-3-64242-021-4.

KARKHIN 2019
Karkhin, V. A.: Thermal processes in welding. Singapore: Springer 2019. ISBN: 978-981-13-5964-4.

KATAYAMA 2020

Katayama, S.: Fundamentals and details of laser welding. Singapore: Springer 2020. ISBN: 978-981-15-7932-5.

KESSLER 2006

Kessler, R. W.: Prozessanalytik. Strategien und Fallbeispiele aus der industriellen Praxis. Weinheim, Germany: Wiley-VCH 2006. ISBN: 978-3-527-31196-5.

KIENDL 1997

Kiendl, H.: Fuzzy Control methodenorientiert. Munich, Germany: Oldenbourg Wissenschaftsverlag 1997. ISBN: 978-3-486-23554-8.

KOGEL-HOLLACHER ET AL. 2014

Kogel-Hollacher, M.; Schoenleber, M.; Bautze, T.: Inline Coherent Imaging of Laser Processing. In: Schmidt, M. et al. (Eds.): Proceedings of the 8th LANE, Laser Assisted Net Shape Engineering 8. Fuerth, Germany, 08.09.–11.09. Amsterdam, Netherlands: Elsevier 2014.

KOGEL-HOLLACHER ET AL. 2016

Kogel-Hollacher, M.; Schoenleben, M.; Bautze, T.; Strebel, M.; Moser, R.: Measurement and closed-loop control of the penetration depth in laser materials processing. In: Schmidt, M. et al. (Eds.): Proceedings of the 9th LANE, Laser Assisted Net Shape Engineering 9. Fuerth, Germany, 19.09.–22.09. Amsterdam, Netherlands: Elsevier 2016.

KOGEL-HOLLACHER ET AL. 2017

Kogel-Hollacher, M.; Schoenleber, M.; Schulze, J.; Pichot, J. F.: Inline measurement for quality control from macro to micro laser applications. In: Neuenschwander, B. et al. (Eds.): Laser Applications in Microelectronic and Optoelectronic Manufacturing (LAMOM) XXII, SPIE LASE. San Francisco, USA, 28.01.: SPIE 2017.

KONUK ET AL. 2011

Konuk, A. R.; Aarts, R. G.; Huis int Veld, A. J.; Sibillano, T.; Rizzi, D.; Ancona, A.: Process Control of Stainless Steel Laser Welding using an Optical Spectroscopic Sensor. Physics Procedia 12 (2011), pp. 744–751.

KOS ET AL. 2019

Kos, M.; Arko, E.; Kosler, H.; Jezeršek, M.: Remote laser welding with in-line adaptive 3D seam tracking. The International Journal of Advanced Manufacturing Technology 103 (2019) 9-12, pp. 4577–4586.

KOS ET AL. 2020
Kos, M.; Arko, E.; Kosler, H.; Jezeršek, M.: Penetration-depth control in a remote laser-welding system based on an optical triangulation loop. Optics and Lasers in Engineering 139 (2020), pp. 106464–106464.

KRAMER 2009
Kramer, O.: Computational Intelligence. Berlin, Germany: Springer 2009. ISBN: 978-3-540-79738-8.

LECUN ET AL. 2015
LeCun, Y.; Bengio, Y.; Hinton, G. E.: Deep learning. Nature 521 (2015) 7553, pp. 436–444.

LEE & NA 2002
Lee, S. K.; Na, S. J.: A study on automatic seam tracking in pulsed laser edge welding by using a vision sensor without an auxiliary light source. Journal of Manufacturing Systems 21 (2002) 4, pp. 302–315.

LIEBL ET AL. 2017
Liebl, S.; Stadter, C.; Ganser, A.; Zaeh, M. F.: Numerical simulation of laser beam welding using an adapted intensity distribution. Journal of Laser Applications 29 (2017) 2, pp. 22405–22405.

LUNZE 2020
Lunze, J.: Systemtheoretische Grundlagen, Analyse und Entwurf einschleifiger Regelungen. Berlin, Germany: Springer 2020. ISBN: 978-3-642-13808-9.

LUO & SHIN 2015
Luo, M.; Shin, Y. C.: Estimation of keyhole geometry and prediction of welding defects during laser welding based on a vision system and a radial basis function neural network. International Journal of Advanced Manufacturing Technology 81 (2015) 1-4, pp. 263–276.

MACKAY 2011
MacKay, D. J.: Information theory, inference, and learning algorithms. Cambridge, USA: Cambridge University Press 2011. ISBN: 978-0-521-64298-9.

MARSLAND 2014
Marsland, S.: Machine Learning. An Algorithmic Perspective. Hoboken, USA: CRC Press 2014. ISBN: 978-1-4665-8328-3.

MICHEL 2004

Michel, J.: Approximatives Modell für das Tiefschweißen mit Laserstrahlung. Diss. Rheinisch-Westfälische Technische Hochschule Aachen. Aachen, Germany: Shaker 2004. ISBN: 978-3-8322-2407-3.

MITTELSTÄDT ET AL. 2019

Mittelstädt, C.; Mattulat, T.; Seefeld, T.; Kogel-Hollacher, M.: Novel approach for weld depth determination using optical coherence tomography measurement in laser deep penetration welding of aluminum and steel. Journal of Laser Applications 31 (2019) 2.

MNIH ET AL. 2015

Mnih, V.; Kavukcuoglu, K.; Silver, D.; Rusu, A. A.; Veness, J.; Bellemare, M. G.; Graves, A.; Riedmiller, M.;Fidjeland, A. K.; Ostrovski, G.; Petersen, S.; Beattie, C.; Sadik, A.; Antonoglou, I.; King, H.; Kumaran, D.; Wierstra, D.; Legg, S.; Hassabis, D.: Human-level control through deep reinforcement learning. Nature 518 (2015) 7540, pp. 529–533.

MOZER 1992

Mozer, M. C.: Introduction of multiscale temporal structure. In: Lippmann, D. S. et al. (Eds.): Advances in neural information processing systems 4. San Mateo, USA. Cambridge: MIT Press 1992, pp. 275–282.
ISBN: 978-0-26256-145-7.

NIEBLES ET AL. 2008

Niebles, J. C.; Wang, H.; Fei-Fei, L.: Unsupervised Learning of Human Action Categories Using Spatial-Temporal Words. International Journal of Computer Vision 79 (2008) 3, pp. 299–318.

NOROOZI & FAVARO 2016

Noroozi, M.; Favaro, P.: Unsupervised Learning of Visual Representations by Solving Jigsaw Puzzles. In: Leibe, B. et al. (Eds.): Computer Vision – ECCV 2016. Cham, Switzerland: Springer 2016, pp. 69–84.
ISBN: 978-3-319-46465-7.

POPRAWE 2005

Poprawe, R.: Lasertechnik für die Fertigung. Berlin, Germany: Springer 2005. ISBN: 978-3-540-21406-9.

PURTONEN ET AL. 2014

Purtonen, T.; Kalliosaari, A.; Salminen, A.: Monitoring and Adaptive Control of Laser Processes. Physics Procedia 56 (2014), pp. 1218–1231.

RENK 2012
Renk, K. F.: Basics of Laser Physics. For Students of Science and Engineering. Heidelberg, Germany: Springer 2012. ISBN: 978-3-642-23564-1.

SCHAFF ET AL. 2017
Schaff, F.; Bachmann, A.; Zens, A.; Zaeh, M. F.; Pfeiffer, F.; Herzen, J.: Grating-based X-ray dark-field computed tomography for the characterization of friction stir welds: A feasibility study. Materials Characterization 129 (2017), pp. 143–148.

SCHAUMBERGER ET AL. 2019
Schaumberger, K.; Beck, M.; Saffer, J.; Kaufmann, F.; Ermer, J.; Roth, S.; Schmidt, M.: Improving process reliability by means of detection of weld seam irregularities in copper via thermographic process monitoring. Procedia Manufacturing 36 (2019), pp. 58–63.

SCHMOELLER ET AL. 2019
Schmoeller, M.; Stadter, C.; Liebl, S.; Zaeh, M. F.: Inline weld depth measurement for high brilliance laser beam sources using optical coherence tomography. Journal of Laser Applications 31 (2019) 2, 022409-1–022409-9.

SCHMOELLER ET AL. 2020a
Schmoeller, M.; Stadter, C.; Wagner, M.; Zaeh, M. F.: Investigation of the influences of the process parameters on the weld depth in laser beam welding of AA6082 using machine learning methods. Procedia CIRP 94 (2020), pp. 702–707.

SCHMOELLER ET AL. 2020b
Schmoeller, M.; Neureiter, M.; Stadter, C.; Zaeh, M. F.: Numerical weld pool simulation for the accuracy improvement of inline weld depth measurement based on optical coherence tomography. Journal of Laser Applications 32 (2020) 2, pp. 022036-1–022036-9.

SCHMOELLER ET AL. 2021
Schmoeller, M.; Stadter, C.; Kick, M.; Geiger, C.; Zaeh, M. F.: A Novel Approach for the Holistic 3D-Characterization of Weld Seams - Paving the Way for Deep Learning Based Process Monitoring. Materials 14 (2021) 1.

SCHMOELLER ET AL. 2022
Schmoeller, M.; Weiß, T.; Goetz, K.; Stadter, C.; Bernauer, C.; Zaeh, M. F.: Inline Weld Depth Evaluation and Control Based on OCT Keyhole Depth Measurement and Fuzzy Control. Processes 10 (2022) 1.

SCHNEIDER 2008
Schneider, W.: Praktische Regelungstechnik. Wiesbaden, Germany: Vieweg 2008. ISBN: 978-3-528-24662-4.

SCHRÖDER & BUSS 2017
Schröder, D.; Buss, M.: Intelligente Verfahren. Identifikation und Regelung nichtlinearer Systeme. Berlin, Germany: Springer 2017. ISBN: 978-3-662-55326-8.

SCHWEIER ET AL. 2016
Schweier, M.; Haubold, M. W.; Zaeh, M. F.: Analysis of spatters in laser welding with beam oscillation: A machine vision approach. CIRP Journal of Manufacturing Science and Technology 14 (2016), pp. 35–42.

SHALEV-SHWARTZ & BEN-DAVID 2014
Shalev-Shwartz, S.; Ben-David, S.: Understanding machine learning. From theory to algorithms. Cambridge, USA: Cambridge University Press 2014. ISBN: 978-1-107-05713-5.

SHEVCHIK ET AL. 2019
Shevchik, S.; Le-Quang, T.; Farahani, F. V.; Faivre, N.; Meylan, B.; Zanoli, S.; Wasmer, K.: Laser Welding Quality Monitoring via Graph Support Vector Machine With Data Adaptive Kernel. IEEE Access 7 (2019), pp. 93108–93122.

SILVER ET AL. 2016
Silver, D.; Huang, A.; Maddison, C. J.; Guez, A.; Sifre, L.; van den Driessche, G.; Schrittwieser, J.; Antonoglou, I.;Panneershelvam, V.; Lanctot, M.; Dieleman, S.; Grewe, D.; Nham, J.; Kalchbrenner, N.; Sutskever, I.; Lillicrap, T.; Leach, M.; Kavukcuoglu, K.; Graepel, T.; Hassabis, D.: Mastering the game of Go with deep neural networks and tree search. Nature 529 (2016), pp. 484–489.

SIMONDS ET AL. 2018
Simonds, B. J.; Sowards, J.; Hadler, J.; Pfeif, E.; Wilthan, B.; Tanner, J.; Harris, C.; Williams, P.; Lehman, J.: Time-Resolved Absorptance and Melt Pool Dynamics during Intense Laser Irradiation of a Metal. Physical review applied 10 (2018) 4.

SOKOLOV ET AL. 2020
Sokolov, M.; Franciosa, P.; Al Botros, R.; Ceglarek, D.: Keyhole mapping to enable closed-loop weld penetration depth control for remote laser welding of aluminum components using optical coherence tomography. Journal of Laser Applications 32 (2020) 3.

SOKOLOV ET AL. 2021
Sokolov, M.; Franciosa, P.; Sun, T.; Ceglarek, D.; Dimatteo, V.; Ascari, A.; Fortunato, A.; Nagel, F.: Applying optical coherence tomography for weld depth monitoring in remote laser welding of automotive battery tab connectors. Journal of Laser Applications 33 (2021) 1.

SRAJBR ET AL. 2011
Srajbr, C.; Tanasie, G.; Dilger, K.; Boehm, S.: Active Thermography for Quality Assurance of joints in automobile manufacturing. Welding in the World 55 (2011) 7-8, pp. 90–97.

STADTER ET AL. 2019
Stadter, C.; Schmoeller, M.; Zeitler, M.; Tueretkan, V.; Munzert, U.; Zaeh, M. F.: Process control and quality assurance in remote laser beam welding by optical coherence tomography. Journal of Laser Applications 31 (2019) 2, pp. 022408-1–022408-9.

STADTER ET AL. 2020a
Stadter, C.; Kick, M. K.; Schmoeller, M.; Zaeh, M. F.: Correlation analysis between the beam propagation and the vapor capillary geometry by machine learning. Procedia CIRP 94 (2020), pp. 742–747.

STADTER ET AL. 2020b
Stadter, C.; Schmoeller, M.; Rhein, L.; Zaeh, M. F.: Real-time prediction of quality characteristics in laser beam welding using optical coherence tomography and machine learning. Journal of Laser Applications 32 (2020) 2, pp. 022046-1–022046-9.

STAVRIDIS ET AL. 2018

Stavridis, J.; Papacharalampopoulos, A.; Stavropoulos, P.: Quality assessment in laser welding: a critical review. The International Journal of Advanced Manufacturing Technology 94 (2018) 5-8, pp. 1825–1847.

STENBERG ET AL. 2017

Stenberg, T.; Barsoum, Z.; Åstrand, E.; Öberg, A.; Schneider, C.; Hedegård, J.: Quality control and assurance in fabrication of welded structures subjected to fatigue loading. Welding in the World 61 (2017) 5, pp. 1003–1015.

STORK GENANNT WERSBORG 2010

Stork genannt Wersborg, I. B.: A Cognitive Architecture For Production Systems such as Laser Material Processing. Diss. Technische Universität München. 2010.

STRITT ET AL. 2016

Stritt, P.; Boley, M.; Heider, A.; Fetzer, F.; Jarwitz, M.; Weller, D.; Weber, R.; Berger, P.; Graf, T.: Comprehensive process monitoring for laser welding process optimization. In: Dorsch, F. et al. (Eds.): High-Power Laser Materials Processing: Lasers, Beam Delivery, Diagnostics, and Applications V, SPIE LASE. San Francisco, USA, 13.02.: SPIE 2016.

SVENUNGSSON ET AL. 2015

Svenungsson, J.; Choquet, I.; Kaplan, A. F.: Laser Welding Process – A Review of Keyhole Welding Modelling. Physics Procedia 78 (2015), pp. 182–191.

TOMLINS & WANG 2005

Tomlins, P. H.; Wang, R. K.: Theory, developments and applications of optical coherence tomography. Journal of Physics D: Applied Physics 38 (2005) 15, pp. 2519–2535.

TRÄGER 2012

Träger, F.: Springer Handbook of Lasers and Optics. Berlin, Germany: Springer 2012. ISBN: 978-3-642-19408-5.

TURAGA ET AL. 2010

Turaga, S. C.; Murray, J. F.; Jain, V.; Roth, F.; Helmstaedter, M.; Briggman, K.; Denk, W.; Seung, H. S.: Convolutional networks can learn to generate affinity graphs for image segmentation. Neural Computation 22 (2010) 2, pp. 511–538.

VALAVANIS & KOSMOPOULOS 2010
Valavanis, I.; Kosmopoulos, D.: Multiclass defect detection and classification in weld radiographic images using geometric and texture features. Expert Systems with Applications: An International Journal 12 (2010) 37, pp. 7606–7614.

VÄNSKÄ ET AL. 2013
Vänskä, M.; Abt, F.; Weber, R.; Salminen, A.; Graf, T.: Effects of Welding Parameters Onto Keyhole Geometry for Partial Penetration Laser Welding. Physics Procedia 41 (2013), pp. 199–208.

VOLPP & VOLLERTSEN 2016
Volpp, J.; Vollertsen, F.: Keyhole stability during laser welding—part I: modeling and evaluation. Production Engineering 10 (2016) 4-5, pp. 443–457.

WEBSTER ET AL. 2010
Webster, P. J.; Yu, J. X.; Leung, B. Y.; Wright, L. G.; Mortimer, K. D.; Fraser, J. M.: Inline coherent imaging of laser micromachining. International Symposium on Optomechatronic Technologies. Toronto, Canada, 25.10.–27.10. Piscataway, NJ: IEEE 2010, pp. 1–4.
ISBN: 978-1-4244-7684-8.

WEBSTER ET AL. 2014
Webster, P. J.; Wright, L. G.; Ji, Y.; Galbraith, C. M.; Kinross, A. W.; van Vlack, C.; Fraser, J. M.: Automatic laser welding and milling with in situ inline coherent imaging. Optics letters 39 (2014) 21, pp. 6217–6220.

WERBOS 1990
Werbos, P. J.: Backpropagation through time: what it does and how to do it. Proceedings of the IEEE 78 (1990) 10, pp. 1550–1560.

WIESNER ET AL. 2010
Wiesner, M.; Ihlemann, J.; Müller, H. H.; Lankenau, E.; Hüttmann, G.: Optical coherence tomography for process control of laser micromachining. The Review of scientific instruments 81 (2010) 3.

YING ET AL. 1990
Ying, H.; Siler, W.; Buckley, J. J.: Fuzzy control theory: A nonlinear case. Automatica 26 (1990) 3, pp. 513–520.

YOU ET AL. 2013

You, D.; Gao, X.; Katayama, S.: Multiple-optics sensing of high-brightness disk laser welding process. NDT & E International 60 (2013), pp. 32–39.

YOU ET AL. 2014

You, D.; Gao, X.; Katayama, S.: Monitoring of high-power laser welding using high-speed photographing and image processing. Mechanical Systems and Signal Processing (2014) 49, pp. 39–52.

YUSOF ET AL. 2020

Yusof, M. F.; Ishak, M.; Ghazali, M. F.: Weld depth estimation during pulse mode laser welding process by the analysis of the acquired sound using feature extraction analysis and artificial neural network. Journal of Manufacturing Processes 63 (2020), pp. 163–178.

ZADEH & ALIEV 2019

Zadeh, L. A.; Aliev, R. A.: Fuzzy logic theory and applications. New Jersey, USA: World Scientific 2019. ISBN: 978-981-3238-17-8.

ZHANG ET AL. 2015

Zhang, S.; Jiang, H.; Wei, S.; Dai, L.: Feed-forward sequential memory neural networks without recurrent feedback. arXiv:1510.02693 (2015).

References

Appendix

A1 List of supervised student research projects

In the context of this work, several student research projects were supervised in terms of content and organization. The supervision was performed at the Institute for Machine Tools and Industrial Management (*iwb*) of the Technical University of Munich. Some of the jointly gained insights have been incorporated into this dissertation and the publications described in section 5.2. The author of this dissertation would like to sincerely thank the students for the valuable discussions and the ideas that have been developed during the collaboration.

Name of Student	**Title and date of student research project**
Schmid, A.	Prozessoptimierung des Remote-Laserstrahlschweißens von Aluminium und Kupfer mittels optischer Kohärenztomografie für Anwendungen in der Elektromobilität, submitted in February 2018
Flaschberger, J.	Anwendung statistischer Methoden zur OCT-gestützten Prozessüberwachung und -prognose beim Remote-Laserstrahlschweißen, submitted in October 2018
Beilfuß, S.	Vorhersage der Einschweißtiefe beim Laserstrahlschweißen unter Verwendung von Methoden des Maschinellen Lernens, submitted in November 2018
Böhm, V.	Analyse von Schweißnahtdefekten beim Laserstrahlschweißen mittels Mikrofokus-Röntgen-Computertomografie, submitted in November 2018
Wagner, M.	Machine-Learning-Algorithmus zur Korrelation der Prozessparameter und der Einschweißtiefe beim Laserstrahlschweißen, submitted in February 2019

Neureiter, M.	Aufbau und Optimierung eines Finite-Elemente-Modells zur numerischen Simulation des Laserstrahl-Tiefschweißens unter Verwendung eines genetischen Algorithmus, submitted in March 2019
Pedri, M.	Entwicklung und Auslegung einer Einschweißtiefenregelung für das Laserstrahl-Tiefschweißen, submitted in April 2019
Pietschmann, R.	Anwendung von Methoden der Künstlichen Intelligenz zur Kalibrierung eines Laserstrahlwerkzeuges unter Zuhilfenahme Optischer Kohärenztomographie, submitted in April 2019
Diebolder, D.	Auswertung des Einschweißtiefen-Messsignals beim Laserstrahlschweißen mittels Methoden des Maschinellen Lernens, submitted in July 2019
Palukov, V.	Qualitätssicherung beim Laserstrahlschweißen von Aluminium in einer Überlappkonfiguration, submitted in January 2020
Weiß, T.	Auslegung und Implementierung einer Steuerung für eine innovative Laserschweißanlage, submitted in January 2020
Wittemer, M.	Entwicklung eines Sicherheitskonzepts für kompakte mobile Laser-Materialbearbeitungssysteme im Multi-kW-Leistungsbereich, submitted in January 2020
Pedri, M.	Entwicklung einer bildbasierten Auswertungsmethode zur Einschweißtiefen-Ermittlung beim Laserstrahl-Tiefschweißen von Aluminiumlegierungen, submitted in November 2020
Götz, K.	Regelung der Einschweißtiefe beim Laserstrahl-Tiefschweißen von Aluminiumlegierungen, submitted in December 2020
Weiß, T.	Inline-Auswertung der Einschweißtiefe beim Laserstrahlschweißen unter Nutzung von Methoden des Maschinellen Lernens, submitted in January 2021

A2 Publications of the author[17]

The author's publications, which were elaborated in the course of writing this dissertation, are listed below in chronological order.

- **Stadter, C.; Schmoeller, M.; Zaeh, M. F.:** "Hochflexibles Remote-Laserstrahlschweißen für den Karosseriebau der Zukunft", translated title: "Highly flexible remote laser beam welding for the car body production of the future ". Automobiltechnologie in Bayern + e-Car (2018), pp. 20–22.
- **Wagner, M.; Schmoeller, M.; Stadter, C.; Zaeh, M. F.:** "Kreuzkorrelation von Prozessparametern und der Einschweißtiefe beim Laserstrahlschweißen von Aluminiumlegierungen mittels Methoden des Maschinellen Lernens". DVS Berichte 355 (2019), pp. 13–21.
- **Stadter, C.; Schmoeller, M.; Zaeh, M. F.:** "Ganzheitliches Qualitätssicherungskonzept für hochflexible Produktionsanlagen im Karosseriebau der Zukunft: Innovative Sensortechnologie und Datenauswertung mittels Künstlicher Intelligenz als Befähiger für hochflexible Fügetechnologien ", translated title: "Holistic Quality Assurance System for Highly Flexible Production Systems in the Body Shop of the Future: Innovative Sensor Technology and Data Evaluation Using Artificial Intelligence as an Enabler for Highly Flexible Joining Technologies". Automobiltechnologie in Bayern + e-Car (2019), pp. 18–21.
- **Stadter, C.; Schmoeller, M.; Zeitler, M.; Tueretkan, V.; Munzert, U.; Zaeh, M. F.:** Process control and quality assurance in remote laser beam welding by optical coherence tomography. Journal of Laser Applications 31 (2019) 2, pp. 022408-1–022408-9.
- **Schmoeller, M.; Stadter, C.; Liebl, S.; Zaeh, M. F.:** Inline weld depth measurement for high brilliance laser beam sources using optical coherence tomography. Journal of Laser Applications 31 (2019) 2, pp. 022409-1–022409-8. **Publication P1 of this dissertation.**

[17] Wherever no bibliographic indices are given, the information is not available or not known to the author.

- **Stadter, C.; Schmoeller, M.; Kogel-Hollacher, M.; Munzert, U.; Zaeh, M. F.:** Holistic sensor concept for process control and quality assurance in laser beam welding based on Optical Coherence Tomography. Proceedings of the Lasers in Manufacturing Conference (2019).
- **Schmoeller, M.; Neureiter, M.; Stadter, C.; Zaeh, M. F.:** A Genetic Algorithm for the Correlation of the Keyhole and the Melt Pool Depth in Laser Beam Welding of AA6082. Proceedings of the Lasers in Manufacturing Conference (2019)
- **Stadter, C.; Kick, M. K.; Schmoeller, M.; Zaeh, M. F.:** Correlation analysis between the beam propagation and the vapor capillary geometry by machine learning. Procedia CIRP 94 (2020), pp. 742–747.
- **Schmoeller, M.; Stadter, C.; Wagner, M.; Zaeh, M. F.:** Investigation of the influences of the process parameters on the weld depth in laser beam welding of AA6082 using machine learning methods. Procedia CIRP 94 (2020), pp. 702–707. **Publication P3 of this dissertation.**
- **Stadter, C.; Schmoeller, M.; von Rhein, L.; Zaeh, M. F.:** Real-time prediction of quality characteristics in laser beam welding using optical coherence tomography and machine learning. Journal of Laser Applications 32 (2020) 2, pp. 022046-1–022046-9.
- **Schmoeller, M.; Neureiter, M.; Stadter, C.; Zaeh, M. F.:** Numerical weld pool simulation for the accuracy improvement of inline weld depth measurement based on optical coherence tomography. Journal of Laser Applications 32 (2020) 2, pp. 022036-1–022036-9. **Publication P2 of this dissertation.**
- **Schmoeller, M.; Stadter, C.; Kick, M.; Geiger, C.; Zaeh, M. F.:** A Novel Approach for the Holistic 3D-Characterization of Weld Seams - Paving the Way for Deep Learning Based Process Monitoring. Materials 14 (2021) 1. **Publication P4 of this dissertation.**
- **Schmoeller, M.; Weiß, T.; Goetz, K.; Stadter, C.; Bernauer, C.; Zaeh, M. F.:** Inline Weld Depth Evaluation and Control Based on OCT Keyhole Depth Measurement and Fuzzy Control. Processes 10 (2022) 1. **Publication P5 of this dissertation.**